A QUALITATIVE AND PHYSICAL ANALYSIS OF PROCESSES AROUND THE MASCARENE PLATEAU

Patrick Vianello

A thesis presented for the Degree of

DOCTOR OF PHILOSOPHY

In the Department of Oceanography

UNIVERSITY OF CAPE TOWN

August 2015

Abstract

The Mascarene Plateau is a submerged volcanic plateau to the east of Madagascar which extends over 2200 km between the Seychelles and Mauritius. It is a complex feature, which is composed of 4 banks separated by 3 channels – namely the Seychelles, Saya de Malha, Nazareth and Cargados-Carajos Banks.

The main objective of this thesis is to analyze cruise data obtained during the October/November 2008 ASCLME (Agulhas Somali Current Large Marine Ecosystem) cruise on board the Dr Fridtjof Nansen which surveyed the region around the Mascarene Plateau. Due to the paucity of data in the region, the cruise was a routine cruise with no specific scientific questions to be answered. A comparison is also made between sea surface temperature (SST) and Acoustic Doppler Current Profiler (ADCP) derived currents on board to satellite estimate to possibly extend cruise results in space and time. Although the resolution of satellite estimate is low compared to cruise measurements, satellite estimate of geostrophic velocities and sea surface temperatures compare well with cruise data and can therefore be used in the region with confidence. This is invaluable since the Mascarene Plateau is relatively poorly understood and it allows us to link cruise data with Rossby waves and currents impacting the region. This is the second cruise in the region as there was a research cruise on board the RRS Charles Darwin during June/July 2002. However, the June/July 2002 cruise did not sample the banks of the Mascarene Plateau.

The water masses in the region can be divided into 3 regions. The northern region (north of 8° S) is characterized by Red Sea Water in the intermediate layers and Arabian Sea High Salinity Water in the surface waters. Mixing of surface waters (Arabian Sea High Salinity Water and Indonesian Throughflow Water) was observed. The central region between 8° - 13° S exhibits mixing between Red Sea Water And Antarctic Intermediate Water in the intermediate waters while surface waters are predominantly Indonesian Throughflow Water, Tropical Surface Water and Sub-Tropical Surface Water. The South Equatorial Current acts as a barrier to Sub-Tropical Surface Water. To the south of 13° S, only water masses of Southern Indian Ocean origin exist (Antarctic Intermediate Water and Sub-Tropical Surface Water) with the exception of Indonesian Throughflow Water (where the South Equatorial Current flows). Many areas in this region exhibit mixing between Sub-tropical Surface Water and Indonesian Throughflow Water. North Indian Deep Water exists throughout the region of the Mascarene Plateau except in regions where the bathymetry is too shallow. South Indian Central Water exists south of 8° S. Corroborating these findings, nutrient rich water associated with Arabian Sea High Salinity Water and

nutrient poor water associated with Sub-Tropical Surface Water, the area is broadly divided into 2 regions of nutrient rich waters to the north of approximately 13° S and nutrient poor waters to the south.

Similarly to the June/July 2002 cruise results, the cruise results from the October/November 2008 Dr Fridtjof Nansen cruise show that the SEC splits into 3 cores to the east of the Mascarene Plateau and is channeled through the 3 major gaps in the plateau. The total transport for the upper 450 m was 36.53 Sv with 14.93 Sv, 14.41 Sv and 6.19 Sv flowing through the Seychelles – Saya de Malha, Saya de Malha – Nazareth and Cargados – Carajos - Mauritius gaps respectively. The only bank to experience flow is the Seychelles Bank due to the South Equatorial Counter Current. The South Equatorial Current does not act as a constant current in the region but rather oscillates in strength. The Saya de Malha, Nazareth and Cargados-Carajos Banks retain similar high Chl-a values throughout the year suggesting that a distinct ecosystem could exist across these banks.

During both cruises conducted in the region (2002 and 2008) there were no major Rossby wave propagations in the area and hence sampling was undertaken during normal conditions with regards to Rossby wave propagations induced by Indian Ocean Dipole (IOD) and/or El Niño. During the period 1994 – 2011, the majority of the major Rossby waves crossed every part of the Mascarene Plateau whilst the Rossby waves which passed through the gaps in the Mascarene Plateau significantly increased the geostrophic velocity in the gaps.

Studying the Mascarene Plateau has many limitations. There have only been 2 research cruises in the area and hence knowledge of dynamical processes is limited. There have been very few modeling studies in the region and have proven to be highly inaccurate of the actual processes occurring. Further understanding of the region would entail further modeling studies, deploying moorings in the 3 major gaps in the plateau (to understand fully the dynamical nature of the volume transport), analyzing satellite data and initiating further cruises to gather more cruise data in the region (a cruise during a Rossby Wave propagation would give more insight into the physical processes of the region during these events).

Plagiarism Declaration

I know that plagiarism is wrong. Plagiarism is to use another's work and pretend that it is one's own.

This thesis has originally been written by me which includes my original research work (analysis of data, creating of figures and writing the discussions of the results), with the full support of my supervisors (Dr. Mathieu Rouault and Prof. Isabelle Ansorge) at the Department of Oceanography, University of Cape Town, South Africa. Wherever contributions are made by others, every effort is made to clearly acknowledge this. Aside from the guidance of my supervisors, I have received no assistance, except as acknowledged.

I have not allowed, and will not allow, anyone to copy my work with the intention of passing it off as his or her own work.

Signature _____

Date _____

Acknowledgements

Firstly, I dedicate this thesis to the memory of Professor Johann Lutjeharms as without him, this thesis would have been impossible to complete. He was my original supervisor but unfortunately passed away during the first year of my PhD. He designed the cruise track over the Mascarene Plateau and hence had an influence on this thesis as cruise data from this cruise track was used.

I would also like to thank my supervisors, Dr. Mathieu Rouault and Dr. Isabelle Ansorge for their continued support and guidance throughout my PhD, without which, I could not have completed. I am also grateful to them for making it possible for me to attend various conferences and workshops during the course of my PhD and especially to Dr. Mathieu Rouault for making a 2 week trip to Japan possible where I was able to obtain model data from our collaborators at JAMSTEC (Japan Agency for Marine-Earth Science and Technology). Additionally, I give thanks to ACCESS SATREPS for funding my trip to Japan.

I thank the scientists and crew on board the Dr Fridtjof Nansen during the October/November 2008 cruise in the region of the Mascarene Plateau for collecting data required for analysis in this PhD. Without this cruise, this PhD would have been impossible.

I am grateful to my family and friends for their continued support during my PhD and always giving me motivation.

I thank the National Research Foundation (NRF) and the Nansen Tutu Centre for funding my research.

Table of Contents

List of Figures

List of Tables

CHAPTER 1: Literature Review

1.1 Overview of the Indian Ocean

The Indian Ocean is the third largest ocean in the world covering 68.56×10^6 km^2. It is smaller than the Atlantic (76.76×10^6 km^2) and Pacific Oceans (155.56×10^6 km^2) but larger than the Southern (20.33×10^6 km^2) and Arctic Oceans (14.06×10^6 km^2). Its boundaries are 20° – 147° E and 30° N – 60° S including the Red, Arabian, Gulf Persian Seas and the Bay of Bengal. The physical oceanography of the Indian Ocean and in particular the southern sector is poorly understood comparatively to the other ocean basins (Pacific and Atlantic). This is largely due to the lack of hydrographic data over the past decades and it is surrounded by economically poor countries (Wyrtki, 1971; Demopoulos et al, 2003). The Indian Ocean differs to the Atlantic and Pacific Oceans in that it is landlocked in the north at approximately 25° N (The Asian continent extends from the northern tropics to the higher latitudes and therefore has no connection with the Arctic Ocean). As a result, the Indian Ocean differs from the Atlantic and Pacific Oceans in that the circulation patterns north of the equator do not mirror those to the south of the equator. Due to the Indian Ocean being landlocked, there is a strong meridional land-sea contrast leading to a seasonal reversal of winds known as the monsoon. This monsoon system is the strongest on Earth, which generates large seasonal variations in ocean circulation (Schott et al, 2009). The seasonal changes in the monsoonal winds force the wind-driven circulation in the Northern Indian Ocean whilst in the South Indian Ocean the conventional anti-cyclonic, wind-driven circulation persists throughout the year (Lutjeharms, 2006b).

The mean depth of the Indian Ocean is 3800m. Many basins have depths exceeding 5000m. The Wharton Basin, which lies between the Ninety East Ridge (~ 90° E) and Australia, exceeds 6000m and the Arabian Sea has depths below 3000m. There are 2 ridge systems, which run through the ocean in a meridional direction dividing it into 3 parts of approximately equal size. The Central Indian Ridge between the western and the central part is a northward extension of the interoceanic ridge system. It is a broad structure, which rises consistently above 4000m. On occasions it reaches above 3000m. The Ninety East Ridge runs in a north-south direction from the Andaman Islands to 33° S. It is narrower than the Central Indian Ridge. South of 10° S, it frequently reaches 2000m and 3000m in depth. South of approximately 30° S, the Ninety East Ridge merges with the Southeast Indian Ridge which is a continuation of the Central Indian Ridge. The central and eastern part of the Indian Ocean is dominated

by single basins of large meridional extent whilst the western part is subdivided by small ridges and Madagascar into a series of smaller deep basins (Tomczak and Godfrey, 1993).

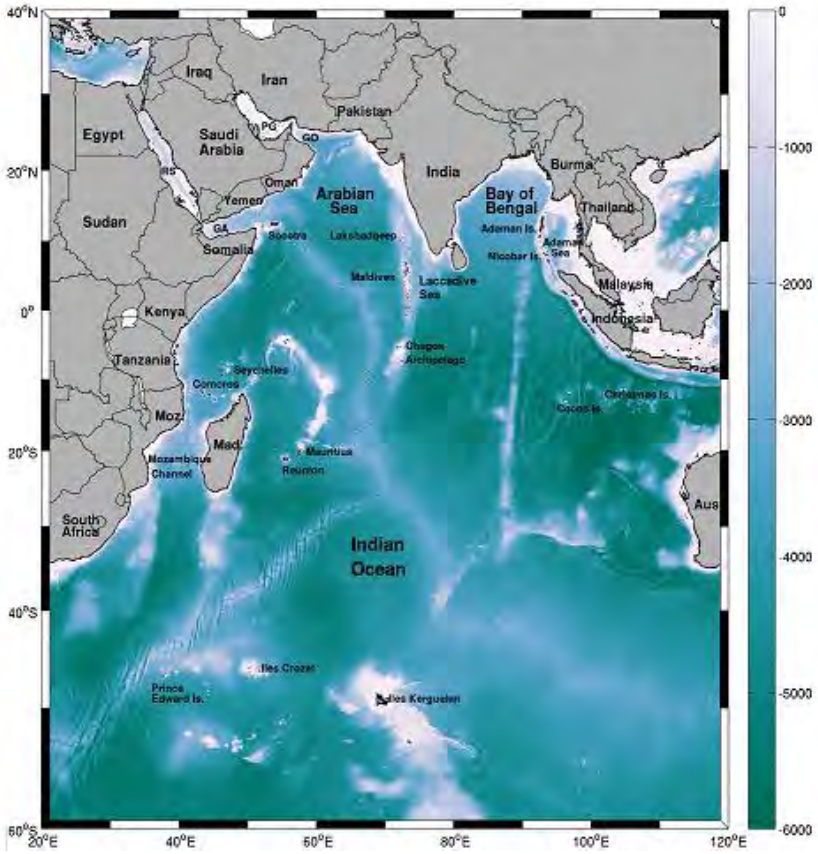

Figure 1. 1: Geographic Map of the Indian Ocean. Abbreviations are as follows: Aus – Australia, Moz – Mozambique, Mad – Madagascar, RS – Red Sea, PG – Persian Gulf, GO – Gulf of Oman, GA – Gulf of Aden. The Indian Ocean is the only ocean that is landlocked to the north at approximately 25° N. The central and eastern part of the Indian Ocean has single basins of large meridional extent whilst the western part is subdivided by small ridges. The deepest basin is the Wharton Basin, which is situated between the Ninety East Ridge and Australia where depths reach below 6000m. (after Collins, 2013)

1.1.1 Previous Research

The Indian Ocean remains the least exploited and most unknown ocean region compared to the Atlantic and Pacific Oceans (Demopoulos et al, 2003). This is due to the fact that it is not surrounded by the world's leading oceanographic institutions and fewer moorings, XBT's, CTD's etc. have been deployed (Domopoulos et al, 2003). An International Indian Ocean Expedition (IIOE) was conducted 1959 – 1965, in which oceanographic data was collected. Data included hydrographic casts using Nansen bottles, phytoplankton

trawl, deep-water fish trawl, vertical series of water samples for primary production, meteorological observations and a bathythermograph down to 275m (Wyrtki, 1971). This International Indian Ocean Expedition was carried out in order to gain more knowledge of the Indian Ocean and reference textbooks to be compiled. Following this expedition others were carried out such as the Indian Ocean Experiment (INDEX) during 1976 – 1979 and the World Ocean Circulation Experiment (WOCE) from 1990 – 1998. Current meter moorings were deployed during the INDEX expedition for the first time in the equatorial Indian Ocean in order to gain more knowledge of the circulation as in-situ data was sparse in the region at the time. One of the moorings was deployed at 0°, 55.67° E in order to ascertain the nature of equatorial currents in the region (Knox, 1976). WOCE is recognized by many as the largest internationally coordinated program conducted. WOCE aimed to provide the largest global data collection such as CTD, ADCP, XBT, etc. The Atlas of the Indian Ocean water masses and properties has been compiled by WOCE (Levitus et al, 1994; Conkright et al, 2002). Subsequently, after further research (research cruises conducted and satellite data obtained) a more in depth understanding of the Indian Ocean was obtained such as the distribution of water masses and the general ocean circulation.

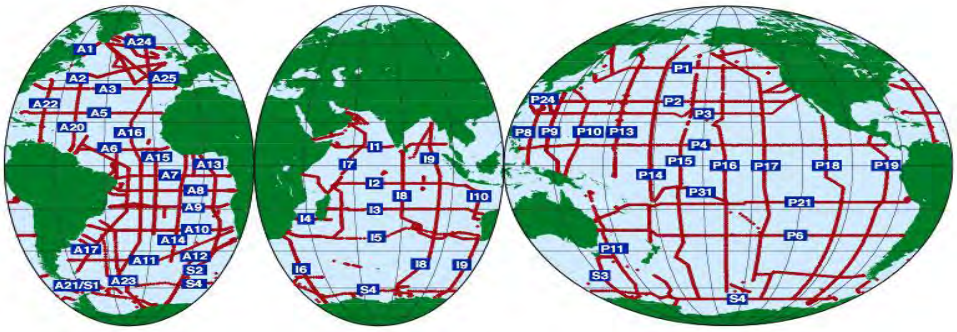

Figure 1.2: Stations Occupied during the WOCE one time survey. Notice that the Indian Ocean has been sampled the least. (Source: http://woceatlas.tamu.edu/Sites/html/atlas/SOA_WOCE.html)

1.1.2 Circulation of the Indian Ocean

The Indian Ocean consists of many wind driven currents and water masses which are in turn transported from the western Pacific Ocean, the Red Sea, Arabian Sea and the Bay of Bengal to other parts of the ocean via these wind driven currents. South of 10° S, the southeast trades are relatively steady with their northern edge shifting northward (southward) during the winter (spring). North of 10° S the winds reverse direction – a phenomenon known as the monsoon (Schott et al, 2009). The monsoon and its

influence on ocean currents will be discussed later. The tropical Indian Ocean is different from the other tropical oceans with regard to the absence of continuous easterly winds along the equator. There is only an easterly component during late winter/early spring, a semiannual westerly component during the intermonsoons and a weak westerly mean (Schott et al, 2009). In the south Indian Ocean an anticyclonic subtropical gyre exists between 40° S and 15° S which extends from South Africa to Australia (Stramma and Lutjeharms, 1997). At approximately 40° S there is an eastward flow in the form of the SIOC (South Indian Ocean Current). Many consider this current to be the northern part of the ACC (Antarctic Circumpolar Current). Approximately 60 Sv flows in the region South East of South Africa but it decreases further east. About 30 Sv circulates northwards between 50° E and 60° E in a SW Indian sub-gyre while the remaining 30 Sv circulates northwards across the remainder of the basin (New et al, 2005)

1.1.3 Currents in the Indian Ocean

1.1.3.1 Eastern Boundary Currents

Eastern boundary currents differ in the Indian Ocean compared to the Atlantic and Pacific Oceans. The temperature and salinity stratification is not fully developed so when upwelling does occur, there is no intensive cooling. Another difference is that twice a year (May and November) the Equatorial jet feeds warm water towards Sumatra which creates a poleward current in the northern and southern hemisphere (Thompson, 1984). The Leeuwin current off Western Australia differs to the eastern boundary currents off the Pacific and Atlantic Oceans. Along the coasts of these two oceans, equatorward winds produce coastal upwelling where there is an equatorward surface flow. Off the coast of Western Australia there are equatorward winds but there is a strong poleward flow against the wind. This phenomenon is because eastern boundary currents are driven by alongshore winds and alongshore pressure gradients. The other two oceans have dynamic heights not exceeding 0.1 m^2s^2 along most eastern coasts whilst the dynamic height off western Australia is 0.5 m^2s^2 (Godfrey and Weaver, 1991; Thompson, 1984). This creates an eastward geostrophic flow and once it reaches the coast the water flows down the pressure gradient resulting in the poleward flow. This poleward flow is stronger than the opposing wind driven equatorward current. The drop in dynamic height drop along the western coast of Australia is related to the connection between the Pacific and Indian Oceans. The connection between the Pacific and Indian Oceans allows the dynamic height to be similar off Northwest Australia and the

Western Equatorial Pacific Ocean. The dynamic height at approximately 34° S is much lower as there is a temperature drop due to strong cooling and convective overturning. The annual average transport of the Leeuwin Current is approximately 5 Sv with velocities averaging 0.1 – 0.2 $m.s^{-1}$ (Thompson, 1984).

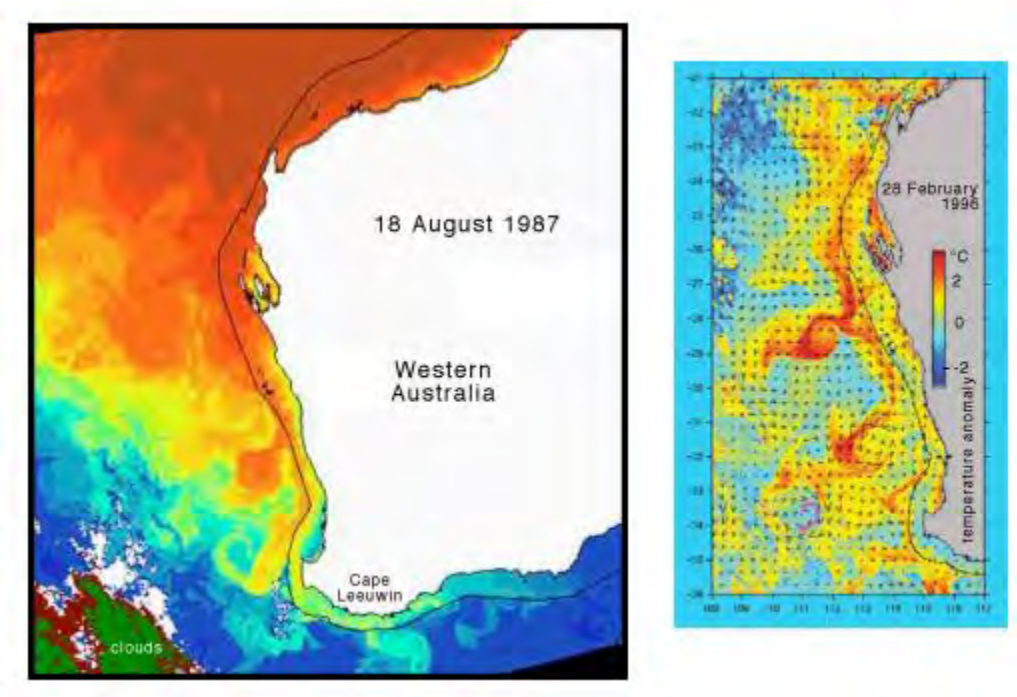

Figure 1. 3: Satellite images of SST in the Leeuwin Current and associated eddies. Left panel – SST in August 1987. The Leeuwin Current is seen as a band of warm water along the western coastline that continues around Cape Leeuwin. The black line indicates the shelf break. Right panel – SST anomalies in February 1996 depicting large eddies. Black arrows indicate surface currents. (Source: http://www.cmar.csiro.au/)

1.1.3.2 Western Boundary Currents

The strongest Western Boundary current in the Southern Hemisphere is the poleward flowing Agulhas Current (Biastoch et al, 2008a). The features of this current are that it is narrow (~ 90 km), 2500 m deep and flows closely along the steep slope of the continental shelf (Casal et al, 2009; Donohue and Toole, 2003; De Ruijter et al, 1999). The steep slope provides the northern extension of the current a stable regime. However, between Durban and Richards Bay (Natal Bight), the Agulhas Current occasionally overshoots seaward (Lutjeharms, 2006). This occurs due to the development of an intermittent cyclonic

meander inshore of the current, termed the Natal Pulse (Lutjeharms and Roberts, 1988). These pulses grow as they move downstream at a propagation speed of ~ 20 km/day and a mean diameter of ~ 200 km (van Leeuwen et al, 2000; Lutjeharms et al, 2001). South of Port Elizabeth, the continental shelf differs considerably due to the presence of the Agulhas Bank. The shallow topography of the bank induces a more unstable regime on the Agulhas Current and a meandering behaviour characterizes the flow in this region (De Ruijter et al, 1999). Measurements taken along the path of the current suggests that the core has Sea Surface Temperatures in the range of 22 – 28 °C, salinity of approximately 35.4 and propagation speeds of up to 2 m/s (Gordon, 1986; Gründlingh, 1980). The volume transport of the Agulhas Current is approximately 76 Sv (Donohue and Toole, 2003; Beal and Bryden, 1999). Towards the south western part of the Agulhas Bank, the current separates from the continental shelf and rotates on itself in a revolving loop known as the Agulhas Retroflection (De Ruijter et al, 1999). The Agulhas Retroflection occurs between 16° E and 20° E (Lutjeharms and van Ballegooyen, 1988b) with an average diameter of approximately 340 km (Lutjeharms, 2006). Rings, eddies and filaments are shed from the Retroflection into the oceanic environment of the South-East Atlantic (Reason et al, 2003; De Ruijter et al, 1999). The Indian Ocean properties (heat and salt) can be transported far beyond the South-Eastern Atlantic Ocean (Gordon, 1986). These properties can be transported into the North Atlantic Ocean (Biastoch et al, 2009). Van Ballegooyen et al, (1994) estimated a volume flux by the Agulhas rings of approximately 7 Sv , a heat flux of approximately 0.9 PW and a salt flux of approximately 78×10^{12} kg per year whilst Richardson, (2007) estimated an Agulhas leakage into the Atlantic of 15 Sv in the upper 1000m of which the vast majority is composed of Agulhas rings. These rings in the Atlantic Ocean lose their energy quickly, 70% after their shedding (Shouten et al, 2000). A significant part of the Agulhas retroflection returns back towards the Indian Ocean via the Agulhas Return Current (ARC). The Agulhas Return Current flows eastwards to approximately 70° E (Lutjeharms and Ansorge, 2001). The ARC forms the northern boundary of the Subtropical Convergence Front. This front acts as barrier to the warmer saltier waters to the north from the colder and fresher waters to the south. As the current moves further to the east, its volume transport decreases as a part of it flows into the subtropical gyre of the South Indian Ocean (Lutjeharms and Ansorge, 2001). The ARC has a volume transport of approximately 55 Sv near the retroflection region.

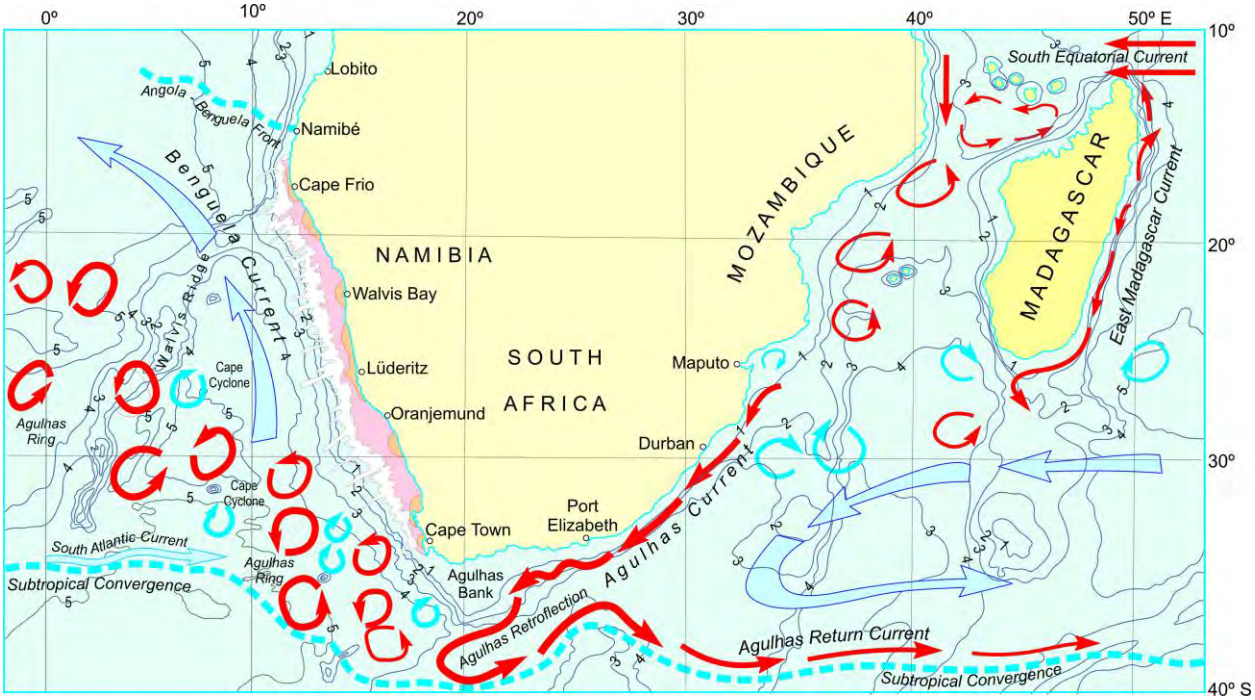

Figure 1. 4: The greater Agulhas Current System. Curvilinear features depicts mesoscale eddies and the arrows the ocean currents. Agulhas rings are depicted south-west of Cape Town whilst Mozambique eddies are depicted in the Mozambique channel. Contours are expressed in km (after Ansorge and Lutjeharms, 2007)

1.1.3.3 East Madagascar Current

The South Equatorial Current (SEC) approaches the eastern coast of Madagascar at approximately 19° S. It then bifurcates into the North East Madagascar Current (NEMC) and the South East Madagascar Current (SEMC). These 2 currents are also commonly known as the northward and southward branches of the East Madagascar Current (EMC). The bifurcation of the SEC may be the result of the wind system. Ekman transport towards the coast (north of the bifurcation) and away from the coast (south of the bifurcation) leads to geostrophic balanced currents both south and north of the bifurcation (Voldsund, 2011). The SEMC acts as a topographically steered western boundary current (150 cm/s and ~ 26 Sv) (Voldsund, 2011). This current flows southwards around Madagascar and part of it flows west to the African coast in the form of eddies and dipoles (de Ruijter, 2005) and contributes to the Agulhas current whilst the remaining part of this retroflects and feeds a shallow eastward jet (Siedler et al, 2006) which is known as the South Indian Ocean Counter-current (SICC). The NEMC is weaker (~ 60 cm/s at the

bifurcation point) but accelerates at approximately 12° S. The volume transport around the northern tip of Madagascar is 62 Sv (Voldsund, 2011). The NEMC which reaches the African coast largely turns northward to form the EACC (East Africa Coastal Current) while some turns southwards through the Mozambique channel and breaks up into eddies (Schott and McCreary, 2001). The EACC may then either link up with the Somali current system or be returned eastward through the South Equatorial Counter Current (SECC).

1.1.3.4 Indonesian Throughflow

The Indonesian Throughflow (ITF) transports water from the Pacific Ocean into the Indian Ocean, mainly in the upper ocean (< 400m). The water mass which is transported is North Pacific water from the Mindanao Current (Gordon, 2005). The ITF also comprises of a subsurface core which has origins in the south Pacific (McCreary et al, 2007). As this water passes through the Indonesian passages, changes happen to this water through tidal mixing and internal wave breaking (Koch-Larrouy et al, 2007) creating a new water mass known as Banda Sea Water. From certain measurements the volume transport is approximately 10 Sv (Gordon, 2005), however certain modeling studies estimate a higher volume transport. Ganachaud et al, (2000) estimated 15 Sv whilst Lumpkin and Speer, (2007) estimated approximately 13 Sv. The ITF has a seasonal cycle with a maximum (minimum) outflow in June (February) and has an amplitude of 3 – 4 Sv (Schott et al, 2001).

1.1.3.5 South Equatorial Current (SEC)

The oceanic wind driven circulation in the SW Indian Ocean (south of 10° S) contains mainly waters of the westward flowing SEC which is a broad westward flow between 10° S and 16° S during the northeast monsoon (December–April) but can extend to 6° S in September/October during the southwest monsoon. The northern part of the sub-tropical gyre in the Southern Indian Ocean takes the form of the SEC. There are various waters which flow into the SEC, including the waters flowing northwards from the sub-tropical gyre, from the Indonesian seas to the east and from waters in the North Indian Ocean through the SW monsoon current and Java current (Schott and McCreary, 2001). Many currents in the North Indian Ocean seasonally reverse direction due to the monsoonal climate.

1.1.4 Monsoons

The monsoonal climate in the Indian Ocean occurs because it is landlocked in the north (Asian land mass). A seasonal reversal of wind direction is the distinguishing feature of monsoonal regions (Gadgil, 2003). There is a seasonal variation of winds in the northern sector of the Indian Ocean. The northern part of the Indian Ocean circulation differs comparatively to that of the Atlantic and Pacific Oceans as the other two Oceans are not inhibited by a land mass to the north. In summer (June–September), the heating of the Asian landmass results in a low pressure system over Asia, while a high pressure system remains over the Indian Ocean (Yamagata et al, 2004). The strong southeast trade winds in the Southern Hemisphere extend north to approximately 5° S and re-curve upon crossing the equator becoming southwesterlies. This system is known as the summer SW monsoon (Yamagata et al, 2004). In winter (December-March) the cooling of the Asian landmass results in a high pressure over the land and a low pressure over the ocean, resulting in a northeasterly wind (Woodberry et al, 1989). These winds cross the equator and change to northwesterlies that converge with the southeast trade winds at approximately 10° S This system is known as the winter NE monsoon (Goes et al, 2005). The intermonsoon periods (April – May and October – November) are characterized by strong equatorial westerlies. During this season there is an equatorial phenomenon known as Wyrtki Jets. These jets do not occur in any of the other oceans due to the existence of the semiannual westerly winds. These jets are important climatically because they carry warm waters eastward, hence increasing the sea level height in the east and decreasing it westwards (Yamagata et al, 2004). Wyrtki jets reflect off the eastern boundary of the basin as Rossby waves (Wyrtki, 1973). During the inter-monsoon periods, the winds along the Somali coast weaken which decreases upwelling in the region.

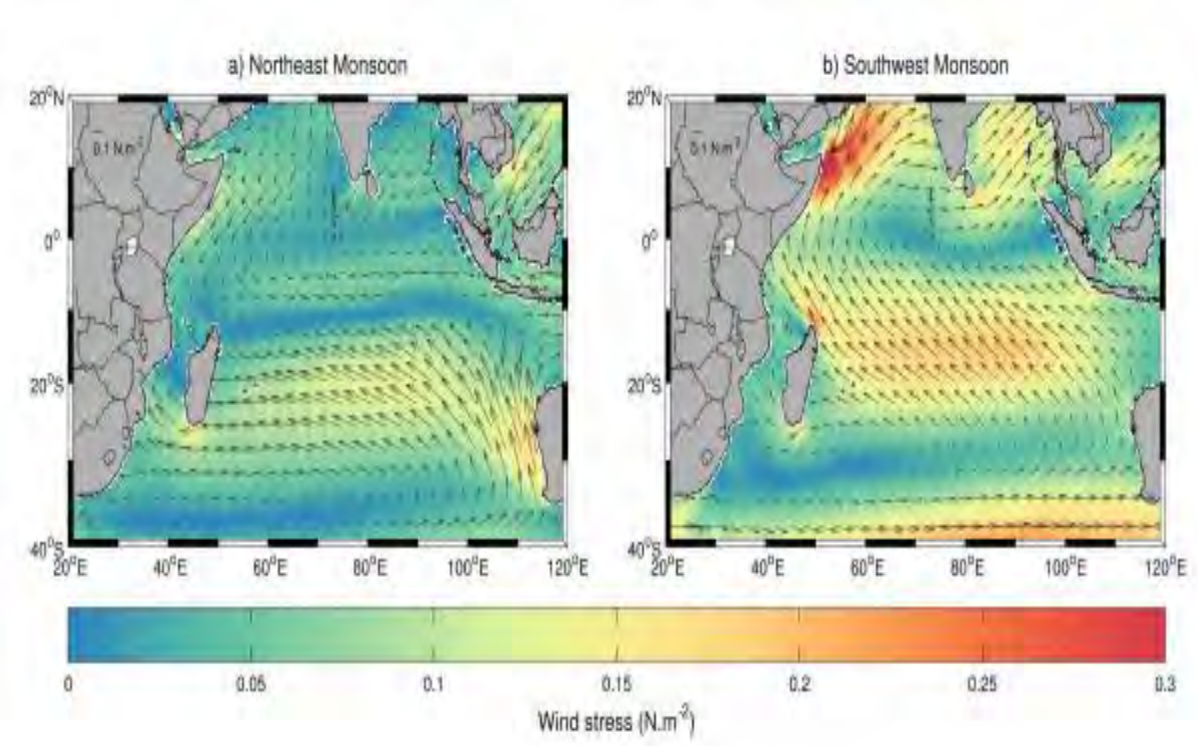

Figure 1. 5: Wind stress (N/m^2) over the Indian Ocean for the (a) Northeast monsoon and (b) Southwest monsoon (after Collins, 2013)

1.1.5 The Monsoon's influence on Ocean Currents and associated SST's

The ocean circulation in the North Indian Ocean undergoes seasonal reversal due to the monsoons (Schott and McCreary, 2001). During the winter NE monsoon, a westward flowing North Equatorial Current (NEC) from 8° N to the equator exists (also known as the Northeast Monsoon Current). This current carries fresh low salinity Bay of Bengal water (origin has a salinity of approximately 33) into the Arabian Sea (Han and McCreary, 2001). During this season, the Somali current flows south and meets with the northward flowing East African Coastal Current (EACC) and supplies water for the eastward flowing South Equatorial Countercurrent (SECC). During this season the South Equatorial Current (SEC) supplies water to the South Equatorial Counter Current (SECC) and the Agulhas Current (Stramma and Lutjeharms, 1997). The SST in the North Indian Ocean (north of 10° S) is influenced by the monsoon winds and associated currents. When the northeast monsoon starts in November, SST decreases until January with significant reduction at the head of the Bay of Bengal from October to December (29° C -

26° C). During January and February between 10° S and 10° N, the SST increases from approximately 28° C from the west to more than 29° C in the east. During this period in the Arabian Sea and the Bay of Bengal, the SST decreases northward (from 28° C at approximately 10° N to 24° C in the northern part). As the sun moves poleward in the northern hemisphere, the Bay of Bengal warms faster than the Arabian Sea (Rao and Ram, 2005).

During the summer SW monsoon, the NEC and Somali currents reverse direction and become an eastward and northward flowing current respectively (Schott et al, 2009). The NEC in combination with the SECC forms a broad eastward flow approximately from 15° N – 7° S termed the Southwest Monsoon Current. This eastward flow flows south of Sri Lanka and then turns north to bring saltier Arabian Sea Water (origin has a salinity > 35.3) into the Bay of Bengal (Jensen, 2003). During this season, the SEC augments with waters flowing in the Somali Current along the African coast. Hence, during the SW monsoon, the SEC, Somali Current and Monsoon Current form a strong wind-driven gyre in the northern Indian Ocean (Pickard and Emery, 1990). It has been observed that there is strong upwelling along the Somali coast during this period. At the start of the summer SW monsoon (June), the SST starts falling until August due to strong winds and the advection of upwelled water from the Somali coast. The decrease in SST in the Bay of Bengal is only approximately 1° C. Towards the end of the southwest monsoon in September, both the Arabian Sea and Bay of Bengal warm up. As can be seen, the monsoonal climate affects the SST significantly in the Northern Indian Ocean. A feature of the Arabian Sea is that the SST in July is 2° C lower than in April whilst the SST in July is almost as low as that in January. This is due to the southwest monsoon (Halpern et al, 1998).

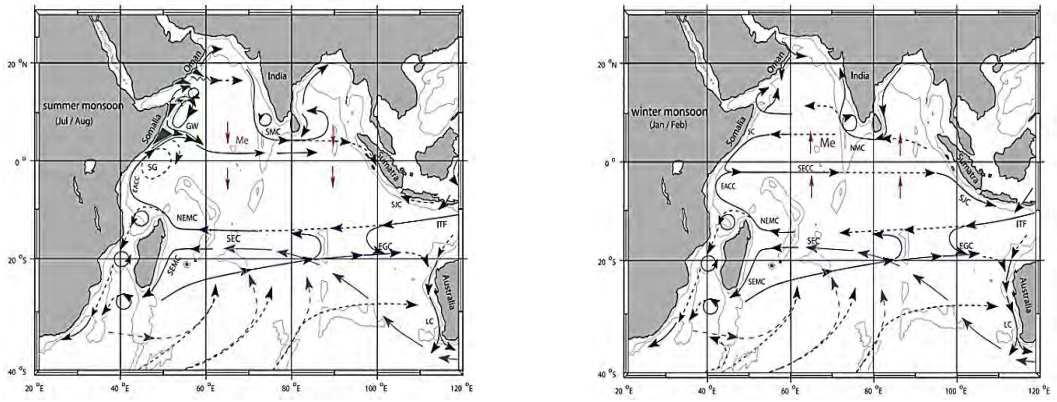

(a) (b)

Figure 1. 6: Diagram of the large scale surface circulation of the Indian Ocean. (a) shows the currents for the summer monsoon whilst (b) shows the currents for the winter monsoon. The circulation in the Southern Indian Ocean is not mirrored in the north due to the presence of the Asian landmass. The Northern Indian Ocean consists of seasonally reversing currents due to the monsoonal climate. Major currents include the westward South Equatorial Current (SEC), eastward South Equatorial Counter Current (SECC) and the seasonally reversing North Equatorial Current (NEC) and Somali Current (after Schott et al, 2009)

1.1.6 Eddies and Eddy Kinetic Energy (EKE)

Mesoscale eddies play an important role in ocean dynamics. They provide important dynamical fluxes for the equilibrium balances of the general circulation and climate (McWilliams, 2013). Mesoscale eddies transport heat and salt across ocean basins (Volkov et al, 2008) and eddy induced mass transport is comparable in magnitude with that of large-scale ocean circulation (Zhang et al, 2014). At the same time, mesoscale eddies modulate nutrient flux into the euphotic zone through vertical transport (Crawford et al, 2005). Submesoscale eddies play a key role through intense upwelling of nutrients and the subduction of plankton (Levy and Klein, 2004). Mesoscale eddies in the South Indian Ocean have been studied using satellite data (Chelton et al, 2011), ocean modeling (Backeberg et al, 2008) and in-situ observations (Ridderinkhof et al, 2010). Altimetry show that anticyclonic eddies propagate westward and equatorward whilst cyclonic eddies propagate poleward in the southeast Indian Ocean (Morrow et al, 2004). Eddy kinetic energy (EKE) in the South Indian Ocean shows a distinct seasonal

cycle. There is a maximum in EKE during the austral summer whilst a minimum occurs during the austral winter (Jia et al, 2011). During the austral spring, heat flux forcing of combined meridional Ekman and geostrophic convergence strengthens the upper ocean meridional temperature gradient and increases the vertical velocity shear. This modulation of the vertical velocity shear changes the intensity of baroclinic instability associated with the surface intensified SICC (South Indian Countercurrent) and SEC, leading to the seasonal variations of EKE (Jia et al, 2011). Compared with altimetry measurements, surface drifters give fine spatial and temporal resolutions. Altimetry can hardly detect eddies with a radius of less than 40 km whereas surface drifters can detect submesoscale eddies with a radius of less than 10 km. The temporal resolution of surface drifters are approximately 6 hours whilst altimetry have a resolution of 7 days.

1.1.7 Intraseasonal Variability

The monsoons in the Indian Ocean are a seasonal phenomenon. However there are also intraseasonal phenomena in the Indian Ocean such as Madden-Julian Oscillations (MJO's).

1.1.7.1 Madden-Julian Oscillations (MJOs)

Madden-Julian Oscillations (MJOs) are a part of a planetary-scale mode of tropical variability where convection develops over the western tropical Indian Ocean. Madden and Julian, (1972) observed variability at periods of 30 – 60 days. This convection propagates eastward across the Indian Ocean and decays east of the international dateline. There are baroclinic circulations associated with the moving convective centre. Anomalous easterlies in the lower troposphere east of the convective centre and anomalous westerlies to the west of it prevail (Salby and Hendon, 1994). SST anomalies of approximately 0.2° C – 0.4° C co-propagate with MJOs in the tropical Indian Ocean (Kawamura, 1988). The cause of the coherence of SST anomalies with MJOs is the variability in surface heat fluxes, latent heat flux and solar radiation. East of the convective centre, anomalous easterlies are superimposed on mean westerlies. As a result, there is a reduction in the latent heat loss from the ocean. At the same time, suppressed convection increases heating by solar radiation. Consequently, positive SST anomalies lead the MJO (Schott et al, 2009). The MJO is an intrinsic mode of atmospheric convection and circulation. MJO dynamics are not that well understood. A reason for this is that MJOs are not well represented in general circulation models (Slingo et al, 1996; Lin et al, 2006). However, the MJO is generally considered to be an intrinsic mode of atmospheric convection and

circulation and it is clear that convection-circulation interactions give rise to the slow eastward propagation of MJOs (Schott et al, 2009).

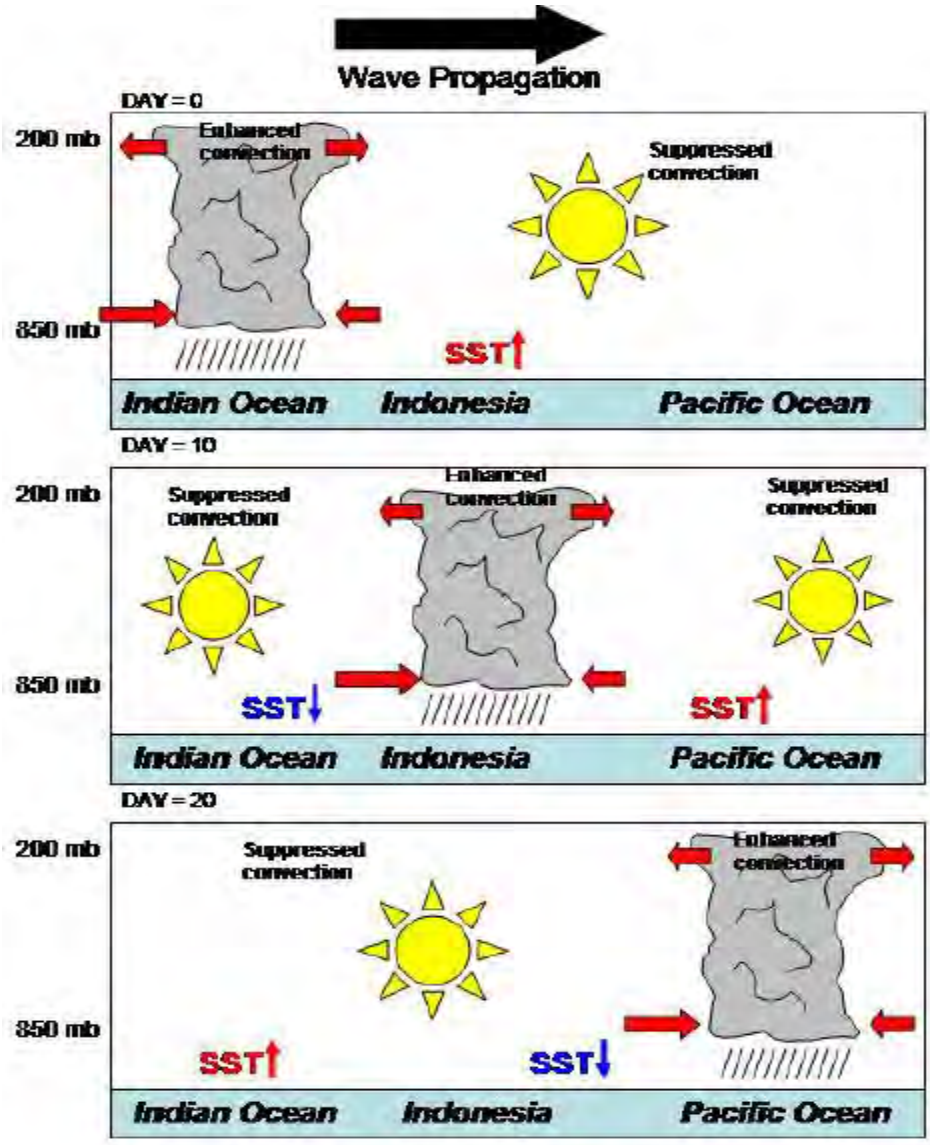

Figure 1. 7: A schematic representation of the Madden-Julian Oscillation, shown as a cross-section along the equator in the Indian Ocean – West Pacific sector. Day 1 – convection in the western Indian Ocean with suppressed convection to the east due to anomalous easterlies being superimposed on mean westerlies resulting in a reduction in latent heat loss. Day 10 – convection in the eastern Indian Ocean with suppressed convection over the western Indian Ocean and the western Pacific Ocean. Day 20 – convection in the western Pacific Ocean with suppressed convection over the Indian Ocean.

1.1.8 Interannual Variability

1.1.8.1 ENSO (El Niño – Southern Oscillation)

El Niño – Southern Oscillation (ENSO) is the primary mode of interannual variability in the Pacific Ocean and influences the climate on a global scale (Yoo et al, 2010). There is an oceanic component (El Niño or La Niña) as well as its atmospheric counterpart (Southern Oscillation). El Niño (La Niña) is characterized by anomalous warming (cooling) of the eastern equatorial Pacific (Schott et al, 2009) developing during the boreal summer, peaking in winter and decaying during the following spring. During these events there is a fluctuation of atmospheric pressure between the eastern and western tropical Pacific (known as the Walker circulation). Sea level pressure tends to be lower (higher) in the eastern Pacific during El Niño (La Niña), and higher (lower) in the western Pacific (Rasmusson and Carpenter, 1982). The tropical Indian Ocean gradually warms during an ENSO year, reaching a maximum during the austral autumn (March-May), approximately one season after the El Niño SST peak (Nigam and Shen, 1993; Klein et al, 1999; Liu and Alexander, 2007). During an El Niño (La Niña) event, the Indian Ocean north of approximately 30° S warms (cools) whilst cooling (warming) occurs in the southern mid-latitudes (Reason et al, 2000; Chambers et al, 1999). During El Niño there is a southward shift of the anomalous easterlies near the equator to approximately 10° S. These anomalous winds associated with the wind stress curl leads to the formation of westward travelling Rossby waves (Xie et al, 2002). Through this, a positive SST anomaly propagates to the west resulting in increased convection (Tourre and White, 1995; 1997). In the Eastern Equatorial Indian Ocean (EEIO), warming is more abrupt which takes place during October-March after an earlier cooling episode. EEIO SST anomalies cool during a growing El Niño (July-October). This cooling is due to intensified southeasterlies off Java and Sumatra, which is associated with the anomalous high-pressure system which in turn is associated with the Southern Oscillation. The southeasterlies weaken after October and the resulting coastal upwelling ceases (Murtugudde et al, 2000). Along with this, evaporation decreases and there is increased solar radiation due to suppressed convective clouds. These factors cause the EEIO SST anomalies to become positive (Tokinaga and Tanimoto, 2004). During an El Niño event there is high precipitation over Indonesia leading to fresher water. Hence Indonesian Throughflow Water (ITW) is fresher during these periods.

1.1.8.2 Indian Ocean Dipole (IOD)

The Indian Ocean Dipole (IOD) and associated westward propagating Rossby waves are an integral part of the interannual variability of the Indian Ocean (Yamagata et al, 2003;2004). A typical IOD event starts with anomalous SST cooling along the Sumatra-Java coast in the eastern Indian Ocean during May-June. The usual equatorial westerly winds during June-August reverse direction (Feng and Meyers, 2003). The event (positive) typically peaks around September with a positive SST anomaly over large parts of the Western Indian Ocean and a negative SST anomaly over large parts of the Eastern Indian Ocean (Saji et al, 1999). Saji et al, (1999) described an Indian Ocean dipole index as the difference between SST anomalies in the Western equatorial Indian Ocean (50 – 70 E, 10 S – 10N) and the tropical southeastern Indian Ocean (90 – 110E, 10S – equator). A negative IOD is the reverse of a positive IOD (ie. positive SST anomaly over the Eastern Indian Ocean and a negative SST anomaly over the Western Indian Ocean).

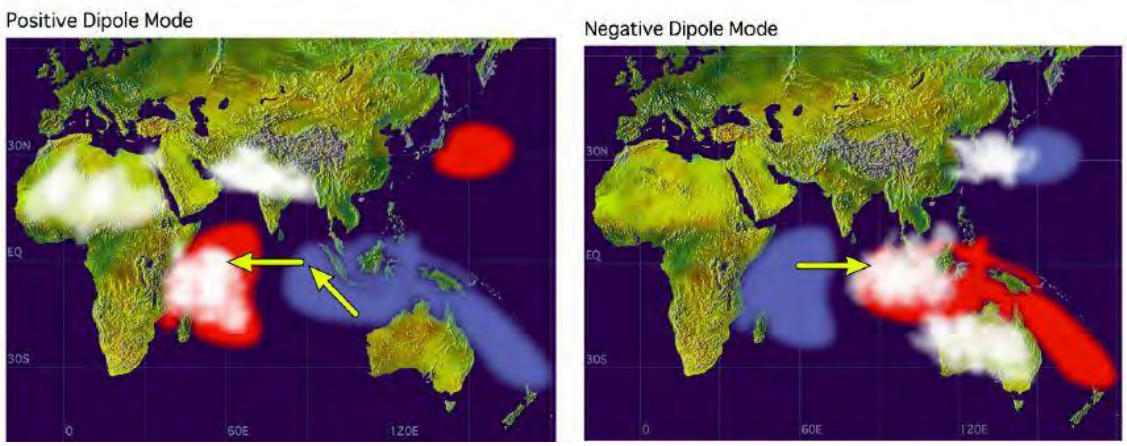

(a) (b)

Figure 1. 8: Positive (a) and Negative (b) Indian Ocean Dipole (IOD). During the positive IOD, SST is above normal in the western Indian Ocean and below normal in the eastern Indian Ocean. During the negative IOD, SST is below normal in the western Indian Ocean and above normal in the eastern Indian Ocean. (Source: http://www.jamstec.go.jp/frsgc/research/d1/iod/e/iod/about_iod.html)

There has been a great deal of controversy as to whether the IOD is related to ENSO. An example as to whether there is a teleconnection between the two was during the 1997 IOD/ENSO event (Schott et al,

2009). However there are examples of IOD years where ENSO is absent such as the strong IOD event in 1994 and also the significant IOD event of 1961 where ENSO is absent (Schott et al, 2009). Observations from 1958 to 1997 identified 11 out of 19 IOD years occurred where ENSO was absent (Saji and Yamagata, 2003). An analysis by Nagura and Konda, (2007) identified IOD development depends on the seasonal switch from normal or La Niña to El Niño. IOD development is favoured if the switch occurs from spring to summer. Nagura and Konda, (2007) concluded that if La Niña continued or if El Niño does not develop until autumn, an IOD event will not occur. In many models, the IOD tends to co-occur with El Niño (Baquero-Bernel et al, 2002; Yu and Lau, 2004). However, certain models show that the IOD is generated within the Indian Ocean region by stronger austral summer winds (Fischer et al, 2005). Results from certain modeling studies and observations conclude that IOD is a natural mode of the Indian Ocean coupled system, which can be triggered by ENSO or can self-generate (Schott et al, 2009). It is not clear what triggers IOD events but there are a few theories. The Westward propagating Rossby waves occur around the time of an IOD event. These waves in the eastern part of the Indian Ocean basin are triggered by the wind stress curl and are strengthened by the arrival of Kelvin waves (Vaid et al, 2006). The Sea Surface Height in the western equatorial Indian Ocean is influenced by the westward propagating Rossby waves and these signals are able to control the evolution of the surface characteristics during IOD events (Vaid et al, 2006). An interesting aspect of Rossby waves is that a rise in the sea surface of only a few centimeters results in the deepening of the thermocline by tens of metres (Mathieu Rouault, *pers comm*). The phase speeds of these waves increase towards lower latitudes and are of big interest due to their ability to transfer energy across ocean basins (Gnanaseelan et al, 2005). The atmospheric response to the anomalous SST is a basin wide anomalous Walker circulation (Yamagata et al, 2002; 2003). This anomaly reverses the direction of the equatorial winds, from westerlies to easterlies during the peak of the positive events (Rao et al, 2002). Additionally, seasonal southeasterly winds along the Sumatra coast are also strengthened during positive IOD events, inducing coastal upwelling and hence there is strong SST cooling in the east (Behera et al, 1999). Convection in the eastern Indian Ocean is suppressed during positive IOD events but is enhanced in the central and western Indian Ocean (Behera and Yamagata, 2003). The eastward propagation of the warm anomaly in the western Indian Ocean initiates the decay of the positive IOD event (Feng and Meyers, 2003). The climate in the vicinity of the Indian Ocean is affected by the IOD (Ashok et al, 2003; Clark et al, 2003; Behera et al, 2003). Countries to the west of the Indian Ocean have an anomalously high precipitation (Behera et al, 2003) whilst countries to the east of the Indian Ocean have an anomalously low precipitation (Ashok et al, 2003; Saji and Yamagata, 2003). Positive (negative) SSH anomalies associated with a positive (negative) IOD phase induces a shift in the intensity and position of the tropical and subtropical gyres

(Palastanga et al, 2006) in the Indian Ocean. A weakening (strengthening) of the intensity of the South Equatorial Current and its branches along east Madagascar occurs. Additionally, an intensification and northward (southward) extension of the subtropical (tropical) gyre occurs (Palastanga et al, 2006). Topographic features in the southwest Indian Ocean such as the Mascarene Plateau may have an influence on westward propagating Rossby waves by affecting the speed, strength or acting as a barrier to the flow. This influence may occur since the plateau is situated in a region where Rossby waves are frequent (Chelton and Schlax, 1996). A description of the Mascarene Plateau is presented in the next chapter.

1.1.9 Circulation Models in the Indian Ocean

1.1.9.1 INDOFOS (Indian Ocean Forecasting System)

INDOFOS is a GODAE OceanView system which incorporates 3 OGCM's (Oceanic General Circulation Models) which encompasses the majority of the Indian Ocean. The INDOFOS system uses atmospheric forcing data from the operational atmospheric prediction system from the National Centre for Medium Range Weather Forecast (NCMRWF) in New Delhi, India. The atmospheric forcing at NCMRWF consists of 1 day analysis fields and gives forecasts for 10 days. The INDOFOS system makes use of these analysis fields as well as the first 5 days of forecasting.

The Global Ocean Data Assimilation System (GODAS) which is used for producing ocean analyses fields is forced by the Global Forecast System (GFS) winds from the National Centre for Environmental Prediction (NCEP). This system assimilates temperature and salinity profiles from ARGO floats, Moored Buoys, XBT's as well as other in-situ observations. The system produces 5 day mean analysis of ocean fields. The HyCOM model setup for the Indian Ocean is forced with the (GFS) winds.

The 3 models used in the system are ROMS version 3.3, MOM 4p0d and HyCOM. There are 40 sigma levels for ROMS, 40 z levels for MOM and 28 Hybrid levels for HyCOM. The horizontal resolution is 1/8° for ROMS, 1/12° for HyCOM and 1/2° (zonal); 1/3° (meridional) for MOM. The domains for the ROMS, HyCOM and MOM models are (30 – 120° E; 30° S – 30° N), (30 - 130° E; 50° S - 30° N) and global respectively. (https://www.godae-oceanview.org/science/ocean-forecasting-systems/ocean-models/)

1.1.9.2 OGCM (OFES) Model

This OGCM is based on the Modular Ocean Model version 3 (MOM3) (Pacanowski and Griffies, 1999) and is developed at the National Oceanic and Atmospheric Administration (NOAA). It is optimized for

the Earth Simulator and is called the OGCM for the ES (OFES) (Sasaki et al, 2008). This is an Eddy-Resolving Model. This model uses the z-level coordinate in the vertical and solves 3 dimensional primitive equations in spherical coordinates under the Boussinesq and hydrostatic approximations. The domain covers the region from 75° S to 75° N but excludes the Arctic Ocean and has a horizontal grid spacing of 0.1°. There are 54 vertical levels and to represent the upper ocean circulation realistically, 20 levels cover the upper 200m. The 54^{th} level has a maximum depth of 6065m. The bathymetry uses the 1/30° bathymetry data set provided from the OCCAM project at the Southampton Oceanography Centre. The temporal resolution is 3 days. The model ocean is driven by the wind stresses and surface tracer fluxes (Masumoto et al, 2004) as the initial state. The daily mean values obtained from the NCEP reanalysis products (Kalnay et al, 1996) are used for wind stresses and atmospheric variables

CHAPTER 2: Introduction

2.1 Description of the Study Area

The Mascarene Plateau is a submerged volcanic plateau which extends over 2200 km between the Seychelles Bank (4° S, 56° E) and Mauritius (20° S, 57° E). This plateau is a complex feature which is oriented in a north-south direction and is shaped similar to a crescent (Figure 2.1) while it has an area of over 115000 km^2 (New et al, 2005). It is composed of a series of banks which are separated by deep channels. From north to south the banks are known as the Seychelles Bank, the Saya de Malha Bank, the Nazareth Bank and the Cargados-Carajos Bank (New et al, 2005). The depths of these banks range between 20-100m deep and are coral topped. However, in some regions of these banks the topography sometimes breaks the surface to form small islands such as the Seychelles archipelago with 120 islands while on either side of the plateau depths rapidly reach approximately 4000m (New et al, 2005). Between the Seychelles Bank and the Saya de Malha Bank, a 400 km ridge exists which is 1000 – 1500m deep (gap 1) (Smith and Sandwell, 1997). The deepest part of the Mascarene Plateau exists in the gap between the Saya de Malha Bank and Nazareth Bank (gap 2) which is 100 km wide and depths exceed 1000m. A very narrow gap exists between the Nazareth and Cargados-Carajos Banks (200m deep and 50km wide). The final gap is that between the Cargados-Caragos Bank and Mauritius (gap 3) where 2 channels (~ 2000m deep), each of which is approximately 50 km wide and separated by the Soudan Bank (New et al, 2007). The Mascarene Plateau affects the ocean circulation in the region which is a key aim of investigation in this study. The currents which interact with the Plateau are the South Equatorial Current (SEC) and the South Equatorial Counter Current (SECC). The interaction of the SEC with the Mascarene Plateau affects its flow downstream (Figure 2.2). Both of these currents contain water masses with different origins which will be investigated in this study. Since this area has not been extensively studied, further investigations/research will be beneficial to surrounding countries such as Mauritius and the Seychelles as these areas are dependent on their fishery resources.

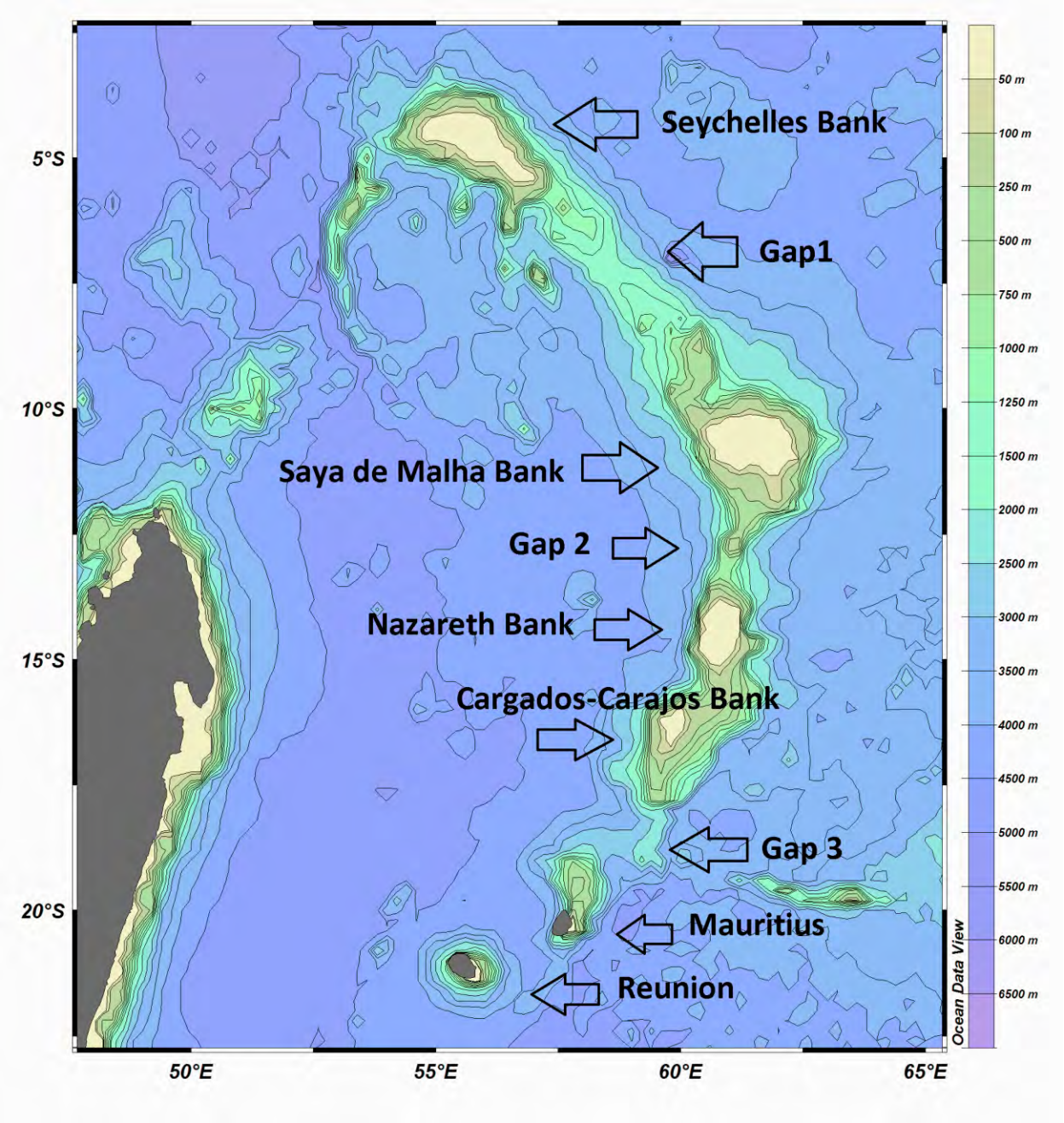

Figure 2. 1: The Mascarene Plateau with its associated Banks and gaps. The Plateau is crescent shaped and is composed of 4 shallow banks and 3 gaps separating these banks. It lies mainly in a meridional direction from the Seychelles to Mauritius. Some of the banks have regions where it breaches the surface to form small islands. The deepest gap is between the Saya de Malha and Nazareth Banks where depths exceed 1000m. Isobath interval: 500m

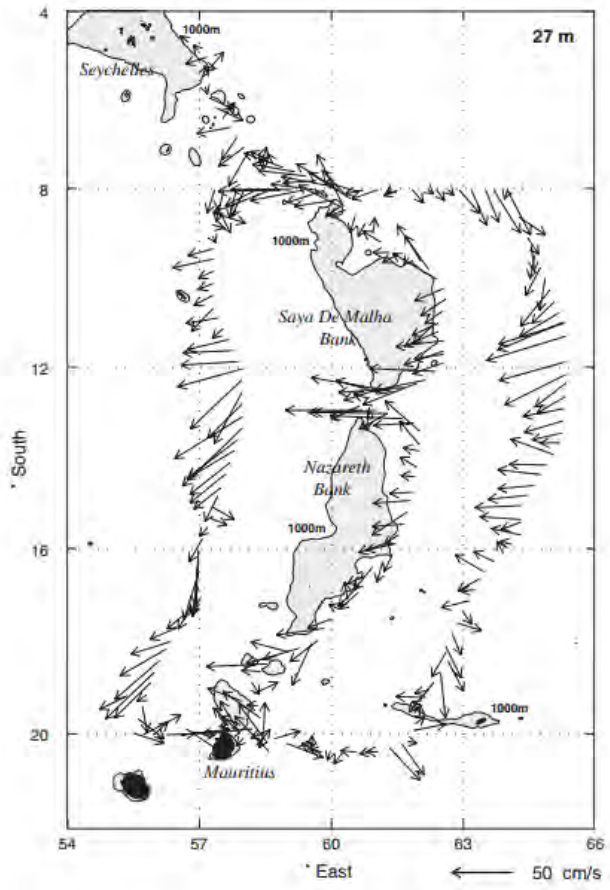

Figure 2. 2: Circulation around the Mascarene Plateau, LADCP obtained currents on board RRS Charles Darwin June/July 2002. Eastward flowing SECC (South Equatorial Counter Current) across Seychelles Bank whilst the region south of approximately 8° S is influenced by the westward flowing SEC (South Equatorial Current). Part of the circulation north of 8° S is influenced by a westward core of the SEC through gap 1. (after New et al, 2007)

2.2 Water Masses associated with the Mascarene Plateau

Since water masses conserve their properties for long periods of time, they can be used to trace the pathway of ocean currents (Emery, 2001). Water masses are classified according to certain properties such as temperature, salinity, oxygen etc (Figure 2.3). The following section will describe the water masses which are found in the Mascarene Plateau region.

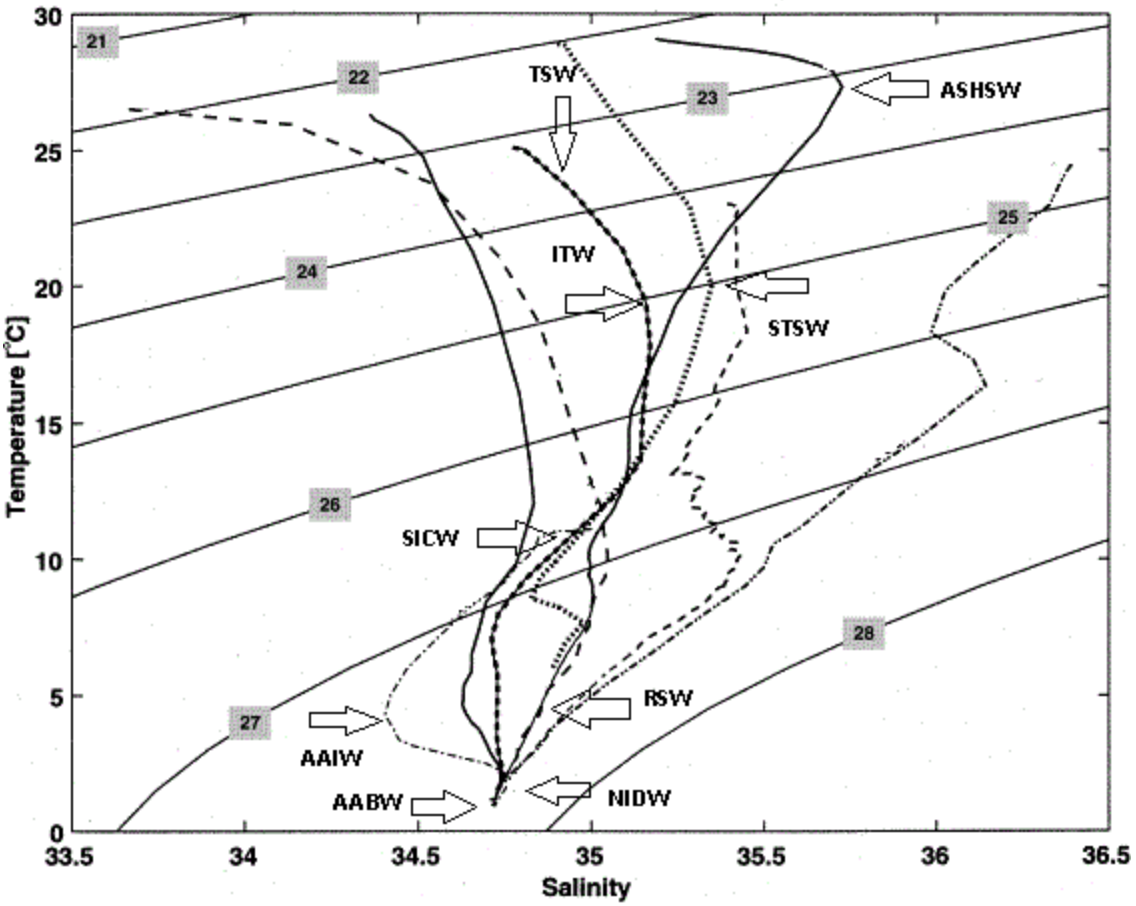

Figure 2. 3: Temperature-Salinity Diagram of Indian Ocean water masses (South-West Indian Ocean) from Levitus and Boyer (1994a,b). The core water masses indicated are NIDW (North Indian Deep Water), AAIW (Antarctic Intermediate Water), RSW (Red Sea Water), SICW (South Indian Central Water), ITW (Indonesian Throughflow Water), STSW (Subtropical surface water), TSW (Tropical Surface Water), ASHSW (Arabian Sea High Salinity Water) and AABW (Antarctic Bottom Water).

Tropical Surface Water (TSW) – TSW is a broad band of fresh water between 4° S and 20° S. Salinity is low (34.7 – 34.9) due to the high levels of precipitation in the tropics. TSW is transported via the westward flowing SEC which in turn transports water masses from the western Pacific Ocean (New et al, 2005). TSW has temperatures greater than 23° C, oxygen values > 4 ml/l and occupies a density range of between 22 kg/m^3 and 23.5 kg/m^3 (Gründlingh et al, 1991; Warren, 1981).

ASHSW (Arabian Sea High Salinity Water) - ASHSW is formed in the Northern Indian Ocean (Kumar and Prasad, 1999) in the Arabian Sea due to an excess of evaporation over precipitation. The salinity in this

source region can be in excess of 36.5. ASHSW is swept eastwards across the Indian Ocean by the South Equatorial Counter Current (SECC). The channel separating the Seychelles and Saya de Malha Banks on the Mascarene Plateau acts as a barrier between fresh TSW from saltier modified ASHSW to the north. ASHSW has temperatures greater than 24° C and salinity greater than 35.3. It forms a shallow salinity maximum (Kumar and Prasad, 1999; Emery, 2001). ASHSW has oxygen values greater than 4 ml/l and occupies the density range between 22.5 kg/m^3 and 24.5 kg/m^3 (Kumar and Prasad, 1999).

Subtropical Surface Water (STSW) – STSW can be found in the subtropical belt between 20°- 35° S. STSW displays characteristically high salinity values (> 35.3) due to the high levels of evaporation associated with the subtropics. Travelling northwards STSW subducts below the fresher TSW to form a subsurface salinity maximum, which at 18° S is centred at 300 m. This salinity maximum extends as far north as 14°S, and may be partly carried westward by the SEC. STSW occupies the temperature range 17 – 18° C, has a shallow oxygen minimum and occupies the density range between 24.5 kg/m^3 and 25.5 kg/m^3 (Gründlingh et al, 1991. Wyrtki, 1973).

Indonesian Throughflow Water (ITW)- Immediately below TSW between 100 - 300m. Song et al, (2004) identified Indonesian Throughflow Water (ITW). An important characteristic of the Indonesian Throughflow is its higher temperature and relatively low salinity (17° C - 23° C and 35.1 - 35.2 respectively) (Song et al, 2004; New et al, 2005) due to its source region (western equatorial Pacific Ocean) being high in precipitation. Consequently the Throughflow transports large amounts of relatively warm and fresh water to the Indian Ocean. When the Indonesian Throughflow through the Lombok Strait and the Timor passage enters the Indian Ocean it is advected towards Africa within the South Equatorial Current. ITW is slightly more saline than TSW and in the region of the Mascarene Plateau has been observed between 100 – 250m at 10° S. Carried within the core of the SEC, ITW has been shown to spread across the western boundary of the Indian Ocean, forming a subsurface oxygen minimum of between 2 – 3 ml/l and within the density range of between 24 kg/m^3 – 26 kg/m^3 (Song et al, 2004).

South Indian Central Water (SICW) – this water mass is formed between 35° and 45° S as a result of deep winter mixing (a variety of Sub-Antarctic Mode Water (SAMW) and subducted northwards in the subtropical gyre recirculation (McCartney, 1982)). SICW is characterized by a temperature range between 8°–15° C, a salinity range of 34.7 – 35.2, an oxygen maximum > 4.5 ml/l and within the density range 26.5 kg/m^3 – 27 kg/m^3 (Toole and Warren, 1993; Emery, 2001).

Antarctic Intermediate Water (AAIW) – AAIW is characterized by a salinity minimum between 800–1500m (33.8 – 34.6) and oxygen levels > 3.5 ml/l. AAIW originates in the Southeast Pacific (McCartney, 1982) and in the South Atlantic (Piola and Gordon, 1989) and appears to enter the South Indian Ocean in its southeastern region (Fine, 1993). AAIW occupies the temperature range of between 2° C – 10° C and the density range between (27.1 kg/m^3 – 27.5 kg/m^3) (Valentine et al, 1993; Gründlingh et al, 1991; Toole and Warren, 1993).

Red Sea Water (RSW) – Warm, saline RSW is formed in the Mediterranean basin of the Red Sea, spreads from the north through the strait of Bab el Manded into the Gulf of Aden where it is modified through mixing (Beal et al, 2000). RSW spreads southward through the Indian Ocean where its salinity content decreases. RSW occupies the temperature range 4° C - 9° C, salinity range >= 34.8, oxygen range of <= 2 ml/l and occupies the density range 27.0 kg/m^3 – 27.6 kg/m^3 (Beal et al, 2000).

North Indian Deep Water (NIDW) – NIDW is often referred to as Circumpolar Deep Water (CDW) It is characterized by a salinity maximum due to the infusion of North Atlantic Deep Water (NADW) which is carried eastward and northward (Stramma and Lutjeharms, 1997). The salinity maximum decreases northward to 10 - 20° S but then increases further to the north due to the southward movement of a deep saline water mass which underlies RSW (Mantyla and Reid, 1995). Very little is known about the spreading pathways of NIDW in the Indian Ocean. NIDW occupies the temperature range 2.5° C - 5° C, salinity range of between 34.8 – 34.9, oxygen values greater than 2.5 ml/l and occupies the density level of approximately 27.8 kg/m^3 (New et al, 2005; Toole and Warren, 1993).

Antarctic Bottom Water (AABW) – AABW spreads northwards in the Indian Ocean through 3 main routes. Namely under the Agulhas Current in the Western Indian Ocean, around the Kerguelen Plateau in the Central Indian Ocean and in a broad region (through the South Australasian Bight) between 50° E and 124° E in the Eastern Indian Ocean (van Sebille et al, 2013). South of Australia, it flows along the western slope of Australia and further north it enters the central Indian Ocean and propagates along the eastern slope of the Ninety-east Ridge (Tomczak and Godfrey, 1993). After crossing the eastern slope, it flows westwards to the northeast coast of Africa. Here it upwells to form North Indian Deep Water (NIDW). AABW in the region of the Mascarene Plateau is identified below NIDW by a decreasing salinity and increasing oxygen content (Read and Pollard., 1993). Table 2.1 presents a summary of the water masses characteristics in the region. AABW is not mentioned in the table as it was not identified during the 2008 ASCLME cruise.

Water Mass	Temperature Range (° C)	Salinity Range	Oxygen Range (ml/l)	Density range (kg/m^3)	References
TSW (Tropical Surface Water)	> 23	< 34.9	> 4	22 – 23.5	Gründlingh et al, 1991; Warren, 1981.
ASHSW (Arabian Sea High Salinity Water)	> 24	> 35.3. Shallow salinity maximum	> 4	22.5 – 24.5	Kumar and Prasad, 1999; Emery, 2001
ITW (Indonesian Throughflow Water)	17 – 23	35.1 – 35.2	2 – 3 (Subsurface Oxygen Minimum)	24 – 26	Song et al, 2004; New et al, 2005
STSW (Subtropical Surface Water)	17 – 18	Subsurface salinity maximum. > 35.3	Shallow oxygen minimum	24.5 – 25.5	Gründlingh et al, 1991; Wyrtki, 1973
SICW (South Indian Central Water	8 – 15	34.7 – 35.2	Oxygen Maximum (> 4.5 ml/l)	26.5 – 27.0 (linear relationship on T/S diagram)	Emery, 2001; Toole and Warren, 1993
RSW (Red Sea Water)	4 – 9	>= 34.8	<= 2	27.0 – 27.6	Roman and Lutjeharms, 2009; Beal et al, 2000; Gordon et al, 1987.
AAIW (Antarctic Intermediate Water)	2 – 10	Salinity minimum. 33.8 – 34.6	> 3.5	27.1 – 27.5	Valentine et al, 1993; Gründlingh et al, 1991; Toole and Warren, 1993.
NIDW (North Indian Deep Water)	2.5 – 5	34.8 – 34.9	> 2.5	~ 27.8	New et al, 2005; Toole and Warren, 1993

Table 2. 2: Water masses characteristics in the SW Indian Ocean based on temperature, salinity, oxygen and density.

2.3 Previous Studies in the Region

The Mascarene Plateau lies directly in the path of the South Equatorial Current. There has been limited research on the area to date. However, there have been several modeling studies in an attempt to investigate how the pathway of the SEC is influence by the shallow Mascarene Plateau. Woodberry et al, (1989) developed a 1.5 layer reduced gravity model with a resolution of 0.2°. The model depicted a SEC transport of approximately 24.3 Sv prior to the Mascarene Plateau at 63° E between 8° S and 23° S. The model showed that the SEC split into 2 cores, which crossed through gap 2 (10.9 Sv) and one branch, which flowed between the Cargados-Carajos Bank and Mauritius. However, the model does not represent a westward flow through gap 1 (Figure 2.4). Lee and Marotzke, (1998) used an ocean general circulation model (OGCM) with a resolution of 1.5°. This model proved ineffective as it did not represent any of the islands in the plateau and showed the SEC as a broad westward flow situated between 5° – 20° S. Garternicht and Schott, (1997) used an OGCM with a horizontal resolution of 0.4° which better resolved the islands in the Mascarene Plateau. The SEC had a greater degree of horizontal structure and variability. It passed over the plateau as a narrow current entirely between the Saya de Malha and Nazareth Banks. These 3 models yielded different results due to the complex bathymetry in the region and also the horizontal resolution.

The shoals of Capricorn program was conducted from 1998 – 2001. The aim of this program was to investigate the Mascarene Plateau and develop knowledge and skills for the management and protection of its resources. It was initiated so that the research was of value to the host nations. The program hosted over 200 scientists from 21 countries and together they investigated different aspects of the marine environment of the Seychelles, Mauritius and Rodrigues. A scientific result out of the program was that waters to the west of the plateau have a similar rich nutrient content as that of the north Atlantic. The reefs of the Seychelles suffered from dramatic coral bleaching in 1997/1998 but this program has revealed that there were signs of new coral recruitment. (Royal Geographical Society, n.d.)

A study by Weijer, (2008) identified the origin of the bi-monthly variability in the Mascarene basin to the west of this plateau, whilst Payet, (2005) studied the management, governance and socio-economics in the area, however it was concluded that management practices of marine resources over the plateau is not easy due to the lack of knowledge in the area.

Prior to the 2008 Agulhas Somali Current Large Marine Ecosystem (ASCLME) cruise, the only extensive research cruise conducted over the Mascarene Plateau was the June/July 2002 cruise on board the RRS Charles Darwin (however, this cruise did not sample the banks). The cruise was largely funded by the UK Natural Environment Research Council through the Southampton Oceanography Centre infrastructure funding, with additional support coming from the James Rennell Division core strategic programmes. It was also partly supported by the Royal Geographical Society – Royal Society Shoals of Capricorn programme, western Indian Ocean, 1998 – 2001. A prior research cruise (June/July 2002) was necessary in order to obtain a synoptic view of the circulation in the region as previous models contradicted each other and hence were not robust. The results from the June/July 2002 cruise revealed that the South Equatorial Current (SEC) split into 3 cores with a volume transport of 50 Sv to the east of the plateau. A major finding of this cruise, was that half of the volume of the SEC (25 Sv) was channeled through gap 2, whilst the remainder of the SEC flowed in equal volumes of 12.5 Sv north of the Saya de Malha Bank and south of the Cargados-Carajos Bank. The variability in the volume of flow associated with the SEC through each gap is unknown but a possible trigger for variability could be the change in the position of the SEC to the east of the plateau. The June/July 2002 cruise identified the distribution of water masses in the region and the degree of mixing which occurred. Once again, the amount of water mass mixing may vary throughout the year due to changes in the circulation patterns. There has been a limited amount of remote sensing being utilized in the area and by using it, much variability can be ascertained since it is able to map seasonal changes in ocean topography, currents etc. It is unknown whether the monsoon seasons have an effect on the variability on the Mascarene Plateau with particular reference to the circulation. However, the effect of monsoons is not a topic of discussion in this study.

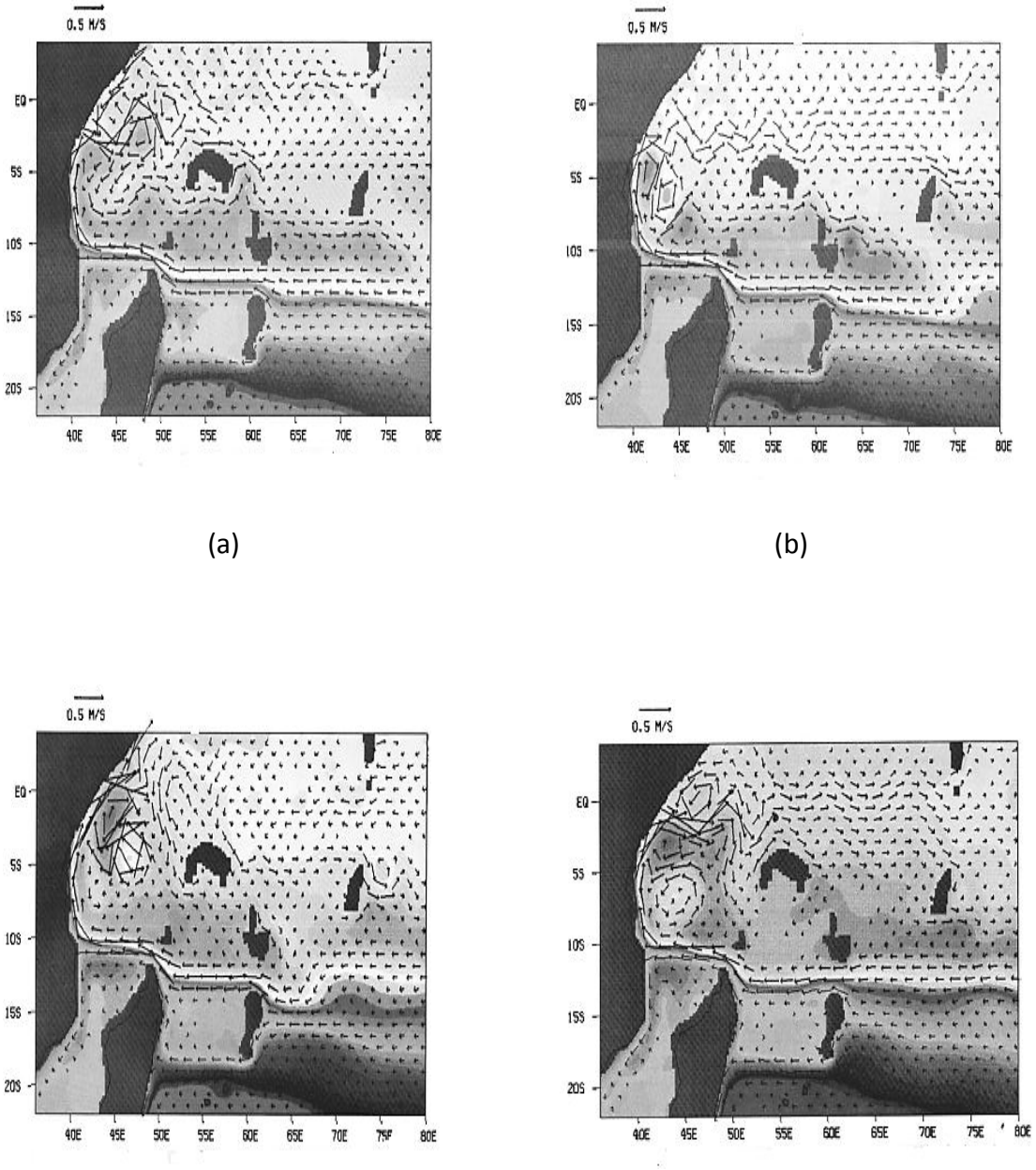

(a) (b)

(c) (d)

Figure 2. 4: Southwestern area of the 1.5 layer reduced gravity model developed by (Woodberry et al, 1989) (from the 10th year of integration). Arrows depict geostrophic velocities. Velocities can be observed through the gaps between the Saya de Malha bank and Nazareth Bank and between the Cargados-Carajos Bank and Mauritius. (a) – January (b) – April (c) July (d) – October

2.4 Key Questions

There have only been a couple of modeling studies (WoodBerry et al, 1989; Lee and Marotzke, 1998; Garternicht and Schott, 1997) in the region of the Mascarene Plateau as highlighted in the previous section. However, these studies did not provide an accurate representation of the circulation in the region, reconfirming the need for a synoptic research cruise to be conducted between June/July 2002. However, the region still lacks understanding and this study will hopefully deepen our knowledge of the area by addressing 8 key questions. In addition to using cruise data obtained via the October/November 2008 cruise on board the Dr Fridtjof Nansen, satellite data will also be utilized.

In Chapter 4

1. *Which water masses are present in the region of the Mascarene Plateau, where are their origins, where do they mix in the region and does the westward flow of the South Equatorial Current (SEC) influence the mixing? (Chapter 4)*

In Chapter 5

2. *How accurate is satellite data in the region and hence what is its viability for use in the region? (Chapter 5)*

In Chapter 6

3. *In what way is the flow of the SEC affected by the gaps in the Mascarene Plateau during the 2008 ASCLME cruise and are there differences to the cruise conducted during the June/July 2002 onboard the RRS Charles Darwin? (Chapter 6)*

In Chapter 7

4. *What seasonal effect does the Mascarene Plateau have on the geostrophic velocities, SST's and eddy kinetic energy in the region? (Chapter 7)*
5. *What is the nature of the SEC in the region and how do the geostrophic velocities during the 2008 cruise year differ from climatology? (Chapter 7)*

In Chapter 8

6. *What is the distribution of Chl-a in the region (climatology) and do the banks differ in Chl-a concentration from its surrounding areas? (Chapter 8)*

In Chapter 9

7. *Were there westward propagating Rossby waves over the Mascarene Plateau during the June/July 2002 cruise on board the RRS Charles Darwin and the October/November 2008 cruise on board the the Dr Fridtjof Nansen? Are these waves capable of crossing every part of the plateau? What effect do these waves have on the general circulation in the region? (Chapter 9)*

In Chapter 10

8. *Is an OGCM (OFES) model viable in the region for further modeling studies? (Chapter 10)*

The data and methodology is presented in the next chapter used to answer these questions.

CHAPTER 3: Data and Methodology

3.1 Agulhas and Somali Current Large Marine Ecosystem Project (ASCLME) 2008 cruise

The key aim of the ASCLME project was to develop a series of coordinated oceanographic research cruises to gather information on the oceanography of the western Indian Ocean and its influence on the biodiversity and economies of the Western Indian Ocean. Although the ASCLME project focused on the Agulhas and Somali Current ecosystems, it was decided that a survey of the Mascarene Plateau was to be conducted to study the nature of the South Equatorial Current (SEC) which is upstream of both the Agulhas and Somali currents. In this study, much of the data obtained from this cruise is used to ascertain further knowledge of the region of the Mascarene Plateau that until 2008 had remained under-sampled.

3.2 Hydrographic Data

3.2.1 CTD measurements

Physical properties of the water column were measured to a maximum depth of 3000m. A Seabird 911 plus CTD plus was used to obtain vertical profiles of temperature, salinity, pressure and oxygen. Real time plotting and hydrographic logging was carried out using the Seabird Seasave software. The profiles along the Mascarene Plateau and surrounding shelf and slope regions were usually obtained to a few metres above the bottom.

The hydrographic component of the cruise comprised of 176 CTD casts which were made across the Mascarene Plateau. For purposes of this study, only 42 CTD stations are used for analysis since many of the CTD casts were made over the banks for biological oceanography research. Commencing in Mauritius and ending in the Seychelles, the survey crossed over the Mascarene Plateau, including gap 3, the Nazareth Bank, gap 2, the Saya De Malha Bank, gap 1 and finally the Seychelles Bank. Intensive sampling was undertaken in the region around gap 2 as previous studies (New et al, 2007) determined that half (25 Sv) the SEC flows through this channel and intensive mixing occurs in this region between water masses of origins lying in the Northern Indian Ocean and Southern Indian Ocean. This is an important region for biological oceanography studies since this main branch of the current divides the

area into nutrient rich areas to the north and nutrient poor areas to the south. Figure 3.1 depicts the cruise tracks and stations for the 2002 and 2008 research cruises on board the Dr Fridtjof Nansen and R.R.S. Charles Darwin respectively.

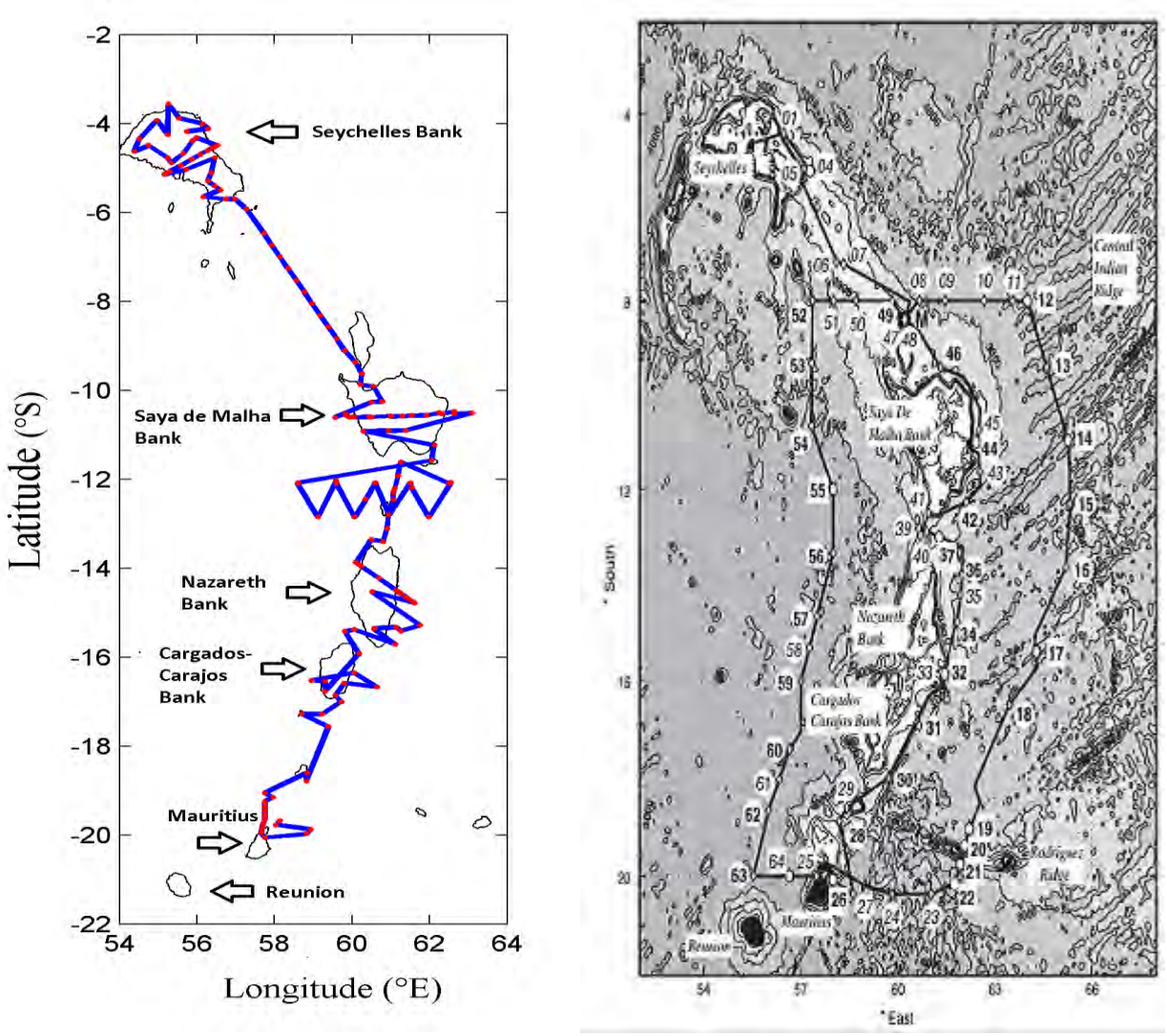

Figure 3.1: (a) Overview of Mascarene Plateau with Banks and cruise track (on board the Dr. Fridtjof Nansen – cruise EAF-N2008/7 in 2008) commencing in Mauritius and ending in the Seychelles. Red dots indicate CTD stations, blue line indicates the cruise track with the 120m isobath overlaid in black and (b) Overview of Mascarene Plateau with Banks and cruise track (on board the R.R.S. Charles Darwin – cruise 141 in 2002). Numbers indicate CTD/LADCP stations (after New et al, (2007)).

3.2.2 ADCP measurements

The currents along the track were measured by using vessel mounted Acoustic Doppler Current Profiler, (VMADCP), Ocean Surveyor from Teledyne RD Instruments. The unit mounted on R/V Dr. F. Nansen consists of a single transducer using electronic beam forming to produce four beams required to measure current velocity. The units operates at frequency is 150 kHz and is triggered synchronously with the onboard EK60 echo sounder. The navigation data are provided by the Seapath Differential Global Positioning System (DGPS). The instrument was run continuously in broadband mode shallower than about 150 meters and in narrow band mode in deeper waters. The practical range of detected currents varied between 200-400 meters, depending on the density of scattering layers in the water column. The ping data were averaged into 4 and 8 m vertical bins for the shallow and deep water data, respectively. Spurious data (near bottom, wire interference, etc) were edited using custom designed, prototype software (Marek Ostrowski, *pers comm*). The currents were estimated over 5 nautical mile horizontal bins using ping-based data. Only the regions where the vessel speed was more than 6 knots were included in the computations. The raw data, computed currents and quality flags from data editing were stored using the hierarchical data format (HDF5, see www.hdfgroup.org).

3.3 Argo Profiling Float Data

In areas of the world's oceans where there is a deficiency of cruise data, Argo float data is particularly useful since they obtain vertical profiles of temperature and salinity, hence water mass properties, geostrophic velocities and fluxes can be assessed. A series of Argo floats were used for the period 2004 – 2010 where temperature and salinity properties were analyzed to 2000m to identify water mass origins. Once water masses are identified from cruise data, they can be backtracked to their origins via Argo floats since they give a synoptic view of the ocean. Since water masses generally move along isopycnals, argo floats across the ocean at a specified isopycnal (determined by what isopycnal the water mass lies in the region of the Mascarene Plateau) are identified and the origin of the water mass can be determined (as well as salinity and temperature changes as it moves through the ocean) (Global Ocean Data Assimilation Experiment (GODAE). 2010. Argo Float Data [Dataset]. Available: http://www.usgodae.org/argo/argo.html.)

3.4 Remote Sensing

3.4.1 Altimetry measurements

Satellite altimetry is an important component of the ocean observing system and was used to compare geostrophic currents to shipboard ADCP data. The Centre for Topographic studies of the Oceans and Hydrosphere (CTOH) database was used to obtain geostrophic velocities at a resolution of ¼° x ¼°. CTOH is a French national observational service for satellite altimetry studies. CTOH maintains online full databases for each mission (TOPEX-Poseidon, Jason-1, ENVISAT and GFO). Weekly merged products are distributed by different operational centres and include algorithms for areas near the equator. The Ssalto/Duacs Gridded Absolute Geostrophic Velocities (1/3° X 1/3°) is incorporated into this product. (Center for Topographic Studies of the Ocean and Hydrosphere (CTOH). 2011. Absolute Geostrophic Velocities [Dataset]. Available: http://ctoh.legos.obs-mip.fr/.) The data downloaded from the internet was processed using Matlab and further analysis was done via Matlab such as the creation of maps, graphs etc.

3.4.2 Ocean Colour Remote Sensing (Chlorophyll-a) measurements

The dataset from the Globcolour Hermes database was used to obtain Chl-data. As early as 1978, the launch of the Coastal Zone Colour Scanner allowed estimation of Chlorophyll-a (Chl-a) using measurements of ocean colour. Chl-a has been used to assess phytoplankton biomass, primary production and the ocean's impact on the climate cycle (Longhurst et al, 1995; Behrenfeld et al, 2006). The estimation of Chl-a by remote sensing relies on the premise that phytoplankton shifts the reflected colour spectrum from predominantly blue to green (Gordon and Morel, 1983). The calculation of Chl-a by satellite involves an empirical relationship developed from field observations of Chl-a and ocean colour collected throughout the global ocean (Zaneveld, 1973). Empirical algorithms have built in assumptions that follow the basic concept of biological oceanography that oligotrophic regions have a low phytoplankton biomass, wheras more productive regions contain larger concentrations of phytoplankton. With the world's ocean changing, phytoplankton composition may change which may create uncertainty (where uncertainties already exist) in empirical approaches (Dierssen, 2010).

(Globcolour Hermes. 2014. Ocean colour [Dataset]. Available: http://hermes.acri.fr/GlobColour/index.php)

3.4.3 Sea Surface Temperature (SST) measurements

The Tropical Rainfall Measuring Mission (TRMM) Microwave imager (TMI) is a passive microwave radiometer primarily designed to measure rain rates over a wide swath under the TRMM satellite that is also used to estimate SST. TRMM was launched on November 27, 1997 and data is available until today. TRMM is a joint program between NASA and the National Space Development Agency of Japan (NASDA). The TMI can estimate SST, rain rates, ocean surface wind speed and cloud liquid water. Data was downloaded and analysed using MATLAB. (Remote Sensing Systems. 2011. Sea Surface Temperature [Dataset]. Available: http://www.remss.com/missions/tmi)

3.5 Wind Stress Curl

In order to calculate the wind stress curl, the wind stress (Zonal and Meridional) needs to be calculated first. The wind speed at 10 metres above sea level was obtained from the Quikscat database. Satellite-based sensors are capable of systematically providing measurements over the entire globe. Sensors operating at microwave frequencies can make measurements of the ocean surface day and night and under nearly all-weather conditions. Both active (radar) and passive (radiometer) microwave sensors have been shown capable of retrieving the ocean surface wind speed, with active microwave instruments being used to also retrieve the wind direction. The wind stress was calculated via the following equations:

$\tau_x = Cd\rho U^2$

Where τ_x = Wind stress (Zonal Direction) (N/m^2)

Cd = dimensionless drag coefficient (typically 0.0013)

ρ = air density (1.2 kg/m^3)

U = Zonal wind speed at 10 metres above sea level (m/s)

$\tau_y = Cd\rho V^2$

Where τ_y = Wind stress (Meridional Direction) (N/m^2)

Cd = dimensionless drag coefficient (typically 0.0013)

ρ = air density (1.2 kg/m^3)

V = Meridional wind speed at 10 metres above sea level (m/s)

The Wind Stress Curl was obtained via the following calculation:

Wind Stress Curl = $\partial\tau_y/\partial x - \partial\tau_x/\partial y$ (N/m^3)

3.6 Eddy Kinetic Energy

Most of the kinetic energy of ocean circulation is contained in ubiquitous mesoscale eddies. Their prominent signatures in sea surface height have rendered satellite altimetry highly effective in observing global ocean eddies. Our knowledge of ocean eddy dynamics has grown since the advent of satellite altimetry in the early 1980s (Fu et al, 2010).

Mesoscale phenomena studies using satellite altimetry allows us a global observation of eddy variability. Eddy Kinetic Energy (EKE) is calculated using the CTOH data described above and applying the following formula:

$EKE = \frac{1}{2}(U^2 + V^2)$

Where U and V are the zonal and meridional geostrophic currents respectively

EKE is the Eddy Kinetic Energy (cm^2/s^2)

3.7 OGCM (OFES) Model

The OFES model was used to compare observations and satellite estimate (SST, geostrophic velocity and Mean Eddy Kinetic Energy) with model output and evaluate the model in the region. Model output was acquired during a trip to Japan at JAMSTEC as part of the ACCESS collaborative project between South Africa and Japan.

3.8 Interannual Variability

To study the interannual variability around the Mascarene Plateau, weekly normalized anomalies are used which is a time series of anomalies from climatology divided by the standard deviation of that week. For instance the Mean Absolute Dynamic Topography (MADT) normalized anomaly is calculated using the following equation:

$MADT_{anonorm}$ = (MADT - $MADT_{average}$) / standard deviation (MADT)

MADT was obtained via the Aviso website (http://www.aviso.altimetry.fr/en/data/data-access/aviso-cnes-data-center.html) and processed into a usable format in Matlab for further analyzing. Time – Longitude plots (Hovmöller Diagrams) are also created in order to observe Rossby Wave propagation across the Indian Ocean. Through these plots, this study will identify the interaction between the Mascarene Plateau and the Rossby Waves. In the analysis of the interaction of the Rossby Waves with the Mascarene Plateau, 6 latitudes are used. The 6 latitudes are the Seychelles Bank (4° - 6° S), gap 1 (7° – 9° S) , the Saya de Malha Bank (10° – 11.5° S), gap 2 (12° – 13.8° S), Nazareth/Cargados-Carajos bank (14° – 16° S) and gap 3 (18° - 18.8° S).

There is a high degree of confidence in the data obtained, either cruise data, satellite estimate or modeling data to answer the key questions proposed above. There is enough data available to address each key question proposed.

RESULTS

CHAPTER 4: The Water Mass Characteristics over the region of the Mascarene Plateau

This chapter consists of the results obtained during the Nansen survey of the Mascarene Plateau conducted between October/November 2008. The objective of this chapter is to define the distribution of water masses in the region and to understand the effect the westward flowing South Equatorial Current (SEC) and eastward flowing South Equatorial Countercurrent (SECC) has on these water masses.

4.1 Analysis of water masses over the Mascarene Plateau

Key Question 1. Which water masses are present in the region of the Mascarene Plateau, where are their origins, where do they mix in the region and does the westward flow of the South Equatorial Current (SEC) influence the mixing?

The Mascarene Plateau affects both the water mass characteristics and circulation patterns in the Southwest Indian Ocean. The Mascarene Plateau creates a splitting of the SEC into 3 branches to the east (New et al, 2007). The following section presents an in depth analysis of the influence the Mascarene Plateau has in the region using 2 datasets (cruise data and Argo data). First a general description of the water masses observed during the October/November 2008 cruise of the Mascarene Plateau is given below.

4.1.1 Water Masses of the Mascarene Plateau - October 2008

New et al, (2007) carried out a detailed study of the water masses in the region of the Mascarene Plateau. From their study, it can be seen that there are prominent differences between the northern and southern regions of the plateau. The northern part of the plateau contained nutrient rich waters (up to 0.6 μg/l) whilst the southern part contained nutrient poor waters (as low as 0.07 μg/l) with the SEC acting as a major barrier. In contrast, there is relatively little difference between water masses characteristics such as oxygen, temperature and salinity found to the east and west of the plateau. Data collected during the 2008 Mascarene survey support past investigations and physical-chemical profiles

give further evidence that the South Equatorial Current (SEC) acts as a barrier between the northern and southern regions of the plateau. Whilst the SEC dominates the general circulation in the vicinity of the Mascarene Plateau, highly saline surface waters over the Seychelles Bank bear resemblance to Arabian Sea High Salinity Water (ASHSW) and suggest the influence of the eastward flowing South Equatorial Counter Current (SECC) on local water masses (Figure 2.2). Furthermore, results collected during this survey provide evidence that the SEC acts as a major conduit for the transport of Indonesian Throughflow Water across the Indian Ocean, originating in the western Pacific Ocean and the Indonesian archipelago, towards the Mascarene Plateau where it is channeled through its various gaps (Figure 2.2). A detailed examination of the water masses identified in the 2008 ASCLME cruise in the region, using the criteria determined in the introduction is given in this section. For ease, the region has been divided into ocean provinces and the water masses associated with these regions are discussed. Cross sections of temperature, salinity and oxygen across the Mascarene Plateau during the October/November 2008 cruise are given in Figure 4.1.

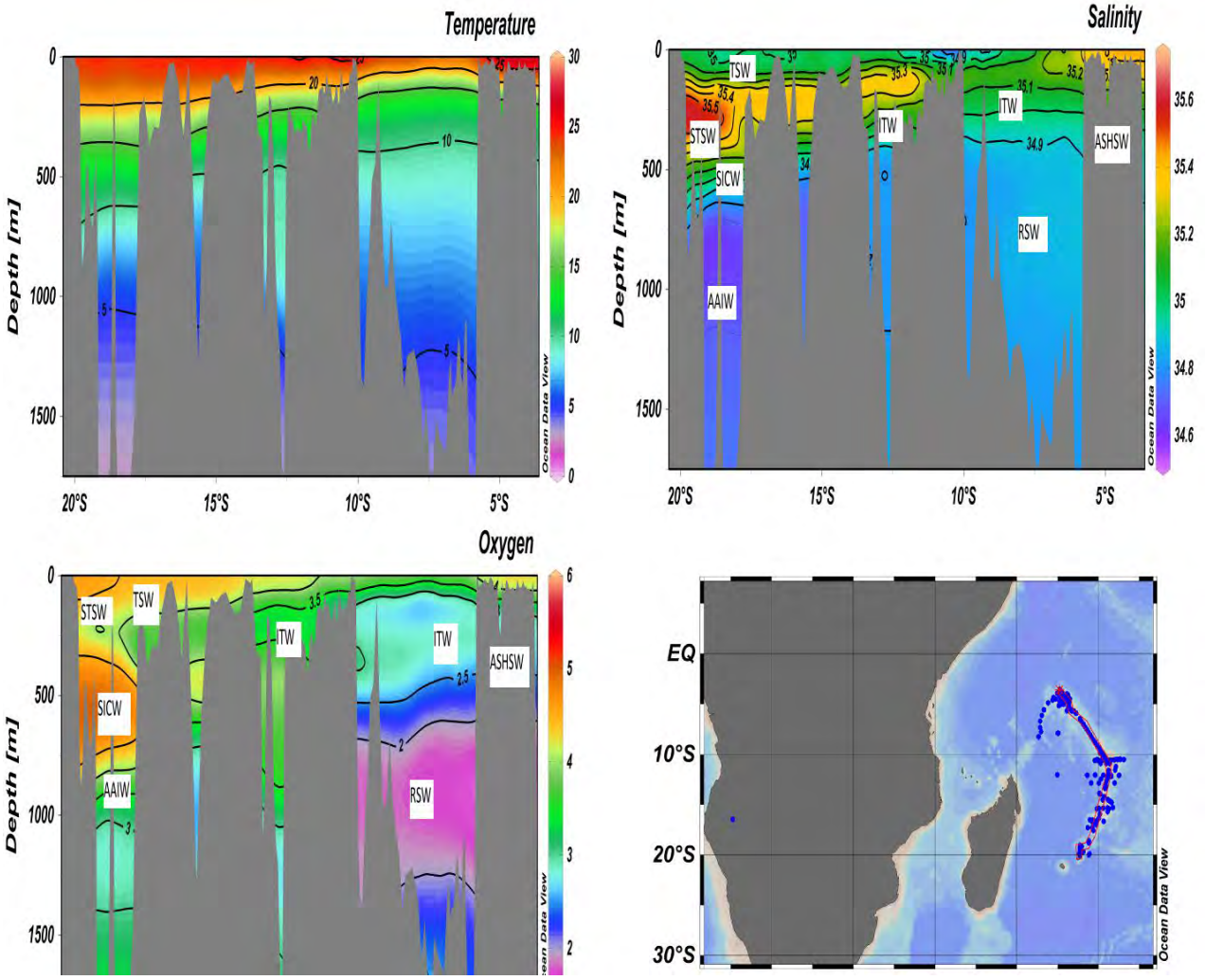

Figure 4. 1: Cross sections across the Mascarene Plateau. In a clockwise direction: Temperature (°C) section, Salinity section , cross section across Mascarene Plateau depicted by red line and Oxygen (ml/l) section. Core water masses are identified, ASHSW (Arabian Sea High Salinity Water), STSW (Sub-tropical surface water), TSW (Tropical Surface Water), ITW (Indonesian Throughflow Water), RSW (Red Sea Water), AAIW (Antarctic Intermediate Water) and SICW (South Indian Central Water).

In the characterization of the water masses in the region, 3 sub-regions are defined in order to determine where the origins of water masses of both Northern and Southern Indian Ocean primarily lie and where the majority of mixing between these water masses occurs in relation to the Mascarene Plateau (Figure 4.2). The first region is defined as the northern sector of the Seychelles Bank, where

predominantly ASHSW surface waters occur (salinity > 35.3, temperature > 24 °C and oxygen > 4 ml/l) to where TSW (Tropical Surface Water) is predominant (salinity < 34.9, temperature > 23 °C and oxygen > 4 ml/l) which is roughly the same latitude as gap 1 (8° S). The second region is characterized by the intrusion of RSW (Red Sea Water), which lies at the same density layer as AAIW (Antarctic Intermediate Water) (Beal et al, 2000; Toole and Warren, 1993). This region extends southwards from 8° S to the approximate latitude of gap 2 (13° S). The 3rd sub-region extends south of this gap and is determined by the lack of RSW and where AAIW is the dominant water mass within the intermediate layers.

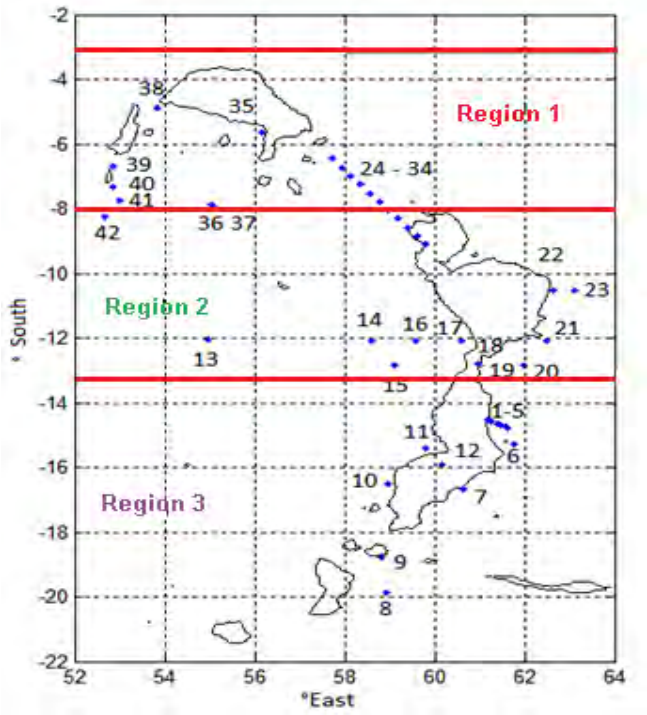

Figure 4. 2: CTD Stations depicted for water mass analysis. Blue dots indicate CTD stations with their respective numbers with the 1000m isobath overlaid in black. Region 1 is defined as where the surface waters are predominantly ASHSW, region 2 is defined by an intrusion of RSW and mixes with AAIW whilst region 3 is defined as where RSW is completely absent.

Surface waters differ between the first region (north of 8° S) and the other two regions due to the influence of the South Equatorial Counter Current (SECC). The SECC flows eastwards across the Seychelles Bank sweeping high salinity Arabian Sea High Salinity Water (ASHSW) across it whilst the other two regions are influenced by the westward flowing South Equatorial Current (SEC) which carries fresh tropical surface

water (TSW) (Figure 2.2). Figure 4.3 depicts all 42 CTD stations analyzed across the Mascarene Plateau. The red scatter plot indicates all the stations north of 8° S, whilst the blue scatters indicates stations south of 8° S.

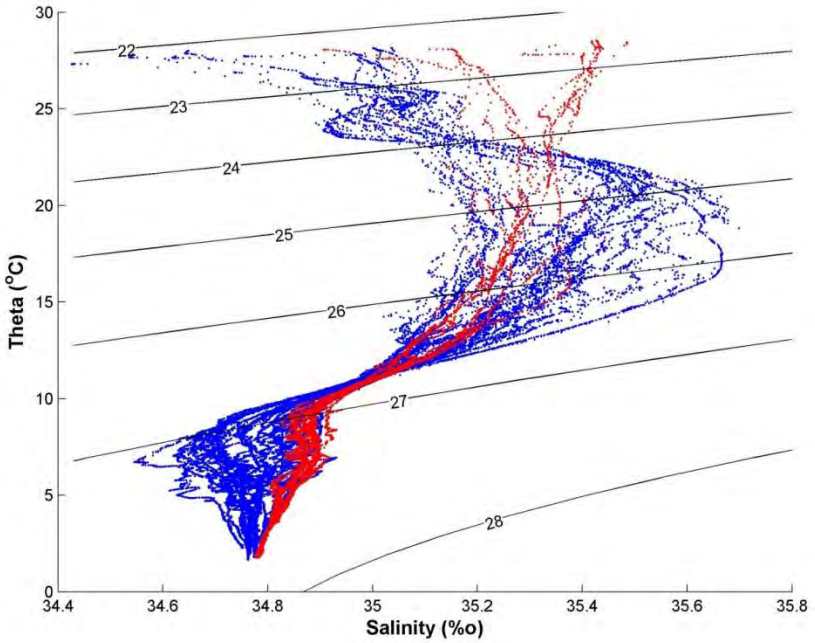

Figure 4. 3: Temperature-Salinity diagram for selected stations across the Mascarene Plateau. Red scatter plot indicates stations north of 8° S, whilst the blue scatter plot indicates stations south of 8° S. There are 13 stations north of 8° S whilst there are 29 stations south of 8° S.

4.1.1.1 Sub-Region 1 (region spanning from the northern sector of the Seychelles Bank to 8° S)

The following section will give results on sub-region 1 which is defined as the region spanning from the northern sector of the Seychelles Bank where predominantly ASHSW surface waters occur to where TSW (Tropical Surface Water) is predominant (8° S). Surface waters differ between the first region (north of 8° S) and the other two regions due to the influence of the SECC. The SECC flows eastwards across the Seychelles Bank sweeping high salinity ASHSW across it whilst the other two regions are influenced by the westward flowing SEC which carries fresh tropical surface water.

Many stations north of 8° S show the presence of NIDW. However, rugged bathymetry (New et al, 2005) in gap 1 prevents NIDW's presence in the gap. All the stations north of 8° S exhibit RSW without any influence

from AAIW. The salinity in the intermediate waters of all these stations do not decrease below 34.8, indicative of RSW (Beal et al, 2000). ITW exists in the stations where one of the branches of the SEC flows in gap 1. Away from the SEC in this region, ITW is not present. Surface waters vary in this region, however ASHSW is predominant. Areas which are close to the branch of the SEC signify mixing with ITW as the salinity decreases below 35.3. Figure 4.4 depicts a T-S diagram and a T-O diagram for 3 stations in the sub-region for water mass analyses.

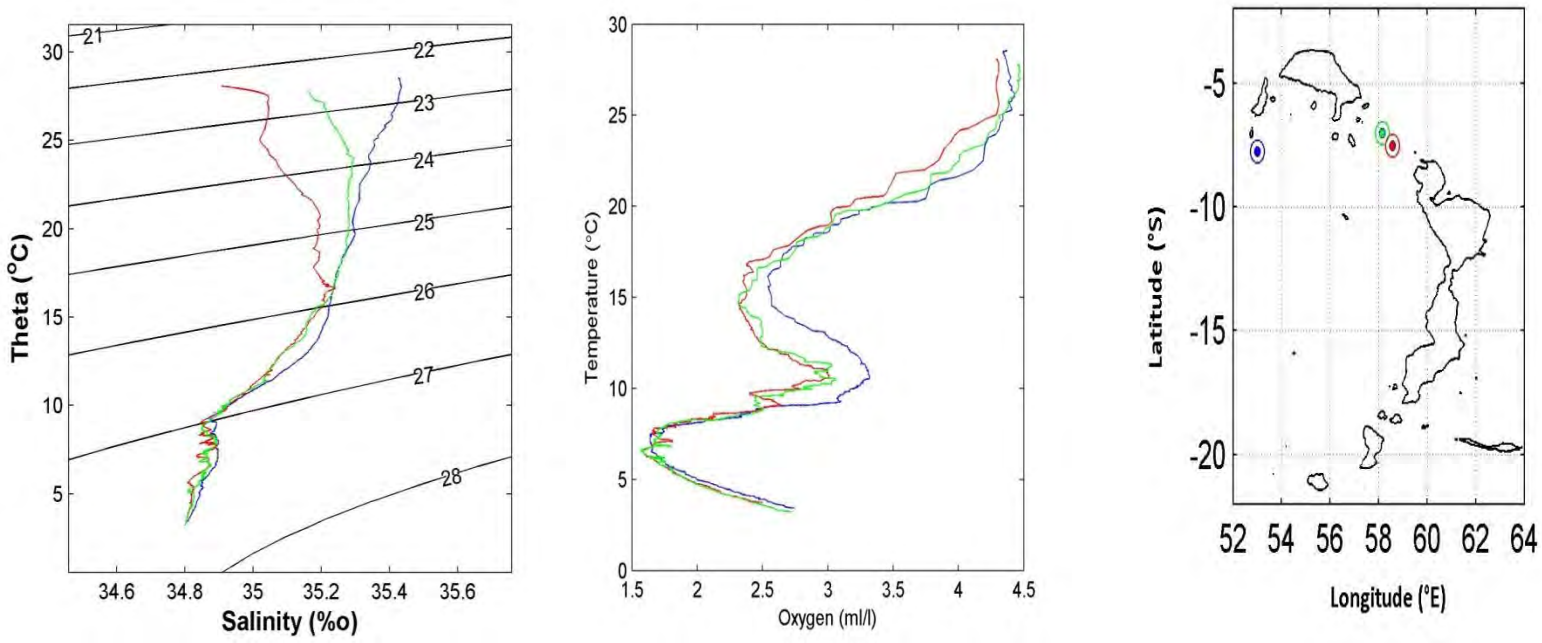

(a) (b) (c)

Figure 4. 4: Temperature-Salinity Diagram (a), Temperature-Oxygen Diagram (b) for Selected Stations north of 8° S and position of stations (c). Stations representing blue indicates station 41 (7.74° S, 53° E), Green indicates station 26 (7° S, 58.14° E) and red indicates station 27 (7.53° S, 58.56° E). These stations are chosen to show that near a branch of the SEC there is mixing between low and high salinity waters whilst the other stations signify no mixing between high salinity waters (away from the branch of the SEC) and low salinity waters (within the core of the SEC)

Three stations are picked to indicate the effect the South Equatorial Current has on the region (station numbers are depicted in Figure 4.2). Station 41 represents a station where there is no influence of the SEC and hence contains water masses typical of Northern Indian Ocean Origin. Station 27 is chosen as it lies within the SEC and shows how the current influences the water properties in the region. Station 26 is chosen as it lies in a region at the edge of the SEC and hence depicts mixing of surface water masses.

Station 41 (7.74° S, 53° E) represents a station with water masses typical of Northern Indian Ocean origin, ie. RSW and ASHSW, since there is no influence from the SEC which carries water mass properties from the Western Pacific Ocean and the Indonesian archipelago as it does not flow across this station. ASHSW is present with temperatures of approximately between 24° C and 28° C, salinity of approximately between 35.3 and 35.45 and oxygen values between 4.3 ml/l and 4.5 ml/l. RSW exists with temperature ranges between 4° C and 7° C, salinity values > 34.82 and oxygen values between 1.6 ml/l and 2 ml/l.

Station 27 (7.53° S, 58.56° E) shows no mixing in the deep and intermediate waters with NIDW having temperatures and a salinity of approximately 3° C and 34.8 respectively. RSW is present in the intermediate waters with temperature and salinity ranges of approximately between 5° C and 8° C and > 34.82 respectively. Oxygen values are similar to that of station 41 in the deep and intermediate waters. The surface waters of this station are clearly influenced by the westward flowing SEC as ITW exists with temperature ranges between 17° C and 20° C, a salinity of approximately 35.2 and an oxygen value of 2.5 ml/l. Above ITW, TSW is present as opposed to ASHSW typical of the region.

Station 26 (7° S, 58.14° E) presents properties similar to the other two stations in the deep and intermediate waters. However, above this, towards the surface waters, mixing occurs between ASHSW, TSW and ITW as temperature, salinity and oxygen values lie between these water mass ranges. The deep and intermediate waters (NIDW and RSW) remain unchanged in this region (similar to that of the Northern Indian Ocean) irrespective of the positioning of the SEC. It appears that the Mascarene Plateau also has no effect on these water masses. However, surface waters in this region vary although ASHSW is the predominant water mass. The region experiences the intrusion of TSW and ITW due to the westward flowing SEC through gap 1 which dilutes the high salinity ASHSW. In the region surrounding the current, there is a mixture of the water masses whilst in the core of the SEC, ASHSW is absent.

4.1.1.2 Sub-Region 2 (region spanning from approximately 8° S – 13° S)

The following section will give the results of sub-region 2, which is defined as the region characterized by the intrusion of RSW which is at the same level as AAIW (Antarctic Intermediate Water). This region extends southwards from 8° S to the approximate latitude of gap 2 (13° S). This region is characterized by mixing between RSW and AAIW in the intermediate waters and mixing between STSW and ITW in the surface waters. The circulation is dominated by the northern core of the SEC which flows through gap 2. Figure 4.5 depicts all the CTD stations within sub-region 2. Certain stations in the region contain water masses in the intermediate layers purely of RSW as salinity values are > 34.8 (Beal et al, 2000), other stations contain water masses in the intermediate layers purely of AAIW as salinity values are between 33.8 – 34.6 (Toole and Warren, 1993) whilst other stations exhibit mixing between the 2 water masses as salinity values lie between that of AAIW and RSW. Figure 4.6 depicts a T-S diagram and a T-O diagram for 3 stations in the sub-region for water mass analyses.

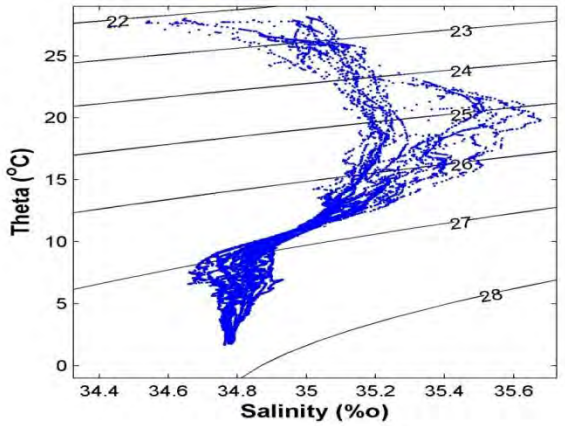

Figure 4. 5: Temperature-Salinity diagram for stations across the Mascarene Plateau between 8° S and 13° S. (15 stations)

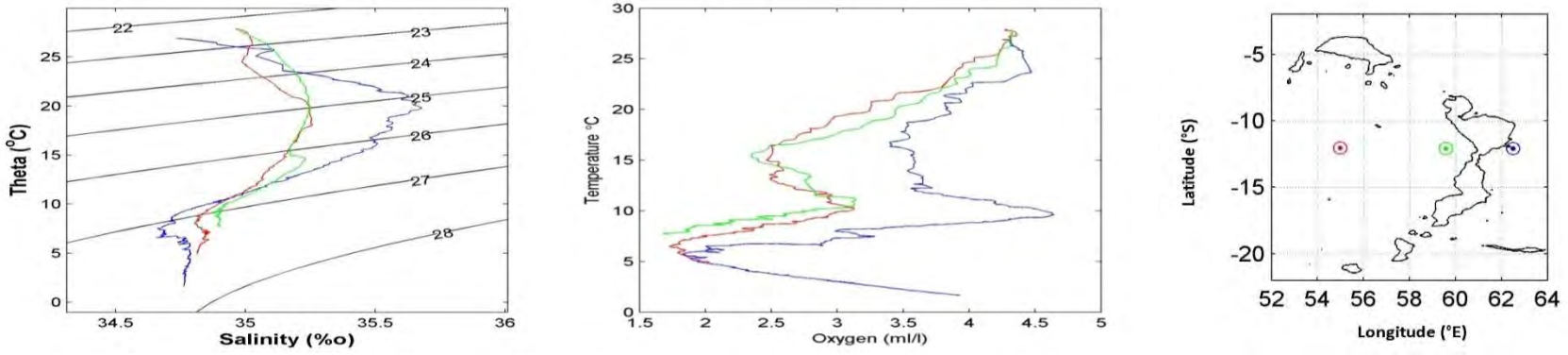

(a) (b) (c)

Figure 4. 6: Temperature-Salinity Diagram (a), Temperature-Oxygen diagram (b) for Selected Stations between 8° S and 13° S and position of stations (c). Blue indicates station 21 (12.09° S, 62.5° E), Green indicates station 16 (12.08° S, 59.6° E) and red indicates station 13 (12.04° S, 54.98° E)

Station 21 exhibits water mass properties typical of the Southern Indian Ocean (ie. AAIW, SICW and STSW), station 16 exhibits intermediate water mass properties that of the Northern Indian Ocean (RSW) and surface water mass properties lack the subsurface salinity maximum indicating the influence of the Indonesian Throughflow while station 13 exhibits the intrusion of RSW.

This region (8° S - 13° S) exhibits mixing in the intermediate waters (AAIW and RSW) as well as between STSW and ITW. The reason for the mixing between STSW and ITW is the transport of the main branch of the SEC through gap 2. Stations away from the SEC exhibit STSW (south of the SEC) with no mixing with ITW whilst certain stations within the SEC exhibit only ITW. AAIW moves northward whilst RSW moves southward, hence there is erosion of AAIW further north. Mixing also occurs between the two water masses in gap 2. Central waters consist of SICW, represented on the TS diagram by the linear relationship between temperature and salinity at densities between 26.5 kg/m^3 and 27 kg/m^3.

Station 21 (12.09° S, 62.5° E) exhibits NIDW with a temperature range of 2.5 °C and 4 °C, a salinity value of approximately 34.8 and oxygen in the range of between 2.5 ml/l and 3.5 ml/l. AAIW exists in the intermediate waters with a temperature of 6° C, a salinity of 34.6 and an oxygen range of 3.5 ml/l and 4 ml/l. Central waters consist of SICW with a temperature range of 9 °C and 11 °C, an oxygen range of 4.5 ml/l and 4.6 ml/l and a salinity range of 35 and 35.1 (Emery, 2001). STSW exists as a subsurface salinity maximum (35.7) (Gründlingh et al, 1991). The strong signature of the STSW is due its positioning as it is not within the SEC and mixing has not occurred with ITW. TSW is present in the surface waters with temperatures > 25 °C, salinity between 34.8 and 34.9 and oxygen values approximately 4.4 ml/l. This station exhibits no influence from waters of Northern Indian Ocean origin.

Station 13 (12.04° S, 54.98° E) does not exhibit NIDW as the bathymetry is too shallow. Intermediate waters indicate mixing between AAIW and RSW as salinity and oxygen values lie between the two water mass ranges. Temperatures are approximately 5° C, salinity ranges between 34.79 and 34.81 while the oxygen is 2 ml/l. ITW is present with a temperature range between 18° C and 20°C, a salinity of 35.2 and an oxygen range of between 2.8 ml/l and 3 ml/l (New et al, 2005). Surface waters consist of TSW with temperatures > 23°C, salinity values of approximately 34.9 with oxygen values between 4 ml/l and 4.4 ml/l.

Station 16 (12.08° S, 59.6° E) consists purely of RSW in the intermediate waters with salinity values of 34.9, a temperature range of between 6°C and 8°C and an oxygen range of between 1.8 ml/l and 2 ml/l. ITW is present with a temperature of 18° C, a salinity of approximately 35.2 and an oxygen value of 3

ml/l. Surface waters consist of TSW with temperatures > 25° C, a salinitiy of approximately 34.9 and oxygen values between 4.3 ml/l and 4.5 ml/l.

In this region there is no current which divides RSW and AAIW, however the mixing which occurs in gap 2 contributes to the gradual change of the properties of the intermediate waters from AAIW to RSW northward. The SEC in this region acts as a barrier to STSW as it exists only to the south of it and there is mixing between STSW and ITW within the SEC and gap 2. NIDW remains unaffected in this region other than where the bathymetry is too shallow for it to exist.

4.1.1.3 Sub-Region 3 (region spanning south of the Saya de Malha – Nazareth gap (13° S) to Mauritius)

The following section gives results for sub-region 3, which is defined as the region which contains AAIW in the intermediate waters with the absence of RSW and is characterized by the southern core of the SEC. The intermediate waters contain no RSW as all stations have a salinity < 34.8 and hence AAIW is present (Toole and Warren, 1993; Beal et al, 2000). There is most likely the presence of IIW (Indonesian Intermediate Water) but is difficult to identify as it occupies the same density and salinity ranges as AAIW. The low salinity AAIW is most likely a mixture of eroding AAIW and IIW, especially closer to the SEC. However, further studies are required. The region spans south of gap 2 (13° S). The region contains water masses only of southern Indian Ocean origin except within the core of the SEC where ITW exists. ITW was identified similarly near the core of the SEC by New et al, (2005). Figure 4.7 depicts all CTD stations within sub-region 3. Figure 4.8 depicts a T-S diagram and a T-O diagram for 3 stations in the sub-region for water mass analyses.

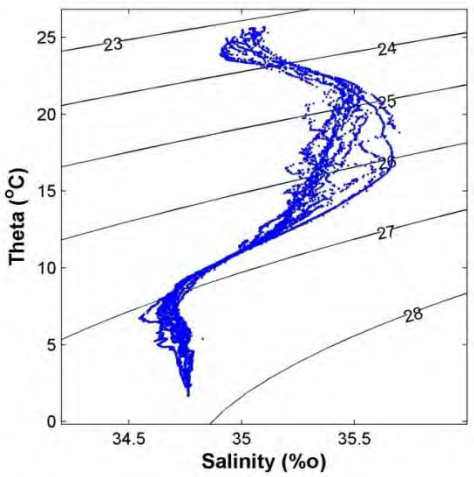

Figure 4. 7: Temperature-Salinity diagram for stations across the Mascarene Plateau south of 13° S.(14 stations)

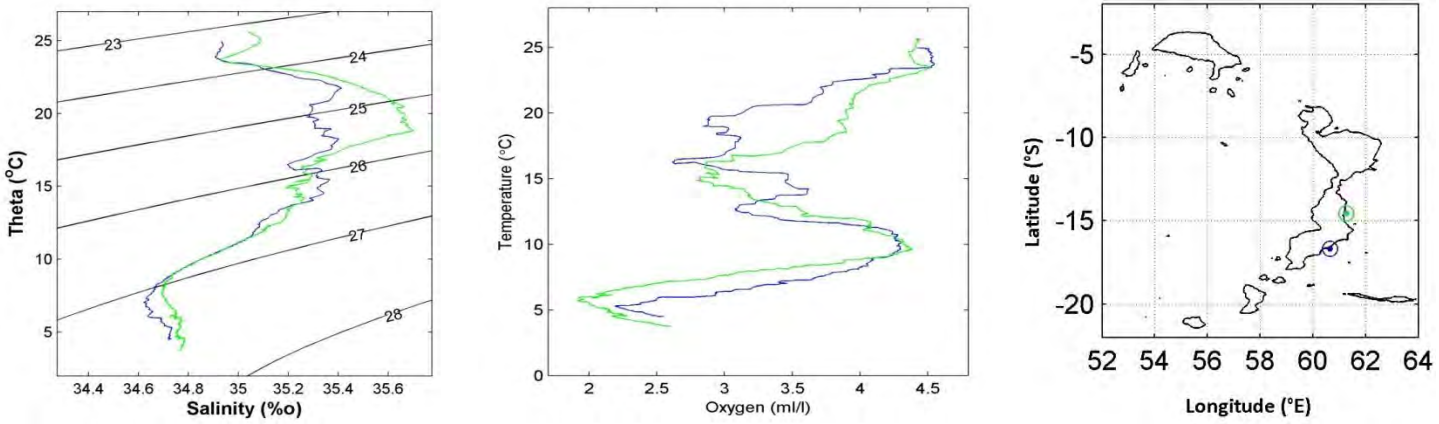

(a) (b) (c)

Figure 4. 8: Temperature-Salinity Diagram (a), Temperature-Oxygen Diagram (b) for Selected Stations south of 13° S and position of stations (c). Blue indicates station 7 (16.6° S, 60.65° E) whilst green indicates station 12 (14.6° S, 61.27° E).

Station 12 is picked as it is not influenced by the South Equatorial Current and exhibits water mass properties purely of Southern Indian Ocean origin whilst station 7 is picked as it depicts the influence of the SEC in the region (mixing between STSW and ITW). Both stations exhibit intermediate and central water masses that of the Southern Indian Ocean (AAIW and SICW) whilst station 12 exhibits a strong subsurface salinity maximum indicating STSW without any influence from the Indonesian Throughflow in contrast to station 7 which indicates mixing between STSW and ITW. South of 13° S, AAIW is present without any mixing. Hence, RSW is not evident this far south in the region. SICW, represented by the linear relationship on the TS diagram between densities of 26.5 kg/m^3 and 27 kg/m^3 exists whilst STSW is predominant below TSW. However, within the branch of the SEC between the Cargados-Carajos Bank and Mauritius, mixing between STSW and ITW occurs. Many stations exhibit characteristics between STSW and ITW.

Station 12 (14.6° S, 61.27° E) exhibits NIDW with temperature ranges between 3° C and 4° C, a salinity of approximately 34.8 and an oxygen value of 2.5 ml/l. Intermediate waters consist of AAIW with temperature ranges of between 5° C and 7° C and the typical salinity minimum. The oxygen value at this depth is approximately 3.5 ml/l. SICW is present in the central waters with temperature values between 9° C and 11° C, salinity values between 34.85 and 34.95 and an oxygen value of approximately 4.5 ml/l (an oxygen maximum). Towards the surface waters, STSW exists as a strong subsurface salinity maximum (35.6) and an oxygen minimum (3 ml/l). TSW overlies STSW with temperatures > 23° C.

Station 7 (16.6° S, 60.65° E) exhibits AAIW with a temperature of approximately 6° C, a salinity of 34.6 with an oxygen value of 3.6 ml/l. Mixing has occurred at this station as water mass properties lie between that of STSW and ITW. The classical isohaline property of ITW exists, however the salinity is too high. Salinity values lie between 35.25 and 35.3 without the classic subsurface salinity maximum. TSW overlies this mixing of water masses. This station clearly shows the influence of the branch of the SEC which is channeled between the Cargados-Carajos Bank and Mauritius due to the presence of ITW which is contained within the current.

From this, it is clear that there are two dividing lines separating firstly surface water masses primarily of Northern Indian Ocean origin (ASHSW) to the north due to the eastward flowing SECC and TSW to the south. However, there is an intrusion of TSW and ITW due to the westward flowing SEC through gap 1. The intermediate waters remain unaffected in this region as RSW is the only water mass present. The second dividing line acts as a barrier to STSW. The SEC which flows between the Saya De Malha Bank and the Nazareth Bank forms this dividing line. Within this region which contains this branch of the SEC there is erosion of AAIW due to the intrusion of RSW from the north. The westward flowing SEC in this

region contributes to the mixing between RSW and AAIW due to the interaction of these water masses in gap 2. The same can be said for the mixing of STSW and ITW within this gap and mixing of these two water masses within the SEC in general. In the southern sector south of 13° S only AAIW exists in the intermediate waters and STSW and TSW in the surface waters except within the southern branch of the SEC where there is mixing between STSW and ITW (salinity values lie between that of STSW and ITW (New et al, 2005; Gründlingh et al, 1991)).

The Mascarene Plateau has an effect on the water masses surrounding the Mascarene Plateau. However, the effect is much smaller than along the north-south divide. The main reason for this is that the plateau is too shallow to have a substantial effect on the deep and intermediate waters (NIDW, AAIW and RSW). From the examples in Figure 4.9, the plateau actually has no effect on NIDW since both the plateau and the channels separating the banks on the plateau are too shallow. The red station (to the east of the Mascarene Plateau) displays a salinity of 34.8, indicating RSW (Beal et al, 2000) whilst the red station to the west of the plateau (similar latitude) displays a salinity of 34.7 indicating mixing with Antarctic Intermediate Water (AAIW). This is due to the SEC (South Equatorial Current) flowing through gap 2 where RSW and AAIW mix. The red station to the east of the plateau indicates a strong subsurface salinity maximum (salinity of approximately 35.5), indicative of STSW (Gründlingh et al, 1991) whilst the red station to the west indicates fresher waters with a salinity of approximately 35.2. This is due to mixing between ITW and STSW through gap 2. Similarly, the blue station to the east of the plateau indicates a strong subsurface salinity maximum with a salinity of approximately 35.5 (STSW) whilst the blue station to the west of the plateau at the same depth has a salinity of approximately 35.3, indicative of mixing between STSW and ITW. In the upper layers of the surface waters, the blue station to the east of the plateau indicates a salinity of approximately 34.9, indicative of TSW (Gründlingh et al, 1991; Warren, 1981) whilst the blue station to the west of the plateau indicates a salinity of approximately 35.05, indicative of mixing between TSW and STSW through gap 2. The Mascarene Plateau also has the effect of displacing the latitude of the SEC (splits it into 3 cores) into 3 regions west of the plateau where mixing occurs at different latitudes. This induces increased mixing between ITW, TSW and ASHSW in the northern branch as the latitudinal position of the SEC is shifted north. Similarly, the plateau induces increased mixing between ITW and STSW within the southern branch as the latitudinal position of the SEC is shifted south.

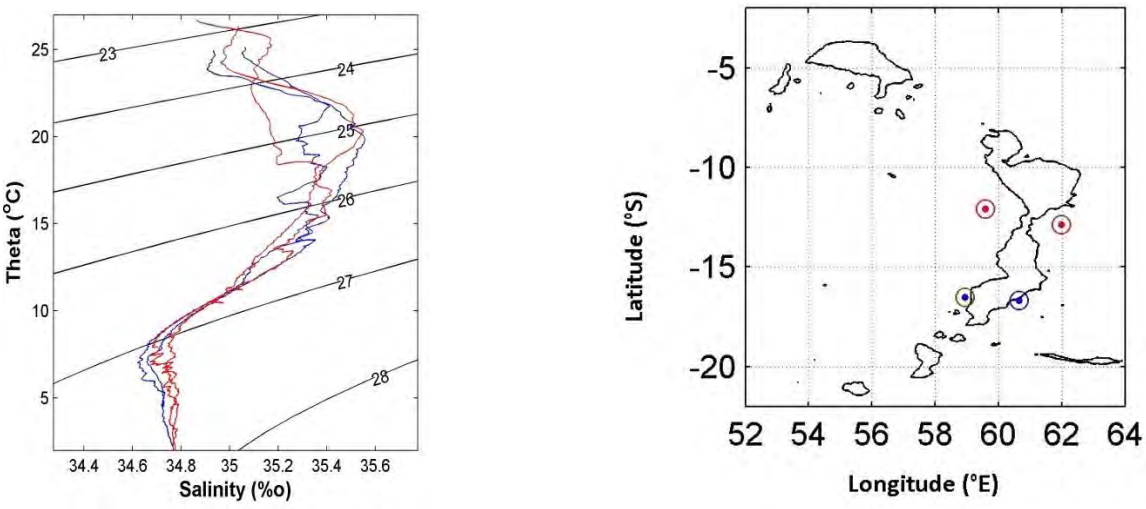

(a) (b)

Figure 4.9: Temperature-Salinity Diagram (a) showing the differences between the western side and eastern side of the Mascarene Plateau and position of stations (b). There is negligible mixing in the intermediate waters whilst mixing increases in the surface waters, however still small compared to the north-south divide.

The overall effect of the Mascarene Plateau is to split the SEC into separate cores centered near 12° and 18° S. Once past the Plateau it seems likely that these 2 cores continue westwards towards the Madagascar coast at 50° E and there form the North East and South East Madagascar Currents. The SEC acts as a main conduit for the westward advection of ITW water across the Indian Ocean bringing with it its subsurface oxygen and salinity characteristics. An interesting circulation exists over the Seychelles Bank, its character influenced by both the SEC flowing westwards to the south and the eastward flowing SECC. The influence the SECC has in bringing highly saline surface waters originating from the Arabian Gulf as well as RSW (Red Sea Water) needs to be further investigated.

4.2 Water Mass Origins

The region surrounding the Mascarene Plateau contains water masses with different origins (New et al, 2007). For evidence of these water mass origins, Argo floats for the period 2004 – 2010 are used to track

water masses. Since water masses in the region of the Mascarene Plateau generally flow along lines of constant density in the Indian Ocean, floats were tracked along isopycnals.

4.2.1 Arabian Sea High Salinity Water (ASHSW) and Tropical Surface Water (TSW)

ASHSW and TSW occur along the isopycnals 22.5 kg/m^3– 24.5 kg/m^3 and 22 kg/m^3 - 23.5 kg/m^3 respectively (Gründlingh et al, 1991; Warren, 1981; Kumar and Prasad 1999; Emery, 2001). Along the 22.6 kg/m^3 isopycnal, ASHSW and TSW with different origins and properties (salinity) occur around the Mascarene Plateau (From Figure 4.4a, TSW (station 27) and ASHSW (station 41) occurs along the 22.6 kg/m^3 isopycnal). ASHSW occurs in the northern sector of the region and is traced back to the Arabian Sea with salinity in excess of 35.8 flowing south whilst low salinity TSW occurs in the southern sector of the region (also in the branch of the SEC in the northern sector) and is traced back to the Indonesian seas (Figure 4.10a). Isopycnal mixing occurs between these water masses in the northern sector.

4.2.2 Sub-Tropical Surface Water (STSW) and Indonesian Throughflow Water (ITW)

STSW and ITW occur along the isopycnals 24.5 kg/m^3 – 25.5 kg/m^3 and 24 kg/m^3 – 26 kg/m^3 respectively (Gründlingh et al, 1991; Wyrtki, 1973; Song et al, 2004; New et al, 2005). Along the 25.5 kg/m^3 isopycnal, STSW and ITW occur around the Mascarene Plateau (From Figure 4.8a, STSW occurs along the 25.5 kg/m^3 isopycnal (station 12) and from Figure 4.6a, ITW occurs along the 25.5 kg/m^3 isopycnal (station 13)). STSW is traced back to the south-eastern quadrant of the Indian Ocean (70° E - 100° E and 20° S – 30° S). STSW is observed in this region by its high salinity in excess of 35.75 and ITW is traced back to the Indonesian seas with salinity as low as 34.7 (figure 4.10b).

4.2.3 South Indian Central Water (SICW)

SICW occurs along the isopycnals 26.5 kg/m^3 – 27 kg/m^3 (Emery, 2001). From Figure 4.8a, SICW occurs along the 26.75 kg/m^3 isopycnal (station 12) around the Mascarene Plateau. SICW is traced back to approximately 40° – 100° E along the 26.75 kg/m^3 isopycnal and spreads along the subtropical gyre reaching the Mascarene Plateau with an increased salinity (Figure 4.10c). The SEC does not form a barrier to it and there is still a presence of SICW north of the SEC.

4.2.4 Antarctic Intermediate Water (AAIW) and Red Sea Water (RSW)

AAIW and RSW occurs along the isopycnals 27.1 kg/m^3 – 27.5 kg/m^3 and 27.0 kg/m^3 – 27.6 kg/m^3 respectively (Toole and Warren, 1993; Roman and Lutjeharms, 2009; Beal et al, 2000). From Figure 4.8a, AAIW occurs along the 27.2 kg/m^3 isopycnal (station 7) whilst in Figure 4.4a, RSW occurs along the 27.2 kg/m^3 isopycnal (station 41) in the region surrounding the Mascarene Plateau and hence this isopycnal is used to trace these water masses (Figure 4.10d). RSW is identifiable along the 27.2 kg/m^3 isopycnal in the north-western region of the Arabian Sea with salinity in excess of 35.7 whilst AAIW is identifiable southward of the Mascarene Plateau with salinity of 34.25. RSW can be seen flowing southward, diluting as it flows south, whilst AAIW flows northward. Isopycnal mixing occurs between these water masses in the region of the Mascarene Plateau. There is a movement of a relatively fresh tongue of water into the region from the Indonesian seas along this isopycnal. This is an indication of IIW (Indonesian Intermediate Water) which is a relatively fresh tongue of water flowing within the SEC at an intermediate depth flowing from the Banda Sea and the Pacific Ocean (Talley and Sprintall, 2005). There is most likely the presence of IIW around the Mascarene Plateau but is difficult to identify as it occupies the same density and salinity ranges as AAIW. The low salinity AAIW in the region is most likely a mixture of eroding AAIW and IIW, especially closer to the SEC. However, further studies are required.

4.2.5 North Indian Deep Water (NIDW)

North Indian Deep Water (NIDW) is a difficult water mass to trace as very little is known about its spreading pathways. According to (Mantyla and Reid, 1995), it is formed from an aged form of North Atlantic Deep Water (NADW) mixing with a deep saline water mass which underlies RSW. Along the 27.72 kg/m^3 isopycnal a deep saline water mass flows southward with decreasing salinity (Figure 4.10e). From Figure 4.8a, NIDW occurs along the 27.72 kg/m^3 isopycnal (station 12).

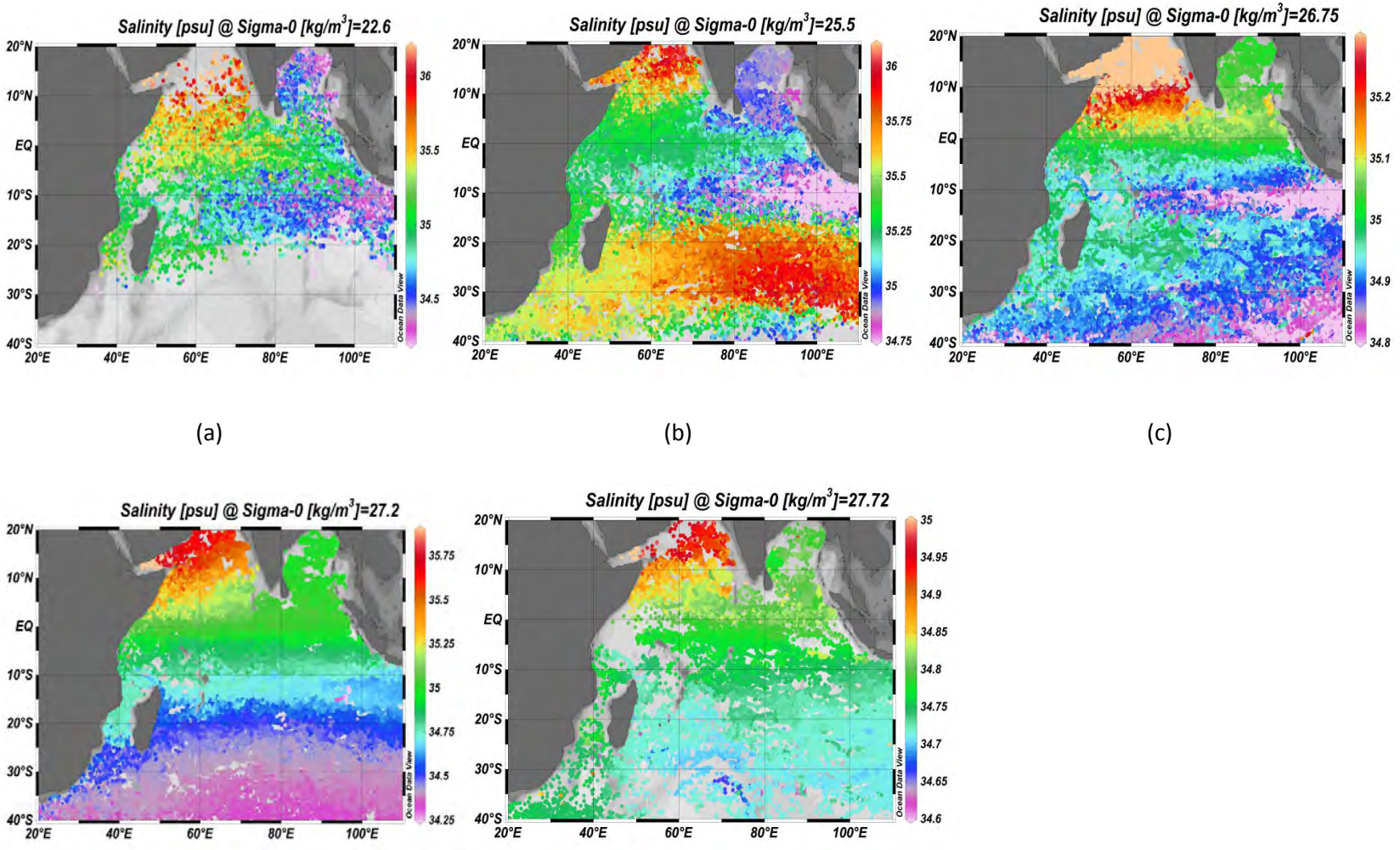

Figure 4. 10: Argo Floats in the Indian Ocean from the period 2004 – 2010 tracking water masses in the region of the Mascarene Plateau back to their origins along different isopycnals.

From the above, key question 1 can be addressed: *Which water masses are present in the region of the Mascarene Plateau, where are their origins, where do they mix in the region and does the westward flow of the South Equatorial Current (SEC) influence the mixing?*

The water masses in the region of the Mascarene Plateau consist of waters of different origins including ASHSW (Arabian Sea High Salinity Water), TSW (Tropical Surface Water), ITW (Indonesian Throughflow Water) and STSW (Subtropical Surface Water) at the surface, RSW (Red Sea Water) and AAIW (Antarctic Intermediate Water) in the intermediate layers, South Indian Central Water (SICW) in the central layers and NIDW (North Indian Deep Water) in the deep layers. The region was too shallow for the identification of bottom waters. IIW (Indonesian Intermediate Water) was most likely present in the region but is hard to identify since it occupies the same density and salinity ranges as AAIW.

These water masses have their origins in the southern Indian Ocean, northern Indian Ocean or the western Pacific Ocean and the Indonesian archipelago. ASHSW has its origins in the northern Indian Ocean (Arabian Sea) and TSW has its origins in the Indonesian archipelago. These 2 water masses travel southwards and westwards along the 22.6 kg/m^3 isopycnal. ITW has its origins in the western Pacific Ocean and the Indonesian archipelago and STSW has its origins in the south-eastern quadrant of the Indian Ocean. These 2 water masses travel westwards (within the SEC) and within the subtropical gyre respectively. SICW is traced back to approximately 40° – 100° E along the 26.75 kg/m^3 isopycnal and spreads along the subtropical gyre. AAIW and RSW has its origins south of the Mascarene Plateau in the southern Indian Ocean and in the north-western region of the Arabian sea respectively. These water masses travel along the 27.2 kg/m^3 isopycnal. NIDW is a difficult water mass to trace as very little is known about its spreading pathways. However, Along the 27.72 kg/m^3 isopycnal, a deep saline water mass flows southward with decreasing salinity which is indicative of NIDW.

South of the northern sector of the Seychelles Bank and north of 8° S the predominant water mass in the surface layers is ASHSW. However, in the region where the northern branch of the SEC flows between the Seychelles and the Saya de Malha Banks there is mixing between ASHSW and TSW. ITW is also present within the branch of the SEC. In this region the westward flow of the SEC does influence the mixing since the TSW within the branch of the SEC in this region mixes with ASHSW (the bathymetry of the Mascarene Plateau steers the branch further north).

The region (8° S - 13° S) exhibits mixing in the intermediate waters (AAIW and RSW) as well in the surface waters between STSW and ITW. This region contains the northern branch of the SEC which

carries TSW and ITW. Mixing between STSW and ITW occurs in the areas close to this branch of the SEC. AAIW moves northward whilst RSW moves southward, hence there is erosion/mixing of AAIW in this region. These 2 intermediate water masses also mix in gap 2 but not to the extent as the erosion/mixing of these water masses moving northwards/southwards (also occurs in the surface waters between STSW and ITW). Once again the westward flow of the SEC influences the mixing of water masses in this region. ITW is carried within the SEC and mixes with STSW.

South of 13° S mixing in the surface waters occur near the branch of the SEC which is channeled between the Cargados-Carajos Bank and Mauritius. Surface waters in this region comprise primarily of TSW and STSW. However, within the core of the SEC, ITW is present. Near the core of this current, mixing occurs between ITW and STSW.

4.3 Summary

Chapter 4 focused on the water masses during the October/November 2008 research cruise on the Fridtjof Nansen. The primary water mass which was carried by the SEC was fresh Indonesian Throughflow Water (ITW) where through the northern gap of the Mascarene Plateau mixed with high salinity Arabian Sea High Salinity Water (ASHSW) and through the southernmost gap mixed with high salinity Sub-tropical surface water (STSW). There are marked differences in water masses between the northern part and the southern part of the Mascarene Plateau. The northern part contains nutrient rich waters (ASHSW) whilst the southern part contains nutrient poor waters (STSW). Intermediate waters consist of Antarctic Intermediate Water (AAIW) in the south whilst the northern part of the Mascarene Plateau consists of Red Sea Water (RSW). Towards the centre of the Mascarene Plateau (~ 13° S), mixing occurs between AAIW and RSW. Whilst there were no new water masses observed during the October/November 2008 cruise on the Dr Fridtjof Nansen compared to the June/July 2002 cruise on the RRS Charles Darwin, new knowledge has been brought to light such as –

- Substantial mixing in the northern branch of the SEC which flows through gap 1 between ASHSW, TSW and ITW.
- Changes in surface water mass properties in the northern sector of the Mascarene Plateau due to this mixing.
- Confirming the water mass origins by using Argo floats and showing that the region around the Mascarene Plateau is an important region for mixing of water masses in the Indian Ocean.

- Due to the bathymetry of the Mascarene Plateau, the SEC is deflected more north and south (different cores) which enhances mixing between ITW, TSW and ASHSW in the north and between ITW and STSW in the south.
- AAIW is not present in region 1 whilst RSW is not present in region 3
- Along the same density level as AAIW and RSW, there appears to be a tongue of relatively fresh water in the intermediate levels which may resemble IIW (Indonesian Intermediate Water) since it is carried within the SEC and the SEC has its origins in the Western Pacific Ocean and the Indonesian archipelago. This water mass requires further investigation since it occupies the same density levels and salinity ranges as AAIW.
- The bathymetry of the banks is understood better as the ASCLME cruise sampled the banks of the Mascarene Plateau whereas the June/July 2002 cruise did not and the predominant water masses over the banks are well known now. Over the Seychelles Bank, high salinity ASHSW is swept across eastwards whilst over the other 3 banks, TSW is predominant.

CHAPTER 5: Comparison between Cruise Conditions and Satellite Data

Satellite data is extremely useful to oceanographers since cruise opportunities are limited by funding. There is an increased need to monitor the oceans and obtain daily estimates of SST, geostrophic velocity, ocean colour etc. Satellite data can be used for this purpose. However, to ensure accurate representation of satellite estimates, in-situ data needs to be compared with satellite estimate which is done in this section. In-situ data around the Mascarene Plateau is cross-referenced to satellite data to ensure that satellite data is an accurate representation of the processes occurring in the region so cruise data can be extended both temporarily and spatially and to link cruise data to large scale circulation and ocean scale Rossby wave propagation.

Key Question 2. How accurate is satellite data in the region and hence what is its viability for use in the region?

5.1 ADCP Current and Geostrophic Current Comparison

Table 5.1 shows the comparison between ADCP currents obtained during the survey and satellite derived altimetry geostrophic currents for the 3 gaps within the Mascarene Plateau (average velocity across the respective gaps).

All values cm/s	Gap 1	Gap 2	Gap 3
ADCP (U)	-21.87	-43.25	-14.79
ADCP (V)	-3.5	21.326	4.9
Total ADCP Velocity	22.1481	48.222	15.58
Satellite Geostrophic Flow (U)	-20.359	-41.096	-14.413
Satellite Geostrophic Flow (V)	-0.61	11.735	1.8879
Total Geostrophic flow	20.3684	42.739	14.5361
Difference	1.78	5.48	1.04

Table 5. 2: Comparison of ADCP velocities with Satellite Geostrophic Velocities

The similarity between the ADCP ship-board currents and satellite altimetry are encouraging, especially for gap 1 and gap 3 where the difference is only approximately 1 cm/s. Whilst gap 2 has a difference of approximately 5 cm/s this is still acceptable since velocities through this gap can easily reach 40 cm/s. The reason for the increased difference through this gap is most likely due to the narrowness of the gap compared to the others (< 200 km) which could have led to an under-estimation of the geostrophic velocity obtained by satellite.

5.2 TRMM Satellite SST and Shipboard SST comparison

Figure 5.1 gives a comparison between ship board SST and satellite SST. Weekly TRMM Satellite SST is used for this purpose.

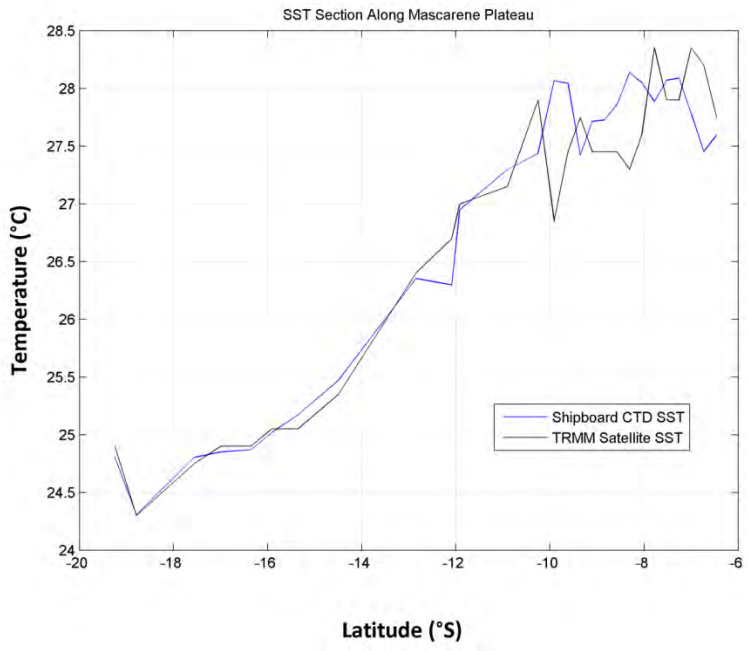

Figure 5.1: Comparison between shipboard SST (October/November 2008) with TRMM Satellite SST. The graph highlights a close similarity between platforms, particularly with distance south. The greatest difference is approximately 1° C which is quite acceptable since satellite data is a weekly product (dates between satellite data and in-situ data are not exactly the same)

From the above, key question 2 can be addressed: *How accurate is satellite data in the region and hence what is its viability for use in the region?*

These comparisons confirm that satellite data can be used within this region with a high degree of confidence and hence cruise data can be extended in space and time. Satellite data which includes altimetry (geostrophic velocities) and SST was compared to ADCP and shipboard SST respectively. This comparison is important in assessing the viability for using satellite data in the region and hence broadening the database for further research in the region.

5.3 Summary

The geostrophic velocities over the 3 major gaps were compared. The difference in geostrophic velocity across gap 1 and gap 3 were approximately 1 cm/s whilst the difference across gap 2 was approximately 5 cm/s. These differences are acceptable for the use of satellite altimetry in the region. The increased difference of 5 cm/s through gap 2 is due to the narrowness of the gap which will produce lower satellite geostrophic velocities. However, the velocity in this region can easily reach above 40 cm/s. Hence the increased difference is acceptable. The greatest difference between shipboard SST and TRMM satellite SST is 1° C. The primary reason for this difference is that the TRMM satellite SST is a weekly product and hence the dates between the satellite data and in-situ data are not exactly the same. However, the comparison is still within an acceptable range for the use of TRMM satellite SST (Kim et al, 2010).

CHAPTER 6: The Circulation around the Mascarene Plateau and its influence on the Equatorial Current System

This chapter consists of further results obtained during the Nansen survey of the Mascarene Plateau conducted between October/November 2008 as well as satellite data. The objective of this chapter is to understand the effect the westward flowing South Equatorial Current (SEC) and the eastward flowing South Equatorial Countercurrent (SECC) has on the general ocean circulation in the region.

6.1 Variability around the Mascarene Plateau

The circulation around the Mascarene Plateau consists mainly of the westward flowing SEC which splits into 3 cores and subsequently flows through the 3 major gaps within the Mascarene Plateau. Downstream of the Mascarene Plateau, two cores of the SEC are formed. The flow between the Cargados-Carajos Bank and Mauritius as well as the augmentation of flows from the south forms the southern branch of the SEC. The northern branch of the SEC is formed from the channeled flow between the Saya de Malha and Nazareth Banks and to a smaller degree the flow between the Seychelles and Saya de Malha Banks. The flow across the Seychelles Bank consists of the eastward flowing South Equatorial Counter Current (SECC). Part of the SEC which flows westward between the Seychelles Bank and the Saya de Malha Bank on occasions recirculate and joins the SECC. There are 4 areas which experience a relatively high variability compared to the rest of the Mascarene Plateau, namely a) the channels between the Saya De Malha and Nazareth Banks, b) Seychelles and Saya De Malha Banks, c) the Cargados-Carajos Bank and Mauritius and d) the area to the east of the Seychelles Bank (Figure 6.1). The high variability through the 3 gaps indicates the 3 pathways of the SEC after splitting to the east of the Plateau whilst the high variability to the east of the Seychelles Bank indicates the SECC.

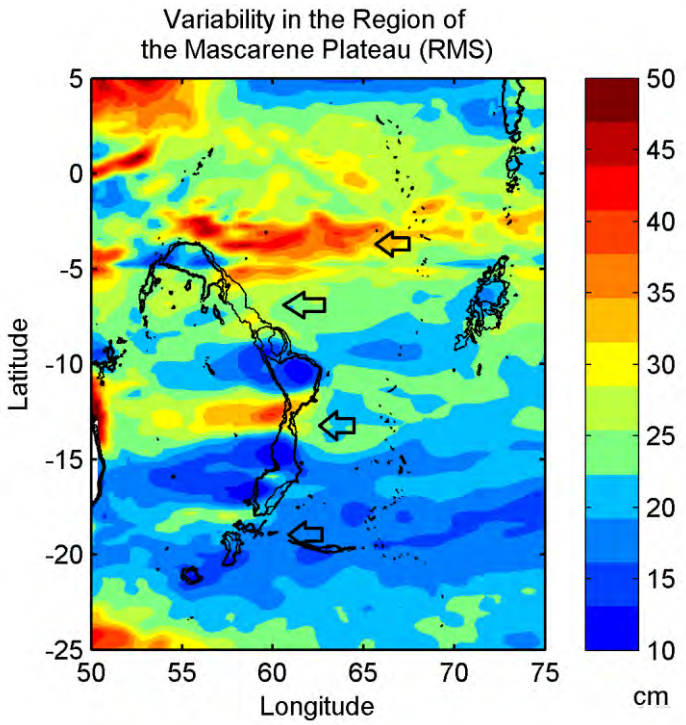

Figure 6.1: Variability in the region of the Mascarene Plateau (root mean square of MADT) for the period 2004 - 2010. The three channels (specifically the channel between the Saya Da Malha Bank and Nazareth Bank) exhibit higher than normal variability. The 4 arrows depict the high variability in the region due to the SEC and SECC. (Data: AVISO Satellite derived Altimetry)

6.2 Circulation around the Mascarene Plateau

Key Question 3. In what way is the flow of the SEC affected by the gaps in the Mascarene Plateau during the 2008 ASCLME cruise and are there differences to the cruise conducted during the June/July 2002 onboard the RRS Charles Darwin?

Circulation patterns in the upper layer of the ocean around and on the banks of the Mascarene Plateau were recorded during the Mascarene Plateau Survey (ASCLME 2008 Cruise between 8 October – 16 November 2008) by a ship-mounted ADCP (SADCP). Velocities at 25 m depth are shown in Figure 6.2 by blue arrows with the 1000 m isobath overlaid in black. This range is well within the mixed upper layer (New et al, 2005). Figure 6.2 illustrates the velocities over the plateau. The SECC (South Equatorial Counter Current) is visible over the Seychelles Bank.

The circulation pattern identified by (New et al, 2005) is confirmed by Figure 6.2. These areas or gaps were thought to contain most of the transport from the broad flowing westward SEC (New et al, 2007) and once again this study proves that most of the SEC flows between these 3 gaps. Quantifying the amount of transport through the 3 gaps during this cruise is difficult since there was no LADCP on board and hence the circulation was not measured to the seabed. However, one can obtain a close approximation of the amount of flow each gap receives as most of the transport is in the upper layer of the ocean and the SEC is strongest in the upper 200 – 250m. The SADCP covers this range. (New et al, 2007) found that the SEC was strongest in the upper 200m (maximum speeds of 70 cm/s) but was still present at depths of 1400m with speeds of 10 cm/s. Hence the volume flux measured from the SADCP for this cruise should be a reasonable estimate, though it will be an underestimation.

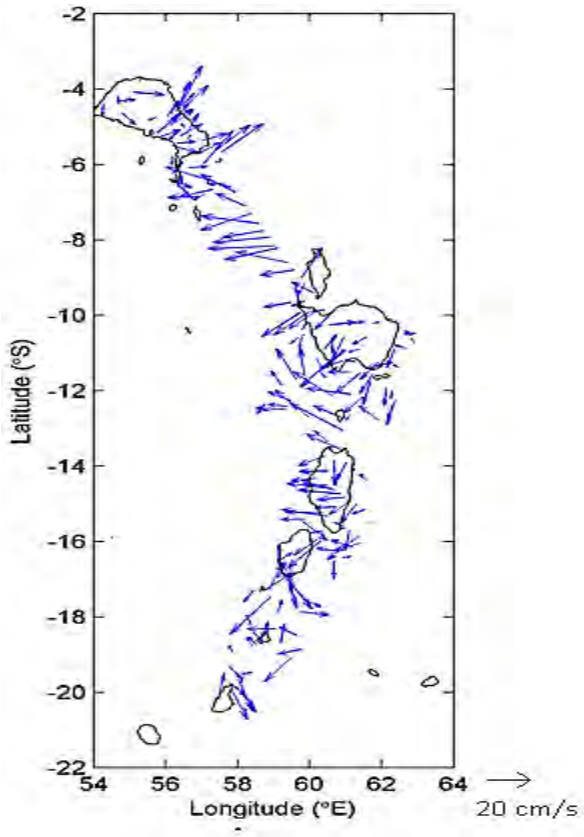

Figure 6.2: Shipboard ADCP Velocities (blue arrows) across the Mascarene Plateau at a depth of 25m with 1000m isobath overlaid in black. Increased velocities through the 3 main gaps within the Mascarene Plateau due to the SEC (South Equatorial Current) are evident whilst increased velocities eastward across the Seychelles Bank are evident due to the SECC (South Equatorial Countercurrent).

During this cruise gap 1 and gap 2 received most of the flow with each having received 14.93 Sv and 14.41 Sv respectively whilst gap 3 received 6.19 Sv. An extra 1 Sv flowed through the relatively small gap between the Nazareth Bank and the Cargados Carajos Bank. Interestingly, part of this latter flow was not shown on maps of altimetry, hence it could have been ageostrophic flow. The ageostrophic component of this flow predominantly occured on the Nazareth bank which could have been due to wind driven influence (a tropical cyclone was present). Thus the total flow across the Mascarene Plateau was (excluding minor amounts flowing over the banks and the flow below the detectable range of the SADCP) 36.53 Sv. 40.87% of the flow was channeled through gap 1, 39.4% was channeled through gap 2, 16.9% was channeled through gap 3 whilst 2.73% was channeled through the minor gap between the Nazareth Bank and the Cargados-Carajos Bank. During the survey conducted by (New et al, 2005), approximately 50 Sv flowed westwards in the SEC between 10° S and 16° S and as it approached the Mascarene Plateau. 50% (25 Sv) of the flow was channeled through gap 2 whilst the remainder past in equal volumes (12.5 Sv) between gap 1 and gap 3. This survey gives an interesting comparison since there is more volume transport through gap 1 (40.87% of total) than gap 3 (16.9% of total). The difference between the 2 cruises could be due to seasonality. Seasonality affects the positioning of the SEC before its encounter with the Mascarene Plateau (Figure 6.3). Figure 6.3a gives the altimetry derived geostrophic velocities in the region for June 2002 (the period of the survey conducted by New et al, (2005) whilst Figure 6.3b gives the altimetry derived geostrophic velocities in the region for October 2008. During June 2002 at 70° E, the SEC existed as a broad band between 10° S and 16° S whilst during October 2008 at 70° E the SEC existed as a broad band between 7° S and 12° S. This is an indication that the variability in the positioning of the SEC may influence the amount of flow through each of the 3 main gaps in the Mascarene Plateau.

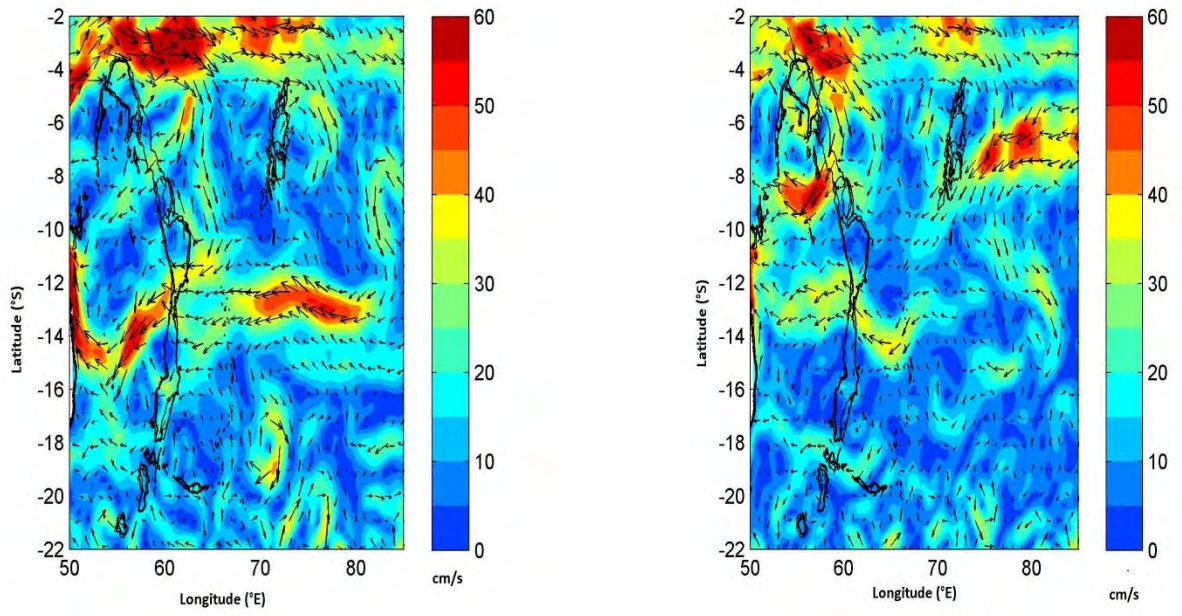

(a) (b)

Figure 6.3: Average altimetry derived Geostrophic Velocities (a) June 2002 and (b) October 2008. A shift in the SEC northward can be seen in October 2008 at approximately 75° E with increased surface geostrophic velocities through the Seychelles – Saya De Malha Bank during this month compared to June 2002

Velocities in the upper layers (45m) of gap 1 averaged approximately 29 cm/s and peaked at 79 cm/s. The structure of the circulation in this gap was non-homogenous in the upper 450m (Figure 6.4). 3 Main areas had velocities in excess of 60 cm/s (westwards) in the upper 60m which appeared to be the main components of the volume transport through this gap. There was an apparent counter-flow between 8.5° S and 9° S. However, from maps of MADT, this counter-flow does not exist (Figure 6.4c).

Gap 2 exhibited 2 areas where flow had a strong westward component (80 cm/s and above) with one area having these velocities down to depths exceeding 200 m (Figure 6.5). These 2 areas (above 50 m) were also accompanied by northward velocities exceeding 50 cm/s. This gap had average velocities in the upper layers (45m) of 50 cm/s and peaked at 95 cm/s. With these westward velocities not fading out at depths of over 250m, this lends to the possibility that this strong flow could have continued further down and hence there could be a higher volume flux than calculated. However, due to a lack of data, this cannot be ascertained and there were not enough CTD stations within this gap to obtain a

geostrophic velocity profile. The higher geostrophic velocities within the gap are clearly evident in Figure 6.5c.

The main feature of gap 3 is the apparent eddy (cyclonic) in the region of 17.5 S (Figure 6.6a). The velocities of this 'eddy' are approximately 40 cm/s to depths of over 150 m. This feature is apparent on maps of surface geostrophic velocity (Figure 6.6c) and hence is geostrophic in nature although it appears weaker than the ADCP velocities (Figure 6.7). A similar feature was noted during the survey conducted during June 2002 (New et al, 2007). This gap has average velocities in the upper 45m averaging 7 cm/s and peaking at 43 cm/s. A reason for the low average velocity in the upper layer is due to the eddy like feature as it is a recirculation cell and hence part of the gap will experience negative velocities. The ADCP currents near Mauritius are South-Eastward which is not picked up in maps of Absolute Geostrophic Velocity (indicates a westward flow). This is most likely due to the course resolution of 1/4°. Increased geostrophic velocity is clearly evident through the channel as compared to the banks to the north and south.

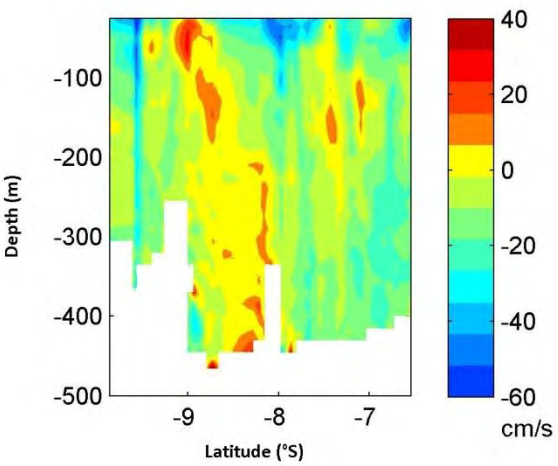

(a)

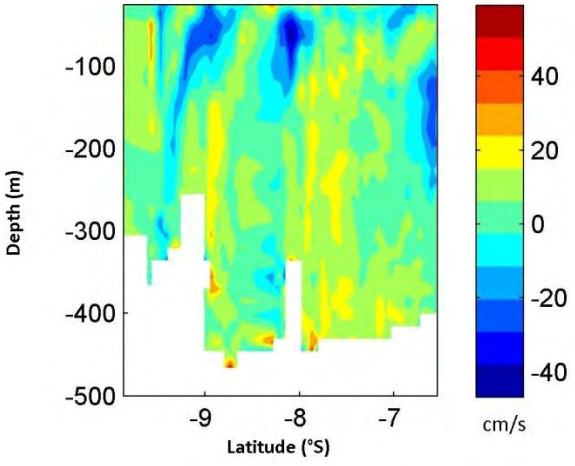

(b)

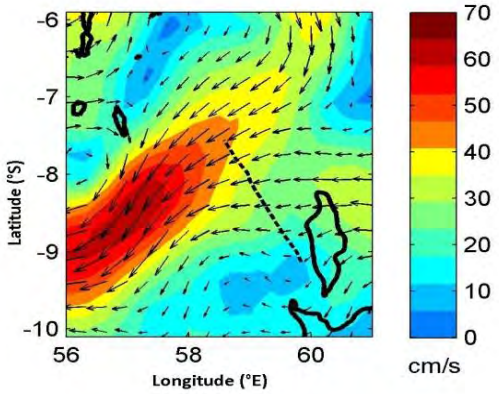

(c)

Figure 6.4: (a) ADCP Velocity Section across gap 1 (vx). (b) ADCP Velocity Section across gap 1 (vy). Flow is non-homogenous with an apparent counter-flow at approximately 9° S with highest westward velocities at 8° S. (c) Surface Geostrophic Velocities, Gap 1 .Dotted line indicates cruise track in region of apparent counter-flow and 1000m isobath overlaid in black. (October/November 2008)

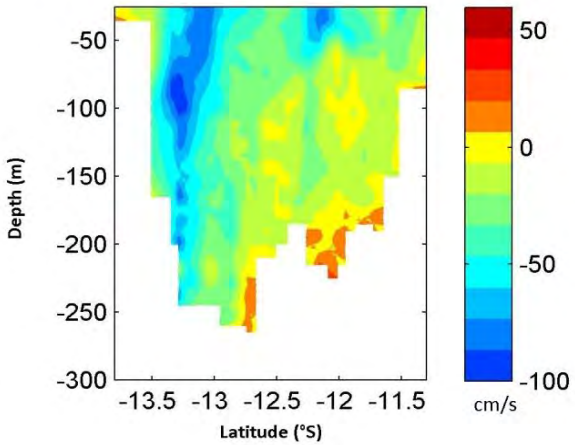

(a)

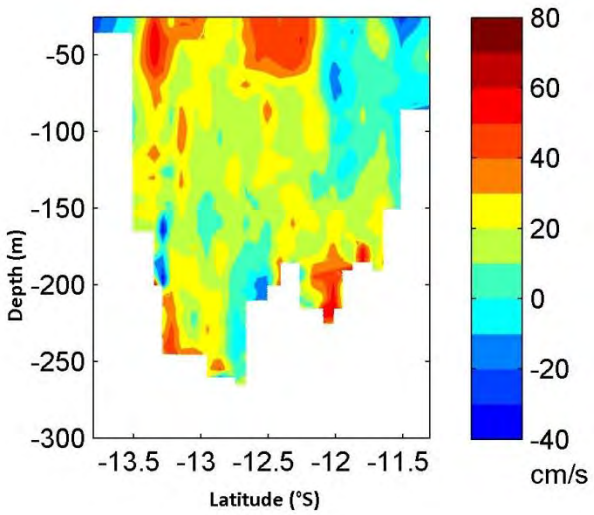

(b)

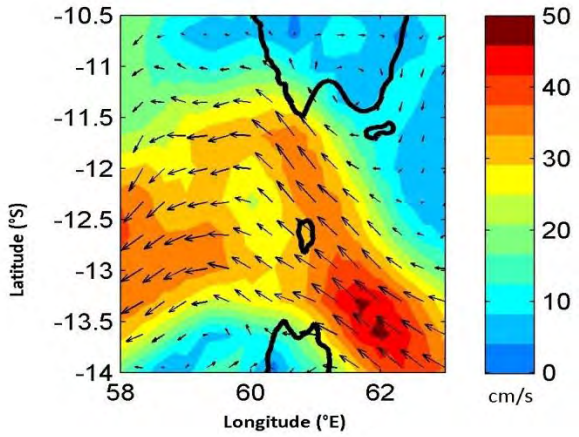

(c)

Figure 6.5: (a) ADCP Velocity Section across gap 2 (vx). (b) ADCP Velocity Section across gap 2 (vy). Highest Westward velocities occur at approximately 13.2° S and extend beyond 250 m in depth. Hence total volume transport through this channel is most likely an under-estimation. (c) Surface Geostrophic Velocities, Gap 2 (Between Saya de Malha Bank and Nazareth Bank) with 1000m isobath overlaid in black. (October/November 2008)

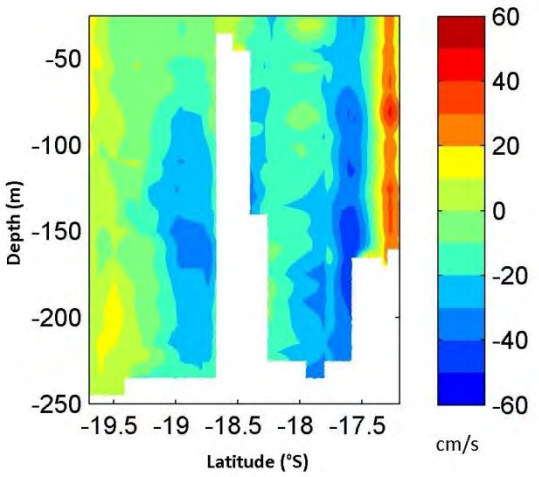

(a)

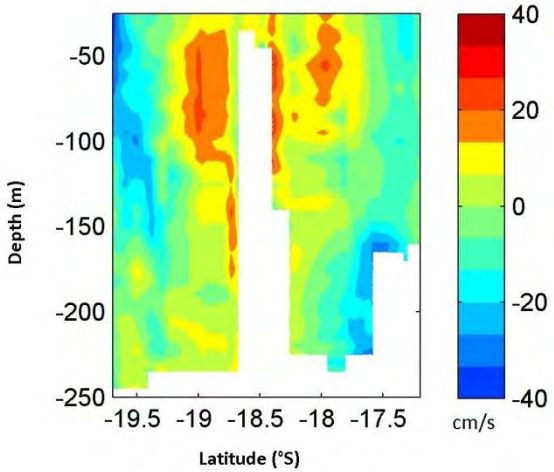

(b)

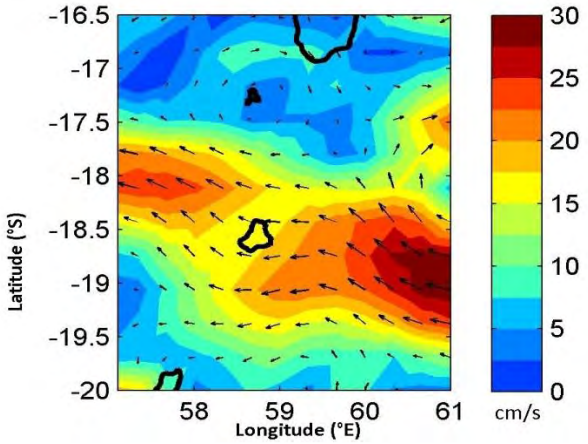

(c)

Figure 6.6: (a) ADCP Velocity Section across gap 3 (vx). (b) ADCP Velocity Section across gap 3 (vy). A cyclonic eddy is apparent at 17.5° S and extends in depth to below 200m. (c) Surface Geostrophic Velocities, Gap 3 (Between Cargados-Carajos Bank and Mauritius) with 1000m isobath overlaid in black. The cyclonic feature can be seen at 17° S near the Cargados-Carajos Bank. (October/November 2008)

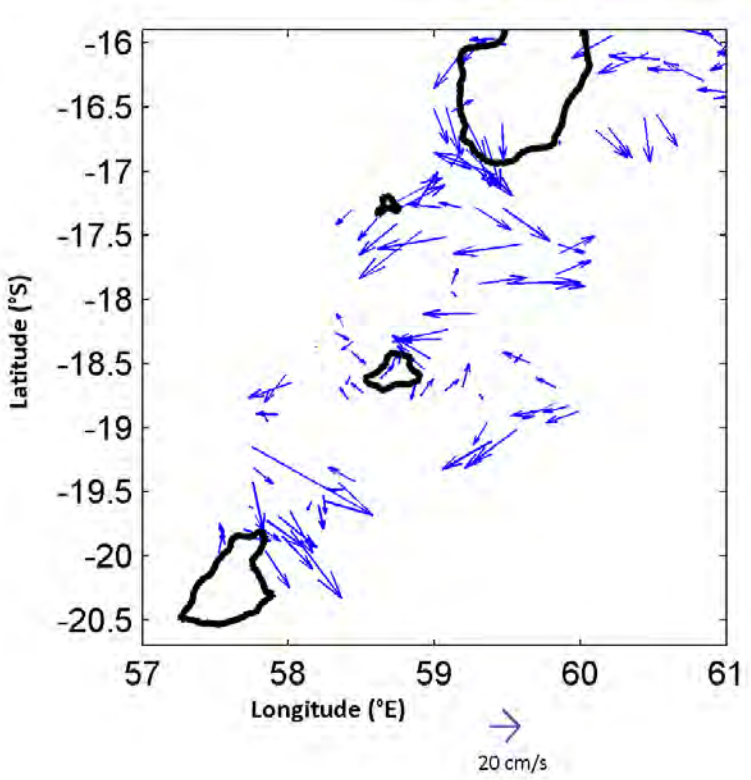

Figure 6.7: Shipboard ADCP velocities, Gap 3 (Between Cargados-Carajos Bank and Mauritius) with 1000m isobath overlaid in black. Surface currents through this channel are not as unidirectional as through the other two channels. This is due to the cyclonic eddy near the Cargados-Carajos Bank and the reversal in current near Mauritius.

Figure 6.8 gives 3 velocity profiles through the centre of each gap where most of the current is channeled through. These profiles are by no means an indication of all the profiles through these gaps as the current is not homogenous as shown in Figure 6.4, Figure 6.5 and Figure 6.6. However, these profiles do give an indication of the strength of the current with depth. The chosen profile for gap 1 indicates that velocities remain above 20 cm/s to depths of 200 m and similarly for gap 3. However, the chosen velocity profile for gap 2 indicates that the velocity remains above 15cm/s down to approximately 225m and there is even an indication of an increase further down although this cannot be ascertained as the SADCP only goes down to approximately 250m.

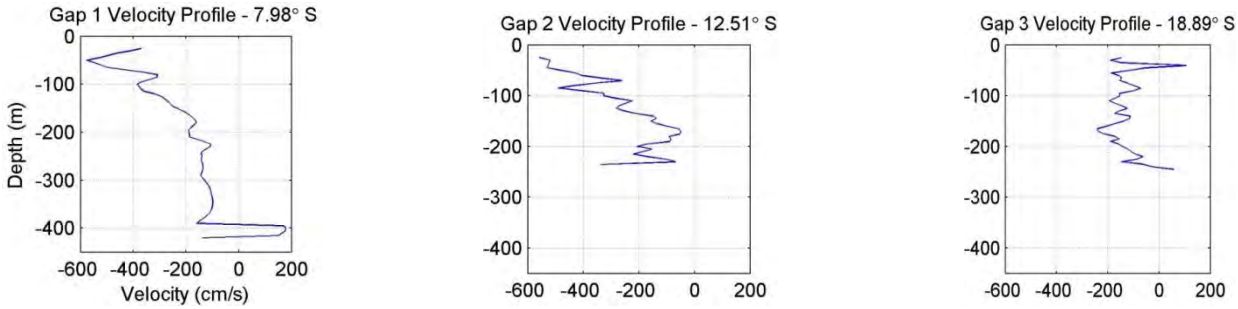

Figure 6.8: Plots showing velocity profiles with depth across stations in Gap, Gap 2 and Gap 3 respectively.

During the 2008 survey across the Mascarene Plateau, the Saya De Malha Bank was the most quiescent bank, in both maps of surface geostrophic velocity and surface ADCP. The SECC (South Equatorial Countercurrent) crosses over the Seychelles bank and from maps of absolute geostrophic velocity (Figure 6.9a) and surface ADCP (Figure 6.9b), the bank has very little effect on the current at the surface, although at 40 m depth, the current has weakened considerably.

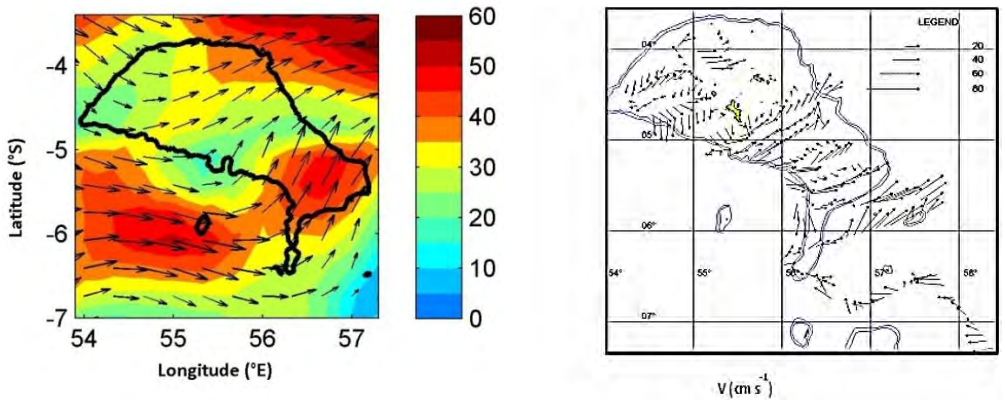

(a) (b)

Figure 6.9: (a) Average Geostrophic Velocities across the Seychelles Bank during October/November 2008 and (b) ADCP Surface Velocities across Seychelles Bank during October/November 2008 with 1000m isobath overlaid in black. Eastward velocities are clearly evident which is an indication of the SECC (South Equatorial Counter-Current).

The Nazareth Bank has a very small geostrophic velocity component flowing over it (figure 6.10b). However, surface ADCP velocities indicates westward flowing currents much stronger than what the geostrophic velocities show (figure 6.10a) but yet again, as with the Seychelles bank, at 45m depth, velocities fade away rapidly. This may be due to wind driven influence but this is not a topic of discussion in this study.

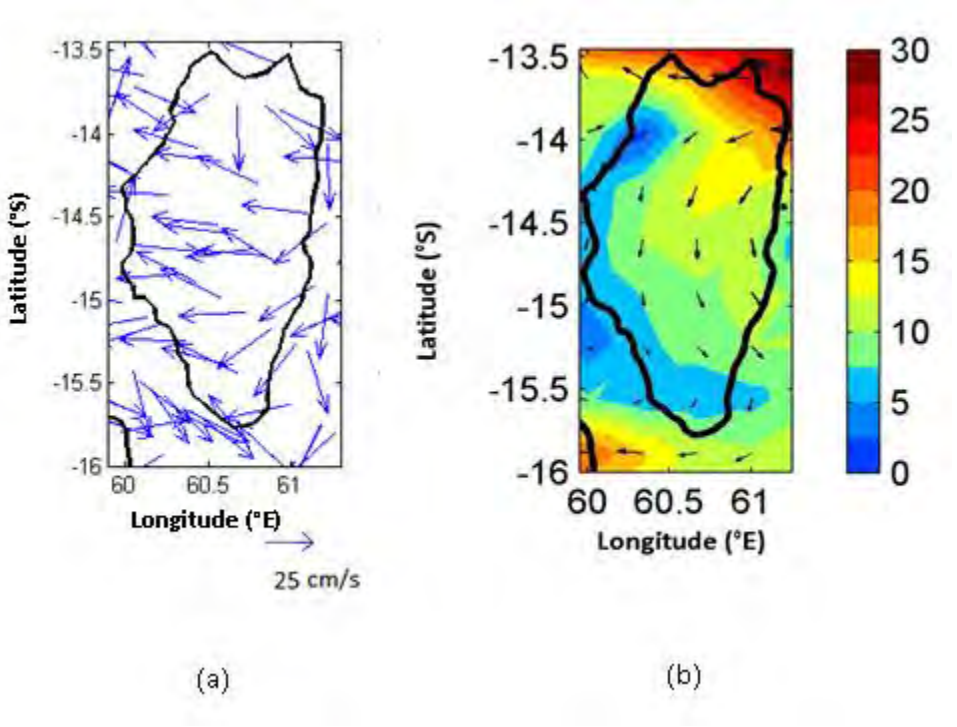

Figure 6.10: (a) ADCP Surface Velocities across Nazareth Bank during October/November 2008 and (b) Average Geostrophic Velocities across Nazareth Bank during October/November 2008 with 1000m isobath overlaid in black. ADCP velocities are westward whilst the geostrophic velocities across the bank are much smaller. This indicates that the ADCP velocities are most likely due to wind influence.

The upper half of the Cargados-Carajos Bank (near the minor gap with the Nazareth Bank) exhibits westward flowing currents. This is the channeled flow which was mentioned previously which is responsible for the small amount of volume flux (~ 1 Sv) across the plateau.

It can be concluded from the ADCP data and the maps of geostrophic velocity that there is very little flow across the banks of the Mascarene Plateau (with the exception of the Seychelles Bank where the flow is dominated by the SECC) and the vast majority of the SEC flows through the 3 main gaps. The study of the circulation over the banks is a new topic since there has been no prior cruise which extensively studied the banks of the Mascarene Plateau.

From the above, key question 3 can be addressed*: In what way is the flow of the SEC affected by the gaps in the Mascarene Plateau during the 2008 ASCLME cruise and are there differences to the cruise conducted during the June/July 2002 onboard the RRS Charles Darwin?*

During the October/November 2008 cruise on the Dr Fridtjof Nansen, the SEC transport to the east of the Mascarene Plateau was 36.53 Sv. This was most likely an underestimate since the volume transport was obtained via an SADCP which did not obtain a full depth profile but only reached a maximum depth of 450m. However, the SEC is strongest in the upper 250m so the underestimation is not likely to be great. The volume transport through each of the major gaps in the Mascarene Plateau are 14.93 Sv or 40.87% through gap 1, 14.41 Sv or 39.4% through gap 2 and 6.19 Sv or 16.9% through gap 3. There is approximately an extra 1 Sv or 2.73% which flows through the small gap between the Nazareth and Cargados-Carajos Bank but is not shown on altimetry maps and hence it could be ageostrophic in nature. Downstream of the Mascarene Plateau, 2 cores of the SEC were formed, a northern and southern core. The northern core composed primarily of the flow between the Saya de Malha and Nazareth Banks with a small amount of flow between the Seychelles and Saya de Malha Bank being augmented into it. The southern core comprised of the flow between the Cargados-Carajos Bank and Mauritius with augmented flow from the south. During the June/July 2002 cruise, 50 Sv flowed east of the Mascarene Plateau with half of the flow being channeled through gap 2 with the rest flowing in equal volumes through gap 3 and gap 1. The difference between the 2 cruises may be due to seasonality and a re-circulation loop existed during the 2008 cruise in gap 1. The SEC existed in a broad band between 10° – 16° S during June 2002 and between 7° – 12° S in 2008. Hence there was a northward shift during October 2008 which may have contributed to extra (less) flow through the most northerly (southerly) gap in the plateau.

6.3 Summary

The volume flux through each gap differs from the 2002 cruise (New et al, 2005) when the SEC transport was 50 Sv east of the plateau and 25 Sv flowed through gap 2 whilst the rest flowed in equal volumes through the other 2 gaps. In the 2008 October/November cruise, the SEC transport was 36.53 Sv east of the plateau (lower than that of 2002). This could be an underestimation due to the SADCP only reaching approximately 450 metres in depth. The total volume through each gap from north to south is 14.93 Sv (40.87 %), 14.41 Sv (39.4 %) and 6.19 Sv (16.9 %) respectively, whilst there was a small amount of flow (~ 1 Sv) through the minor gap between the Nazareth Bank and the Cargados-Carajos Bank. The difference with the 2002 cruise may be due to shifts in the position of the SEC upstream and/or whether there was a recirculation loop within gap 1 which could have increased the volume transport. The flow across the Saya de Malha, Nazareth and Cargados-Carajos Banks is negligible whilst the Seychelles Bank experiences the eastward flowing South Equatorial Counter Current (SECC) which contains ASHSW. A cyclonic eddy was detected south of the Cargados-Carajos Bank with the SADCP and was geostrophic in nature since it was picked up in maps of geostrophic velocity. This feature may be semi-permanent or permanent since a similar feature was detected during the June/July cruise in 2002.

The following chapter analyses the Mascarene Plateau with regards to the climatology of certain variables (geostrophic velocities, SST and eddy kinetic energy). The climatology is also used to ascertain the effect the Mascarene Plateau has on these variables mentioned above. Towards the end of the chapter, examples are given which proves that the SEC acts as an oscillating current as the current does not have a constant strength/velocity. The examples are all taken during 2008 (the year which the Nansen cruise took place, however none of the major pulsations occurred during the cruise within the gaps).

CHAPTER 7: Climatology and Dynamics in the Region of the Mascarene Plateau estimated with Satellite remote sensing

In chapter 5 it was ascertained that satellite remote sensing (satellite altimetry and TRMM SST) can be used confidently in the region of the Mascarene Plateau. This chapter uses altimetry derived geostrophic velocities and SST to study the annual cycle of those parameters and extend the cruise data in time and space. For instance, this chapter presents seasonal cycles of geostrophic velocities through the 3 major gaps of the Mascarene Plateau, increased velocities through the gaps and modification of eddy kinetic energy in the region. It also allows us to compare with a previous cruise led in the region at a different time of the year and to investigate if the different results are due to seasonality, interannual variability or other reasons for instance Rossby wave propagation associated with a positive Indian Ocean Dipole (IOD) year.

7.1 Seasonal Cycle

Key Question 4. What seasonal effect does the Mascarene Plateau have on the geostrophic velocities, SST's and eddy kinetic energy in the region?

7.1.1 Geostrophic Velocities

Similarly to the previous chapter, the region around the Mascarene Plateau will be divided into 3 sections. Section 1 comprises of the region from the northern sector of the Seychelles Bank to the southernmost part of gap 1 (9.05° S). Section 2 comprises of the region between the southernmost part of gap 1 (9.05° S) to gap 2 (13.95° S) whilst section 3 comprises of the region south of 13.95° S to Mauritius.

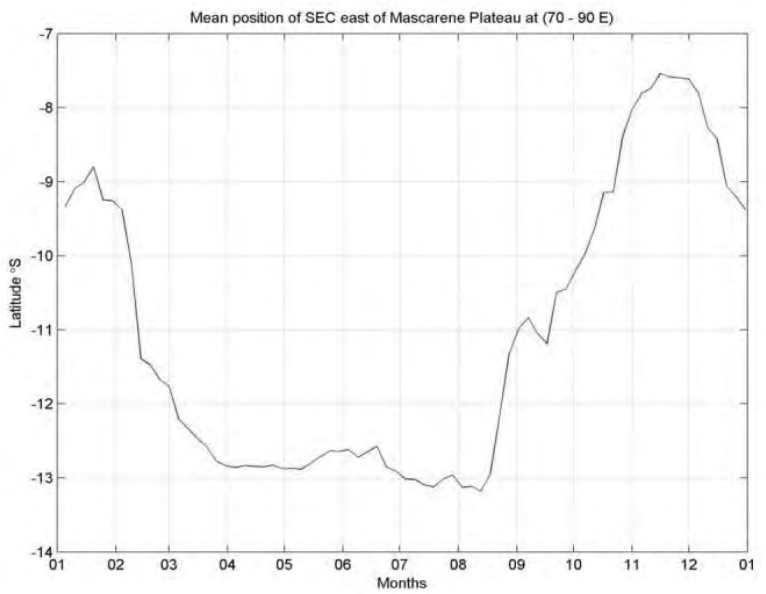

Figure 7. 3: Climatological position of the core (1995 – 2011) of the South Equatorial Current at 70° – 90° E. The core position is calculated from the maximum westward geostrophic velocities which occur between 6° - 20° S (New et al, 2005). (Data: AVISO Altimetry derived Geostrophic Velocities)

The mean position of the core ranges from a minimum of 7.5° S in November to a maximum of approximately 13° S from April to September (Figure 7.1). It is bimodal with a secondary maximum of 9° S in mid-January. The SEC moves northward during the austral summer. During this time, the volume transport increases through the northern gap (gap 1) within the Mascarene Plateau (chapter 6). However, there are other factors responsible for the increased volume transport through the northern gap such as a recirculation cell which will be discussed later.

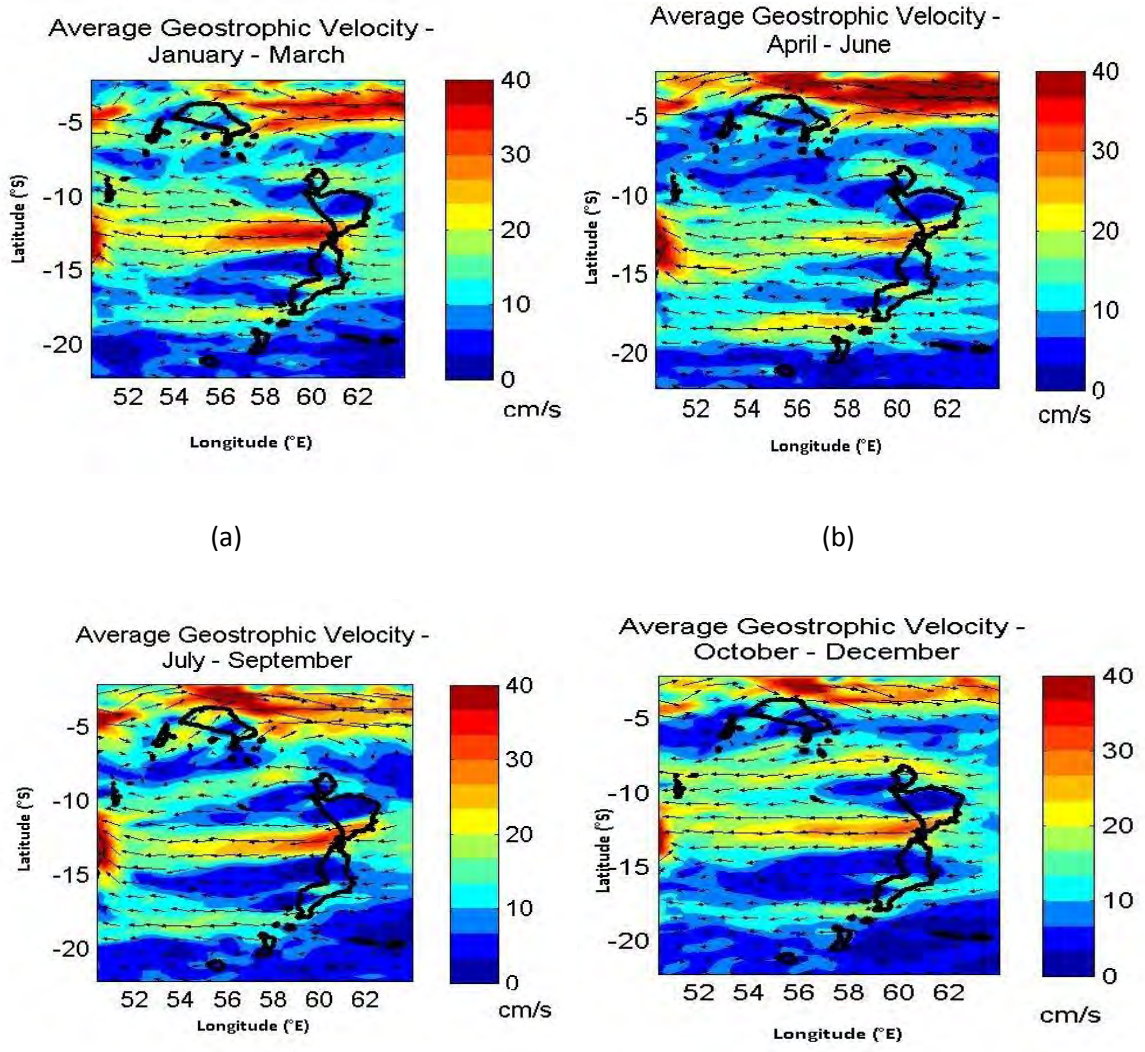

Figure 7. 4: Maps of Geostrophic Velocities (Climatology) for 4 seasons (cm/s). (a) – January – March (summer). (b) – April – June (autumn). (c) – July – September (winter). (d) October – December (spring). 1000m isobath overlaid in black. (Data: AVISO Altimetry derived Geostrophic Velocities).

Figure 7.2 depicts maps of Geostrophic Velocities (Climatology – 1995 - 2011) for 4 seasons. Main features are identified such as the SECC (South Equatorial Counter Current) north-east of the Seychelles Bank, the flow of the SEC (South Equatorial Current) through the 3 major gaps (SEC splits into 3 cores to the east of the Mascarene Plateau) and the 2 cores of the SEC downstream of the SEC. The SECC is

strongest during April to June (45 cm/s) and weakest during October to December (25 cm/s). The highest velocities in the Mascarene Plateau region occur within or just westward of all the gaps.

7.1.1.1 Section 1 (Northern sector of Seychelles Bank (3° S) – 9.05 °S)

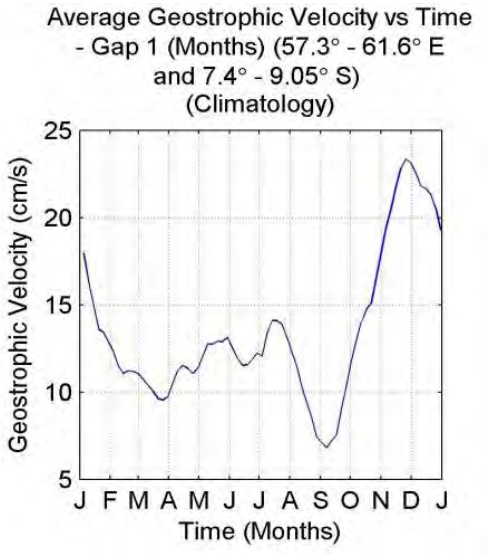

Figure 7. 5: Climatology (1995 – 2011) of altimetry derived geostrophic velocities through the Seychelles – Saya de Malha Gap. (units: cm/s) (Data: AVISO Altimetry derived Geostrophic Velocities)

Figure 7.3 depicts the climatological geostrophic velocity (1995 – 2011) through gap 1. This geostrophic velocity is due to one of the cores of the SEC which split to the east of the Mascarene Plateau. Gap 1 experiences highest velocities during October – December, peaking during December (23 cm/s) and its lowest velocities during August – September (7 cm/s). The climatological geostrophic velocity during the time of the Nansen cruise in October-November 2008 was 15 cm/s through gap 1. The geostrophic velocity during the time of the Nansen cruise was 20 cm/s (5 cm/s or 33% higher than the climatology data) through gap 1. The velocities were higher during the cruise as there was a re-circulation event through the gap during September 2008 which increased the geostrophic velocities and during the cruise in October/November 2008 there was still a minor effect on the circulation in the region which kept geostrophic velocities above the climatological average. As the year progresses, there is a gradual westward shift in the maximum geostrophic velocities of the SECC due to changes in ocean circulation in the northern Indian Ocean caused by the monsoon. It is apparent that a part of this current recirculates

and mixes with the SEC whilst flowing back westward through the gap 1. This then either supplements the northern core of the SEC or joins the SECC to the north in a recirculation loop. Gap 1 experiences the highest annual variation in maximum geostrophic velocity. Velocities during January – March do not increase from east to the west of the bank and remain at 11 cm/s. However, as the flow passes through the gap the velocity increases to 15 cm/s. Similarly, during April – June the velocity remains unchanged from the eastern side and western side of the plateau (9 cm/s) but through the gap it increases to 18 cm/s. During July – September velocities remain at 9 cm/s but increase to 20 cm/s through the gap whilst during October – December velocities increase from 10 cm/s to 18 cm/s (there is no decrease in velocity after it crosses the gap). All velocities to the west of the plateau are taken at 54° E.

7.1.1.2 Section 2 (9.05 °S – 13.95 °S)

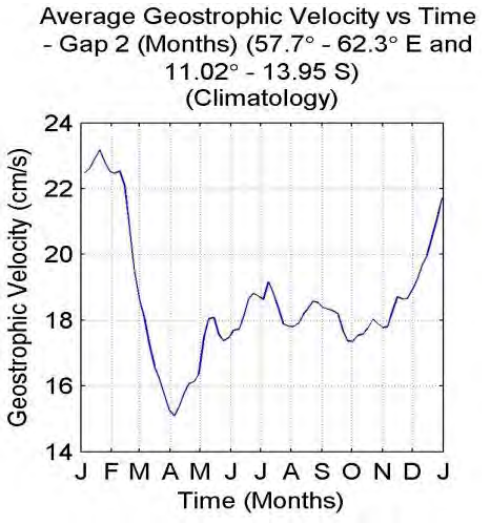

Figure 7. 6: Climatology (1995 – 2011) of altimetry derived geostrophic velocities through gap 2. (units: cm/s) (Data: AVISO Altimetry derived Geostrophic Velocities)

Figure 7.4 depicts the climatological geostrophic velocity (1995 – 2011) through gap 2. gap 2 experiences highest velocities during January – March peaking during January (23 cm/s) with its lowest velocities during April – June (16 cm/s). The geostrophic velocity through this gap has its origins in one of the cores of the SEC which split to the east of the Mascarene Plateau. The Northern core of the SEC downstream of the Mascarene Plateau forms between the Saya de Malha and Nazareth Bank with strongest velocities during January to March (~ 45 cm/s) and weakest velocities during April to June (~ 25 cm/s). The climatological geostrophic velocity during the time of the Nansen cruise in October-November 2008

was 18 cm/s. The geostrophic velocity during the time of the Nansen cruise through this gap was 40 cm/s (22 cm/s or 122% higher than climatology). The reason for the difference is due to the SEC not being a current of relative constant strength with time. However, the SEC can reach higher velocities through this gap as shown in section 5.3. Gap 2 has the effect of increasing the geostrophic velocity the greatest. From January – March the geostrophic velocity increases from 10 cm/s to a maximum value of 32 cm/s through the gap and drops to 20 cm/s westward of the Mascarene Plateau. From April – June the geostrophic velocity increases from 15 cm/s to a maximum of 25 cm/s and drops to 20 cm/s westward of the gap. From July – September the velocity increases from 15 cm/s to a maximum value of 30 cm/s and drops to 20 cm/s westward of the plateau whilst from October – December the velocity increases from 10 cm/s to 28 cm/s but drops to 20 cm/s westward of the plateau. All velocities to the west of the plateau are taken at 54° E.

7.1.1.2 Section 3 (13.95 °S – Mauritius (~ 20 °S))

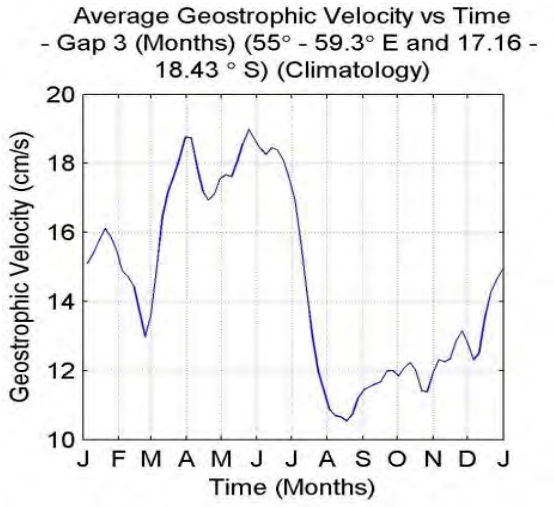

Figure 7. 7: Climatology (1995 – 2011) of altimetry derived geostrophic velocities through gap 3. (units: cm/s) (Data: AVISO Altimetry derived Geostrophic Velocities)

Figure 7.5 depicts the climatological geostrophic velocity (1995 – 2011) through gap 3. Gap 3 experiences highest velocities during April – June with its lowest velocities during August – November. The geostrophic velocity through this gap has its origins in 1 of the 3 cores of the SEC which split to the east of the Mascarene Plateau. The southern core to the SEC forms between the Cargados – Carajos Bank and Mauritius with strongest velocities during April to June (~ 25 cm/s) and weakest velocities

during October to December (~ 15 cm/s). The climatological geostrophic velocity during the time of the Nansen cruise in October-November 2008 was 11 cm/s. The geostrophic velocity during the time of the Nansen cruise through this gap was 15 cm/s (4 cm/s or 36% higher than climatology). This fits in well with the seasonal shift in the SEC upstream between 70° – 90° E (Figure 7.1) as this is the southernmost gap and the weakest velocities occur during October – December when the SEC migrates northward (to the east (70° – 90° E of the Mascarene Plateau). The velocity westward of gap 3 increases due to the constriction of the gap as well as augmented flows from further south (New et al. 2007). Velocities during January to March increase from approximately 5 cm/s in the east to 15 cm/s to the west of the plateau. During April – June velocities increase from 10 cm/s to 19 cm/s. During July – September velocities increase from 5 cm/s to 18 cm/s whilst during October – December velocities increase from 5 cm/s to 12 cm/s. All velocities to the west of the plateau are taken at 54° E.

As mentioned previously, these variations through the 3 gaps (highest and lowest geostrophic velocities at different times of the year depending on the gap) were most likely due to the seasonal shift in the SEC.

7.1.2 Sea Surface Temperatures (SST)

Figure 7.6 shows maps of SST climatology (1998- 2011) over the Mascarene Plateau for all seasons whilst Figure 7.7 depicts the seasonal cycle of SST through the 3 major gaps in the Mascarene Plateau. All gaps have a similar seasonal cycle (and is slightly bimodal in nature) except for a general decrease in SST from gap 1 to gap 3. The gaps experience highest temperatures around March (28 – 30 °C) whilst lowest temperatures occur around July to August (24 – 26 °C) (Figure 7.7). From Figure 7.6, on the large scale (entire Mascarene Plateau region), changes in temperature remain fairly zonal throughout the year. There is an increase in SST around shallower areas and the small islands which breach the surface such as within the Seychelles archipelago and Mauritius simply due to shallower water requiring less solar irradiance to heat up. The highest temperature through gap 1 is 30° C during April, whilst through gap 2 the highest temperature is 29.5° C and through gap 3 the highest temperature is 28.5° C during March. The lowest temperature through gap 1 is 26° C during August, whilst through gap 2 the lowest temperature is 25.5° C and through gap 3 the lowest temperature is 24° C during August.

The SST gradient (climatology) is calculated to see the effect the banks have on the SST (whether there is a significant change). The Seychelles Bank exhibits the greatest change in SST gradient in the order of 8

e^{-3} °C/km, whilst the change in SST gradient across the Saya de Malha and Nazareth Bank is relatively small, in the order of < 1 e^{-3} °C/km. The Seychelles Bank will exhibit the greatest change in SST gradient as this bank contains the shallowest bathymetry and there are many small islands over the bank. The change in SST gradient across the Cargados-Carajos Bank and gap 3 is in the order of 2 e^{-3} °C/km. As gap 3 is relatively small Mauritius has the effect of increasing this gradient.

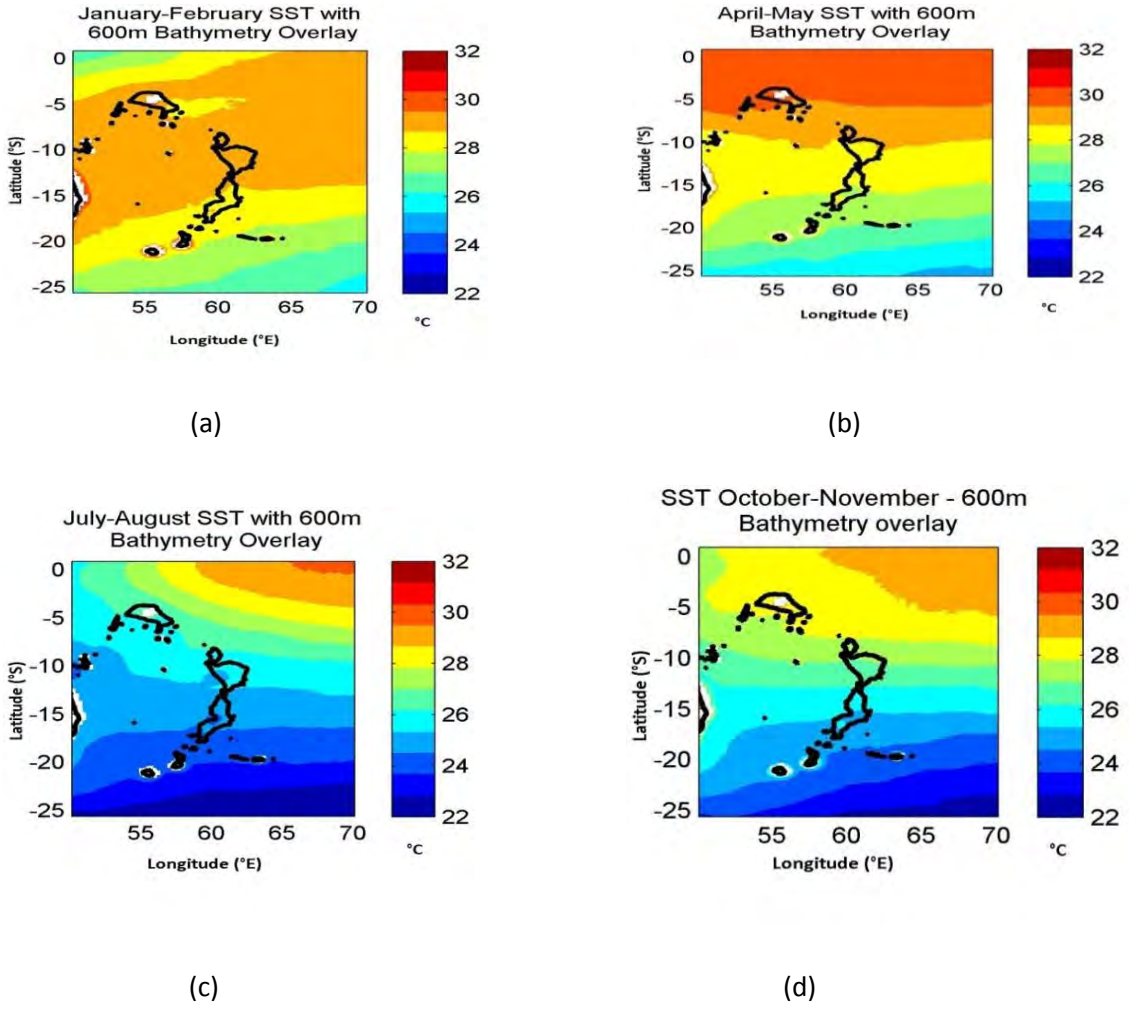

(a) (b)

(c) (d)

Figure 7. 8: Maps of seasonal TRMM SST climatology (°C) (1998 – 2011) across Mascarene Plateau (a – d). Isobath overlaid in black. (a) – January – February (summer), (b) – April – May (autumn), (c) – July – August (winter) and (d) – October – November (spring) (Data: TRMM Satellite SST)

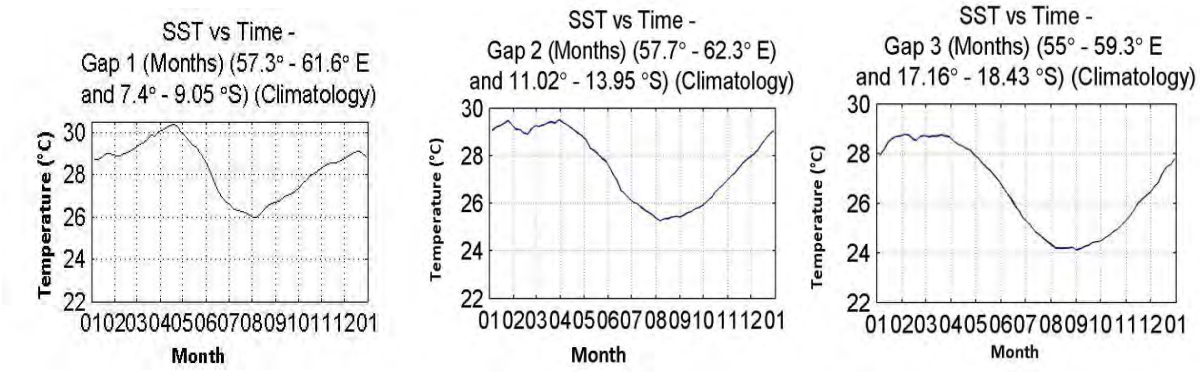

(a) **(b)** **(c)**

Figure 7. 9: SST Seasonal Cycle (°C) through the 3 Main Gaps in the Mascarene Plateau. Highest temperatures occur around March whilst lowest temperatures occur around July/August for all gaps.

7.2 Eddy Kinetic Energy

In this section eddy kinetic energy is investigated in the Mascarene Plateau region as well as the effect the plateau has on the EKE from the eastern side to the western side. It is important to investigate eddy kinetic energy since it serves as a proxy for eddy development (Fu et al, 2010). If eddies form in the region, they potentially have the ability to transport water masses away from the region.

7.2.1 Climatology

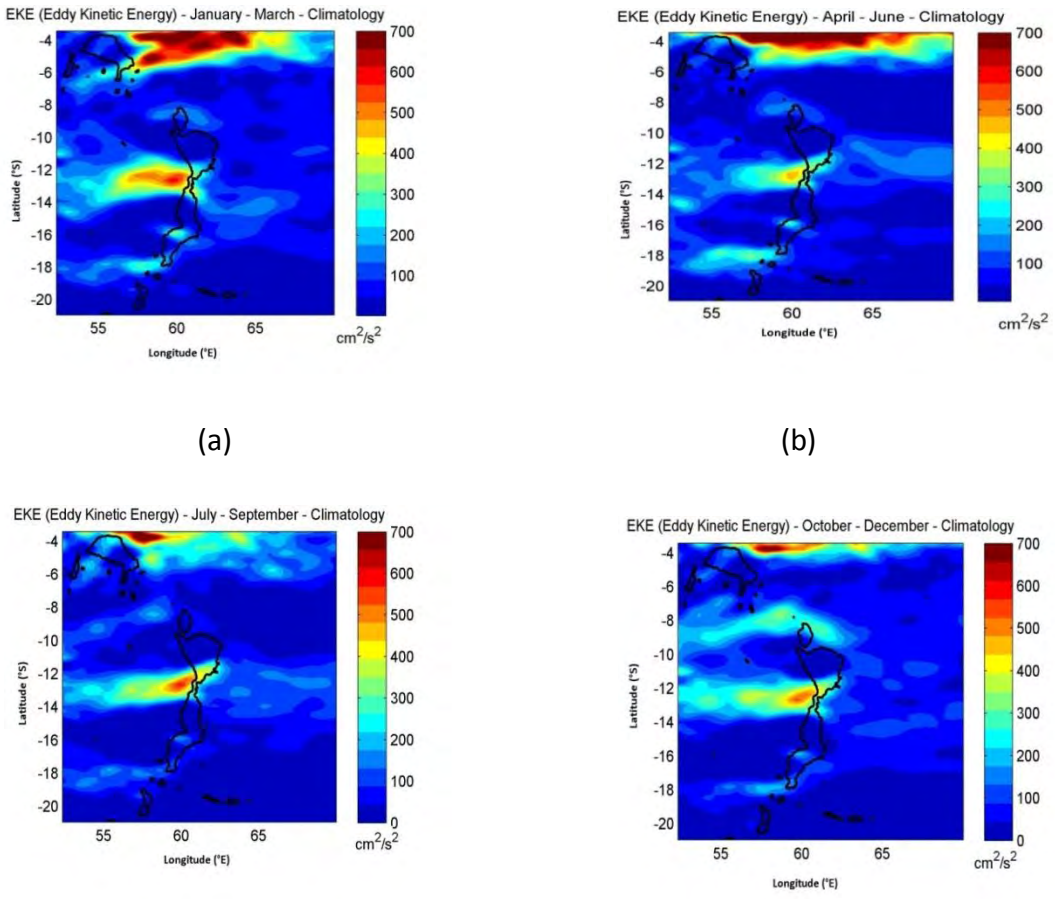

Figure 7. 10: Eddy Kinetic Energy Climatology (1997 – 2010) – 4 seasons. a) – summer, b) – autumn, c) – winter, d) – spring. There are 4 areas where EKE is pronounced (to the east of the Seychelles Bank due to the South Equatorial Counter Current (SECC) and to the west of the 3 major gaps due to the South Equatorial Current (SEC) in the Mascarene Plateau). 1000m isobath overlaid in black. (units: cm^2/s^2)

Figure 7.8 depicts the Eddy Kinetic Energy (cm^2/s^2) Climatology (1997 – 2010) – 4 seasons (a – summer, b – autumn, c – winter and d – spring). There are 3 major areas of high Eddy Kinetic Energy, namely, to the east of the Seychelles Bank, gap 2 and to the west of gap 3. There is also a pronounced signal from October – December in gap 1. All these areas of heightened EKE in the region are due to the South Equatorial Counter Current (SECC) passing through the region to the east of the Seychelles Bank and the

South Equatorial Current (SEC). The increased EKE through gap 1 from October – December (Figure 7.8d) is due to the position of the SEC upstream (70° – 90° E). The average position from October – December is 9° S (Figure 7.1) which is within the range of the latitude of gap 1. Since the SEC northward/southward migration during the year is linked to the monsoon circulation, the EKE climatology is linked to the monsoon. The average position of the SEC upstream during January – March is approximately 11.5° S (Figure 7.1) whilst the season with the highest EKE through gap 2 is during January – March (Figure 7.8a). The most southerly gap (gap 3) in the Mascarene Plateau experiences highest EKE's during April – June (Figure 7.8b) when the SEC upstream is at its most southerly point, 13° S (Figure 7.1). Note that all SEC positions upstream are taken at its core. Thus, the strength of the climatological EKE through the gaps in the Mascarene Plateau is proportional to the position of the SEC upstream.

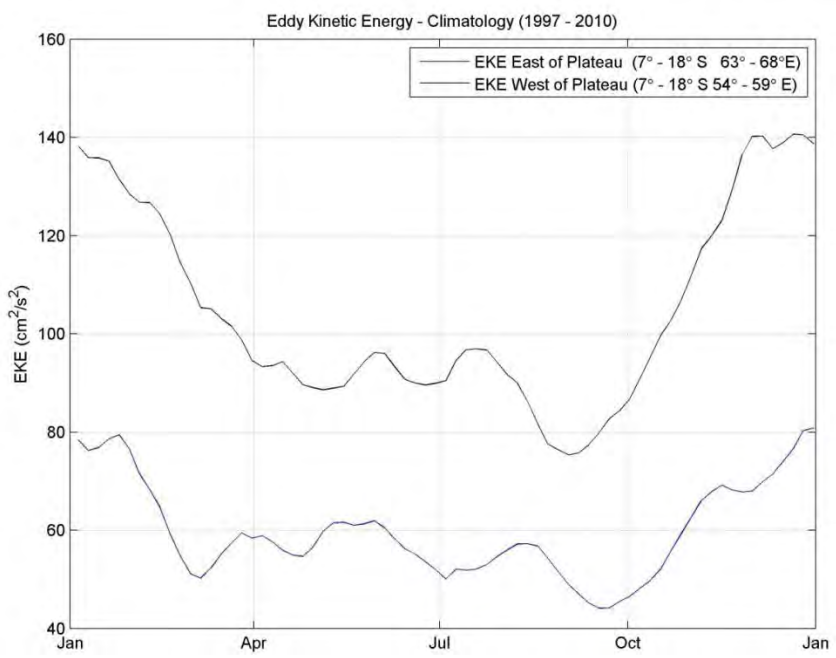

Figure 7. 11: Eddy Kinetic Energy (climatology – 1997 – 2010) west and east of the Mascarene Plateau averaged over the area 7° – 18° S and 63° – 68° E to the east of the plateau and 7° – 18° S and 54° – 59° E to the west of the plateau. Blue represents EKE to the east of the plateau whilst black indicates EKE to the west of the plateau.

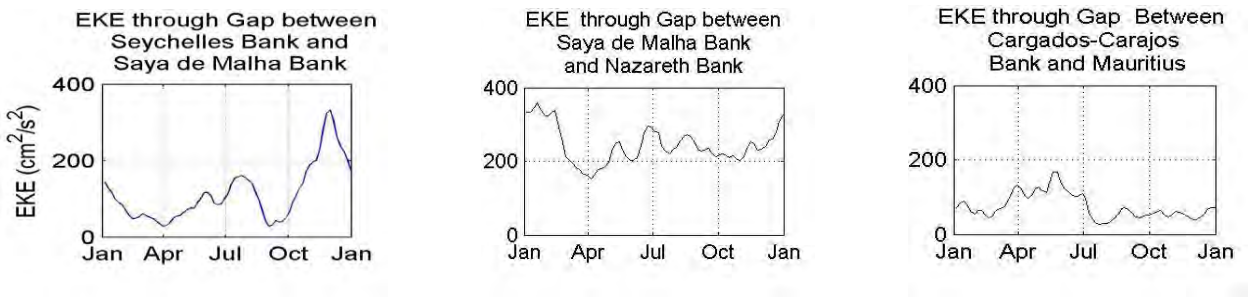

Figure 7. 12: Seasonal Cycle of Eddy Kinetic Energy through the 3 Major Gaps within the Mascarene Plateau. Highest EKE in gap 1 occurs during December (~ 350 cm^2/s^2) and highest values occur during January (~ 360 cm^2/s^2) through gap 2. Values remain below 200 cm^2/s^2 throughout the year in gap 3.

Figure 7.9 shows the EKE climatology (1997 – 2010) to the west and east of the Mascarene Plateau averaged over the areas depicted in the figure. The EKE to the west of the plateau is greater throughout the year due to the constriction of the gaps within the plateau which increases the geostrophic velocity. Figure 7.10 shows the seasonal cycle of Eddy Kinetic Energy through the 3 major gaps within the Mascarene Plateau. Highest EKE in gap 1 occurs during December (~ 300 cm^2/s^2, the highest EKE in gap 2 occurs during January (~ 300 cm^2/s^2) whilst gap 3 has the lowest EKE values for all the gaps (maximum values of approximately 190 cm^2/s^2).

There is a distinct seasonal cycle in the average EKE to the west and east of the Mascarene Plateau. To the west, maximum values reach 140 cm^2/s^2 around December/January whilst minimum values reach 75 cm^2/s^2 around September. To the east, maximum values reach 80 cm^2/s^2 around December/January and drop to a minimum of approximately 45 cm^2/s^2 during September. The major reason for the increased EKE to the west of the Mascarene Plateau is due to the increased speed of the SEC through the gaps of the Mascarene Plateau (specifically through gap 2). Eddy Kinetic Energy is highest in the region when the SEC flows through gap 1 (350 cm^2/s^2 - approximately December) and through gap 2 (360 cm^2/s^2 - approximately January). Here, the possibility for eddy formation is the greatest in the region. However, there has been no identification through satellite data or otherwise to suggest that mesoscale eddies are produced in this region apart from the stationary cyclonic eddy identified during the October/November 2008 Nansen cruise south of the Cargados-Carajos Bank (Figure 6.6) and the eddy formed during the re-circulation event during September 2008 (Figure 7.13). This is probably due to the coarse resolution of satellite estimate (1/3°). There may very well be smaller eddies in the region (< 50 km) which satellite data cannot detect. As the latitude of the core of the SEC to the east of the Mascarene Plateau increases (Fig 7.1), there is a drop in the EKE (both to the west and east of the

Mascarene Plateau). Thus, during the summer SW monsoon (Austral winter), the area surrounding the Mascarene Plateau experiences lower EKE's than during the winter NE monsoon (Austral summer) where the EKE's increase.

7.2.2 EKE during October/November 2008 Nansen Cruise

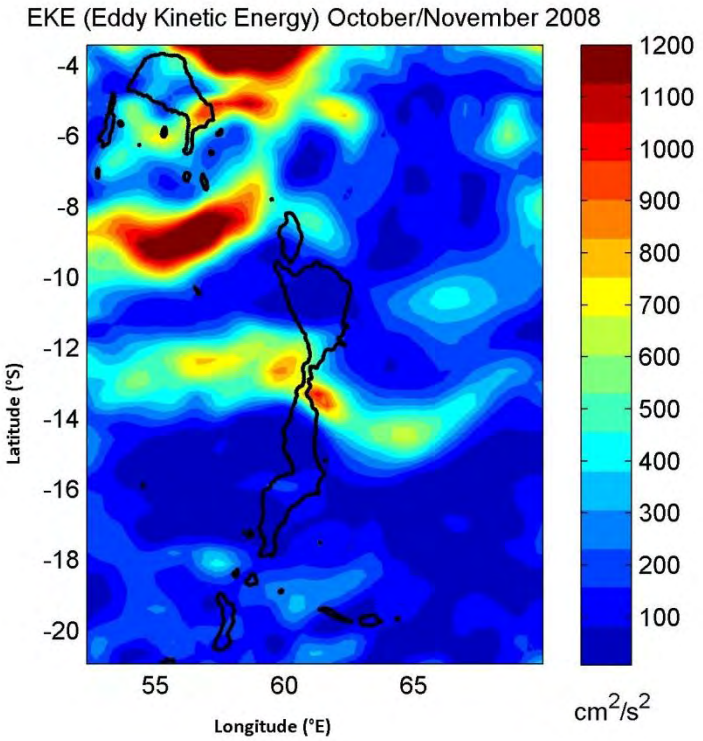

Figure 7. 13: EKE during the October/November 2008 Nansen Research Cruise. 1000m isobath overlaid in black. 2 areas of high eddy kinetic energy are observed to the west of gap 1 (> 1200 cm^2/s^2) and to the north-east of the Seychelles Bank (> 1200 cm^2/s^2).

Figure 7.11 shows EKE during the October/November 2008 Nansen Research cruise. There is a region of high EKE (> 1200 cm^2/s^2) to the west of gap 1 and to the north-east of the Seychelles Bank. The primary reasons for the relatively high EKE in these 2 regions is due to the above average speed of the SEC and SECC in the respective regions. Climatological values during October/November in the region of heightened EKE west of gap 1 and to the North-East of the Seychelles Bank are approximately 136.104 cm^2/s^2 and 408.96 cm^2/s^2 respectively whilst during October/November 2008 values were approximately

1250 cm^2/s^2 west of gap 1 and 1470 cm^2/s^2 to the north-east of the Seychelles Bank. The other 2 gaps within the Mascarene Plateau exhibited similar values to the climatology (500 cm^2/s^2 and 300 cm^2/s^2 through gap 2 and gap 3 respectively).

From the above, key question 4 can be addressed: *What seasonal effect does the Mascarene Plateau have on the geostrophic velocities, SST's and eddy kinetic energy in the region?*

The geostrophic velocities in the region are composed primarily of 2 currents, namely the westward flowing SEC (South Equatorial Current) and the eastward flowing SECC (South Equatorial Counter Current). The Mascarene Plateau has the effect of splitting the westward flowing SEC into 3 cores which flows through the 3 major gaps in the plateau. Westward of the plateau, the SEC is composed of a northern and southern core. The maximum velocity through gap 1 is approximately 24 cm/s during December whilst the minimum velocity is approximately 7 cm/s during September. The maximum velocity through gap 2 is approximately 23 cm/s during January whilst the minimum velocity is approximately 15 cm/s during April. The maximum velocity through gap 3 is approximately 19 cm/s during April whilst the minimum velocity is approximately 11 cm/s during August. The main reason for these differences in time of maximum/minimum geostrophic velocities is due to the position of the SEC upstream during the year. The re-circulation loop which occasionally forms in gap 1 also affects the climatology of that gap. The changes in SST in the region remain fairly zonal throughout the year (a general decrease with increasing latitude). The gaps experiences highest SST's during March with lowest SST's around August. Gap 1 experiences highest SST's of approximately 30° C with its lowest SST's of approximately 26° C, gap 2 experiences highest SST's of approximately 29° C with its lowest SST's of approximately 25° C whilst gap 3 experiences highest SST's of approximately 29° C with its lowest SST's of approximately 24° C. The Seychelles Bank has the effect of increasing the SST the greatest over the Mascarene Plateau as it is composed of the shallowest bathymetry and there are many small islands which has the effect of increasing the SST. The region around the Cargados-Carajos Bank and gap 3 has an effect of increasing the SST. As the gap in this region is not great (compared to gap 1), Mauritius has the effect of increasing the SST in the region. The region with the least effect on the SST is the region around the Saya de Malha and Nazareth Bank. However, it still has higher SST's than its surroundings offshore of the Mascarene Plateau. The eddy kinetic energy (EKE) has a distinct seasonal cycle through the 3 main gaps in the Mascarene Plateau. The maximum EKE through gap 1 is approximately 350 cm^2/s^2 during December with the lowest EKE during April with values of approximately 50 cm^2/s^2. The maximum EKE through gap 2 is approximately 360 cm^2/s^2 during January with the lowest EKE during

April with values of approximately 160 cm^2/s^2. The maximum EKE through gap 3 is approximately 150 cm^2/s^2 during June with minimum values of approximately 40 cm^2/s^2 during July. The Mascarene Plateau has the effect of increasing the EKE as the SEC is channeled through the 3 major gaps in the plateau and increases in velocity due to the constriction of the gaps. Hence the EKE is greater to the west of the Mascarene Plateau.

New information in this section obtained includes:

- The core of the South Equatorial Current between 70° – 90° E changes in latitudinal position depending on the season and seems to have an effect on the speed of the SEC through the 3 gaps in the Mascarene Plateau. The core of the SEC moves northward during the austral summer whilst remains at approximately 13° S from April – September (most southerly extent throughout the year). From April – September, gap 3 experiences its highest geostrophic velocities whilst during the austral summer gap 1 and 2 experiences an increase in geostrophic velocities.
- SST gradients over the banks of the Mascarene Plateau are greatest over the Seychelles Bank, followed by the region surrounding Mauritius and gap 3 and finally over the Saya de Malha and Nazareth Banks. The gradient will be highest over the Seychelles Bank as this bank contains the most islands over the Mascarene Plateau.
- The eddy kinetic energy (EKE) in the region increases from the eastern side of the Mascarene Plateau to the western side. The primary reason for this is due to the constriction of the 3 gaps in the Mascarene Plateau which increases the velocities and hence the EKE increases. There is a distinct seasonal cycle in the EKE in this region throughout the year with highest EKE's during the austral summer. The EKE during the Nansen cruise in October/November 2008 was generally greater than the EKE during the RRS Charles Darwin cruise in June/July 2002.
- Since EKE serves as a proxy for eddy development, there is a greater chance for the formation of eddies to the west of the Mascarene Plateau as well as during the austral summer.
- Any eddy development in the area has the ability to transport water masses away from the region most likely towards Madagascar.

7.3 General Dynamics around the Mascarene Plateau (Geostrophic Velocity and SST)

Key Question 5. What is the nature of the SEC in the region and how do the geostrophic velocities during the 2008 cruise year differ from climatology?

The region around the Mascarene Plateau will be divided into 3 sections which have the same boundaries as that in 4.1.1.

7.3.1 Section 1 (Northern sector of Seychelles Bank (3° S) – 9.05 °S)

Figure 7.12 depicts a time series of geostrophic velocities in 2002 (red), 2008 (blue) as well as the climatology (black) through gap 1. 2002 and 2008 were the years when the 2 cruises occurred. The time series are shown to see if there are any substantial differences between the climatology and 2002/2008. The time series indicates that there are geostrophic velocities during both 2002 and 2008 which are significantly greater than the climatology.

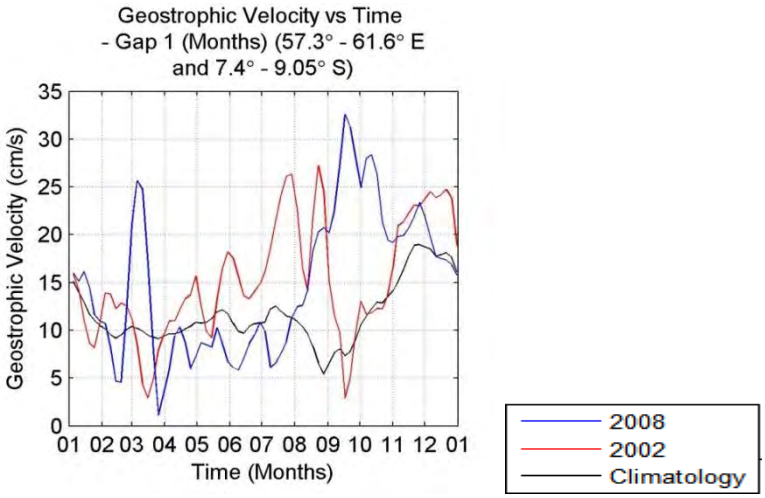

Figure 7. 14: Time Series of Geostrophic Velocities through gap 1 (Climatology, 2002 and 2008). Blue represents 2008, red represents 2002 whilst black represents the climatology (1995 – 2011) of the geostrophic velocities. Areas of heightened geostrophic velocity can be seen during September 2008

Geostrophic velocities are significantly higher during September 2008 when compared to the climatology. Velocities are 20 cm/s greater than the climatological value of 10 cm/s during September 2008.

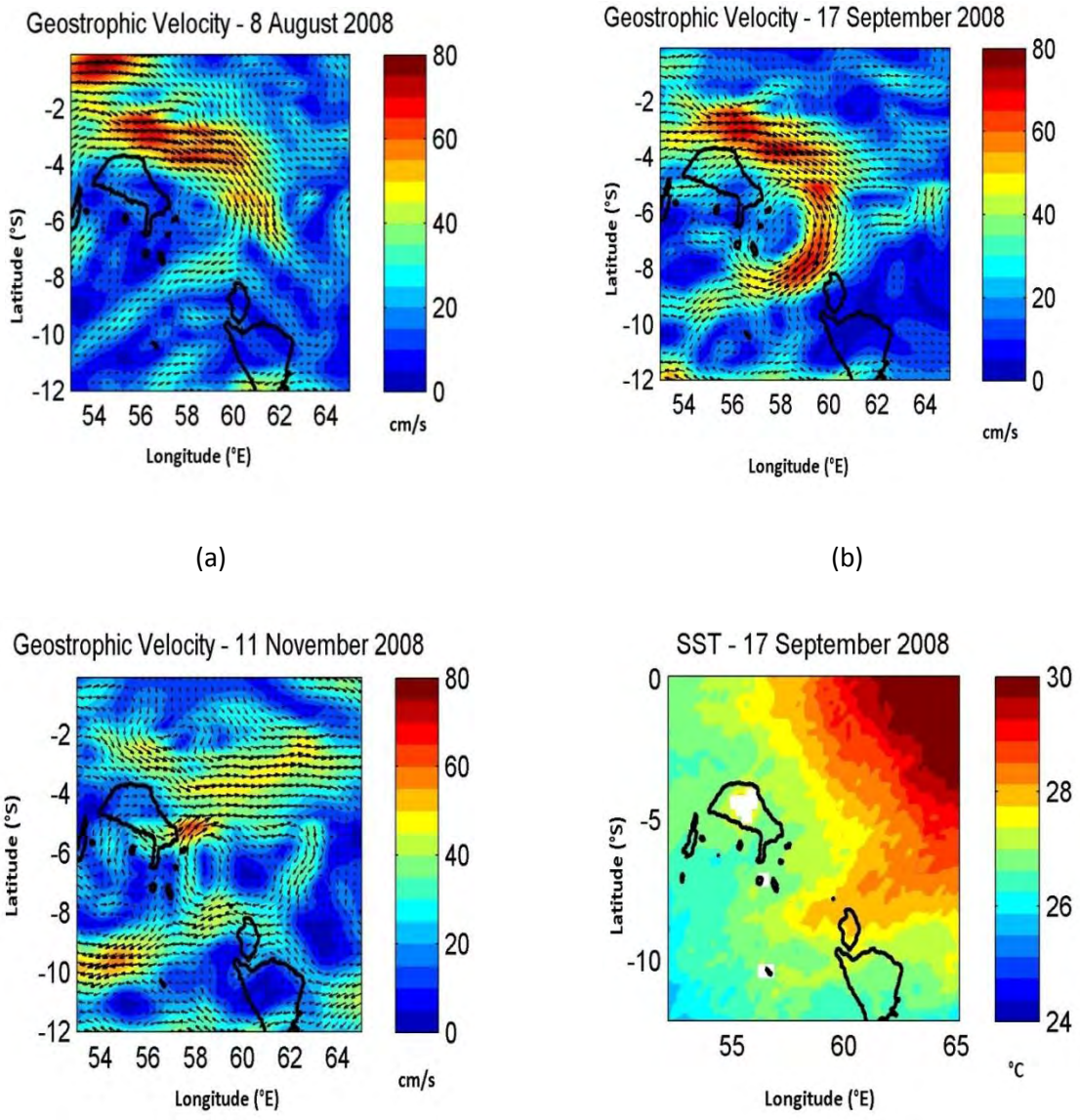

Figure 7. 15: Maps of Geostrophic Velocities (cm/s) and SST (°C) across gap 1. 1000m isobath overlaid in black. (a) Start of the re-circulation event date (8 August 2008) (b) maximum speeds of the re-circulation event through the gap (17 September 2008), (c) geostrophic velocity at the end of the event on 11 November 2008 whilst (d) SST during the peak of the event.

The anomalous velocity during September 2008 (maximum velocities reach 32 cm/s) is due to re-circulation from the SECC through gap 1 and hence geostrophic velocities increase. Figure 7.13 represents the geostrophic flow in the area before, during and after the re-circulation event in 2008. (a) Represents the start of the re-circulation event where a cyclonic eddy forms which starts to draw in flow from the eastward flowing SECC, (b) represents the maximum speeds of the re-circulation event through the gap which are approximately 70 cm/s (17 September 2008), (c) represents the end of the event on 11 November 2008 where speeds diminish to approximately 40 cm/s whilst (d) represents the SST in the region during the peak of the event (27° C). Minimal change in SST is evident as SECC has little variation in temperature to its surrounding regions. This event lasted for approximately 3 months. Towards the end of the event (11 November 2008), the cyclonic eddy drastically reduces in size and there is slightly extra flow from the south. The ASCLME research cruise in 2008 missed this event by a couple of weeks. During the re-circulation, the salinity content in the gap is higher since there is more Arabian Sea High Salinity Water (ASHSW) in the area as much of the water in the re-circulation loop has its origins from the SECC (the SECC primarily contains ASHSW in the surface waters). These re-circulation events increase the variability of the geostrophic velocities within gap 1.

The comparison between the 2002 and 2008 average geostrophic velocities through gap 1 vary substantially from each other and the climatology. The average geostrophic velocity from January – May of 2002 and 2008 are similar with the exception of a spike at the beginning of March 2008 where the average geostrophic velocity was 25 cm/s whilst during March 2002 the average geostrophic velocity was less than 10 cm/s. From May – August, the average geostrophic velocities were greater during 2002 than during 2008 by approximately 10 – 15 cm/s whereas from August – November the average geostrophic velocities were greater during 2008 than during 2002. Here, the maximum difference reached approximately 30 cm/s. During the rest of the year the average geostrophic velocities were similar. The reasons for the difference in these geostrophic velocities are either due to the development of a recirculation loop or an oscillation in the strength of the SEC.

7.3.2 Section 2 (9.05 °S – 13.95 °S)

Figure 7.14 depicts a time series of geostrophic velocities in 2002 (red), 2008 (blue) as well as the climatology (black) through gap 2. The time series are shown to see if there are any substantial differences between the climatology and 2002/2008

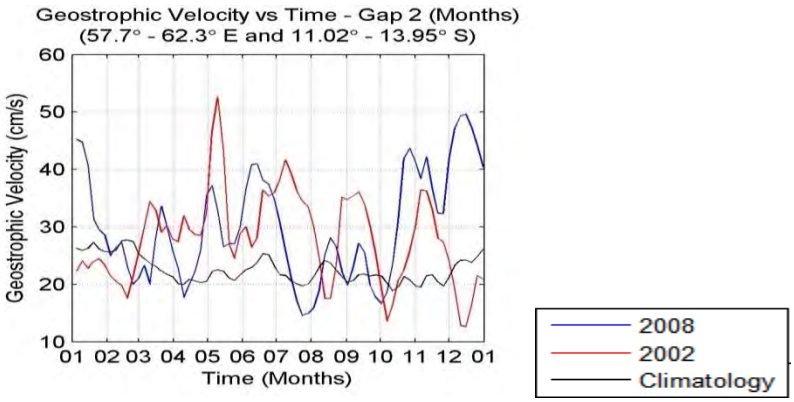

Figure 7. 16: Time Series of Geostrophic Velocities through gap 2 (Climatology (1995 – 2011), 2002 and 2008). Blue represents 2008, red represents 2002 whilst black represents the climatology of the geostrophic velocities. Areas of heightened geostrophic velocity can be seen during December 2008

Geostrophic velocities are significantly higher during December 2008 when compared to the climatology. Velocities are 25 cm/s greater than the climatological value of 25 cm/s during December 2008.

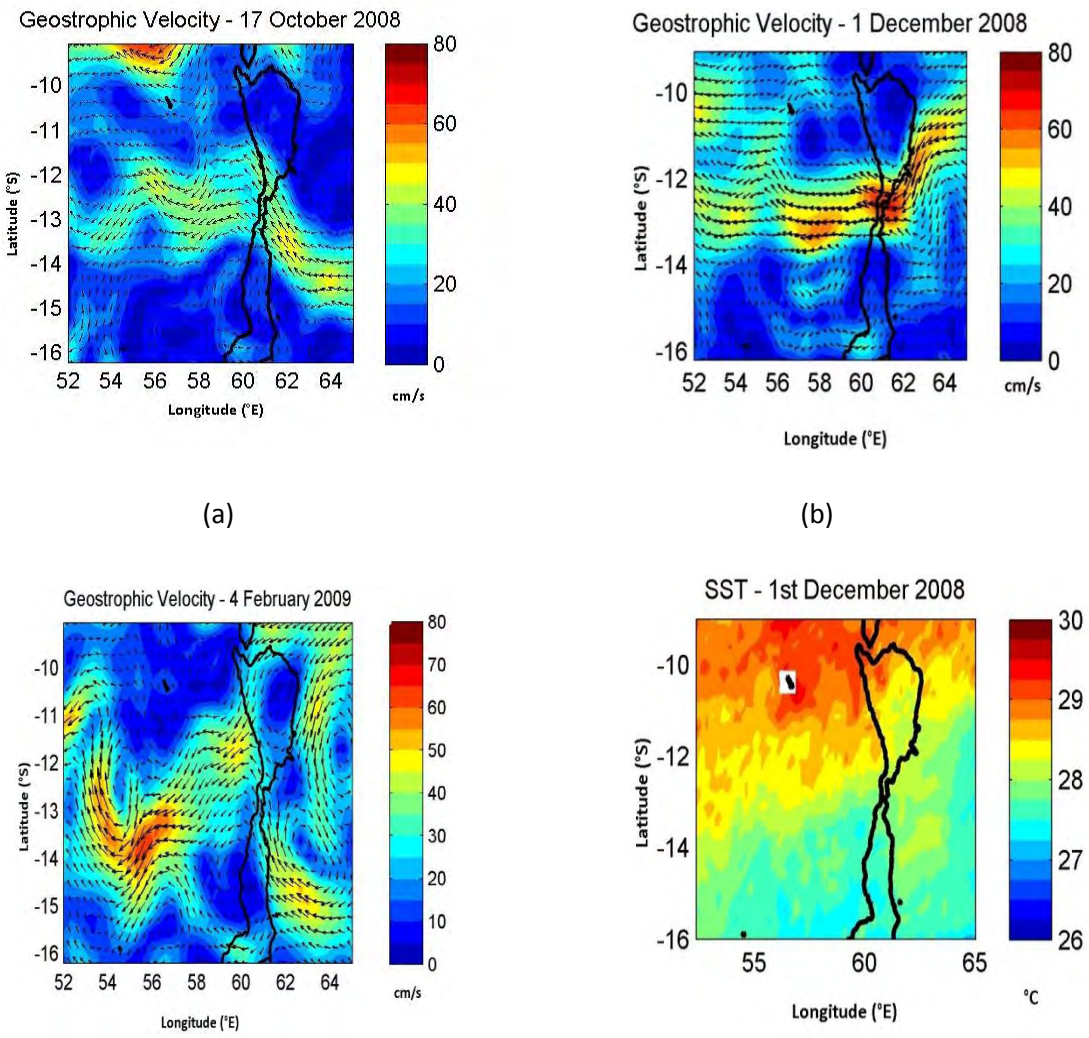

Figure 7. 17: Maps of Geostrophic Velocities (cm/s) and SST (°C) across gap 2. 1000 m isobath overlaid in black. (a) Start (17 October 2008) of the event, (b) maximum geostrophic velocity in the gap (1 December 2008), (c) end of the event (4 February 2009) and (d) SST during the event.

From mid October 2008 – early February 2009 there is an increase in geostrophic velocity through gap 2 as shown in Figure 7.15. The South Equatorial Current (SEC) in this region appears to oscillate. (a) Represents the start (17 October 2008) of the event where there is an oscillation in geostrophic velocity in gap 2 where geostrophic velocities reach approximately 35 cm/s, (b) represents the maximum geostrophic velocity (50 cm/s) in the gap (1 December 2008) whilst (c) represents the end of the event on 4 February 2009 where geostrophic velocities reduce to approximately 20 cm/s and (d) shows little

temperature variation during the event as the SEC has a similar SST to its surroundings. The peak in velocity of this event shows that the strength of the current can be much greater than during the 2008 ASCLME cruise since there was no strong oscillation during October/November 2008. The nature of the SEC (the oscillating current) increases the variability of the SEC in gap 2. The time series during both 2002 and 2008 shows that the SEC oscillates throughout the year but it remains higher than the climatology for most of the respective years.

The comparison between the 2002 and 2008 average geostrophic velocities through gap 2 indicate spikes in the average geostrophic velocities at different times of the respective years. For example, during May 2002, the average geostrophic velocity reached 53 cm/s whilst at the same time of the year during 2008 (May) there was no spike in the average geostrophic velocity (compared to the average geostrophic velocity for 2008). However, there was a spike in average geostrophic velocity during December 2008 where velocities reached 50 cm/s but in December 2002 velocities were below the climatological norm and were approximately 15 cm/s.

7.3.3 Section 3 (13.95 °S – Mauritius (~ 20 °S))

Figure 7.16 depicts a time series of geostrophic velocities in 2002 (red), 2008 (blue) as well as the climatology (black) through gap 3. The time series are shown to see if there are any substantial differences between the climatology and 2002/2008.

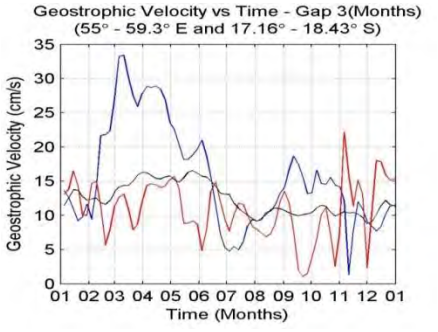

Figure 7. 18: Time Series of Geostrophic Velocities through gap 3 (Climatology (1995 – 2011), 2002 and 2008). Blue represents 2008, red represents 2002 whilst black represents the climatology of the geostrophic velocities. Areas of heightened geostrophic velocity can be seen during March 2008

Geostrophic velocities are significantly higher during March 2008 when compared to the climatology. Velocities are 15 cm/s greater than the climatological value of 15 cm/s during March 2008. Similarly to gap 2, the current oscillates during the year through gap 3 but during most of 2002, the current is weaker than the climatology.

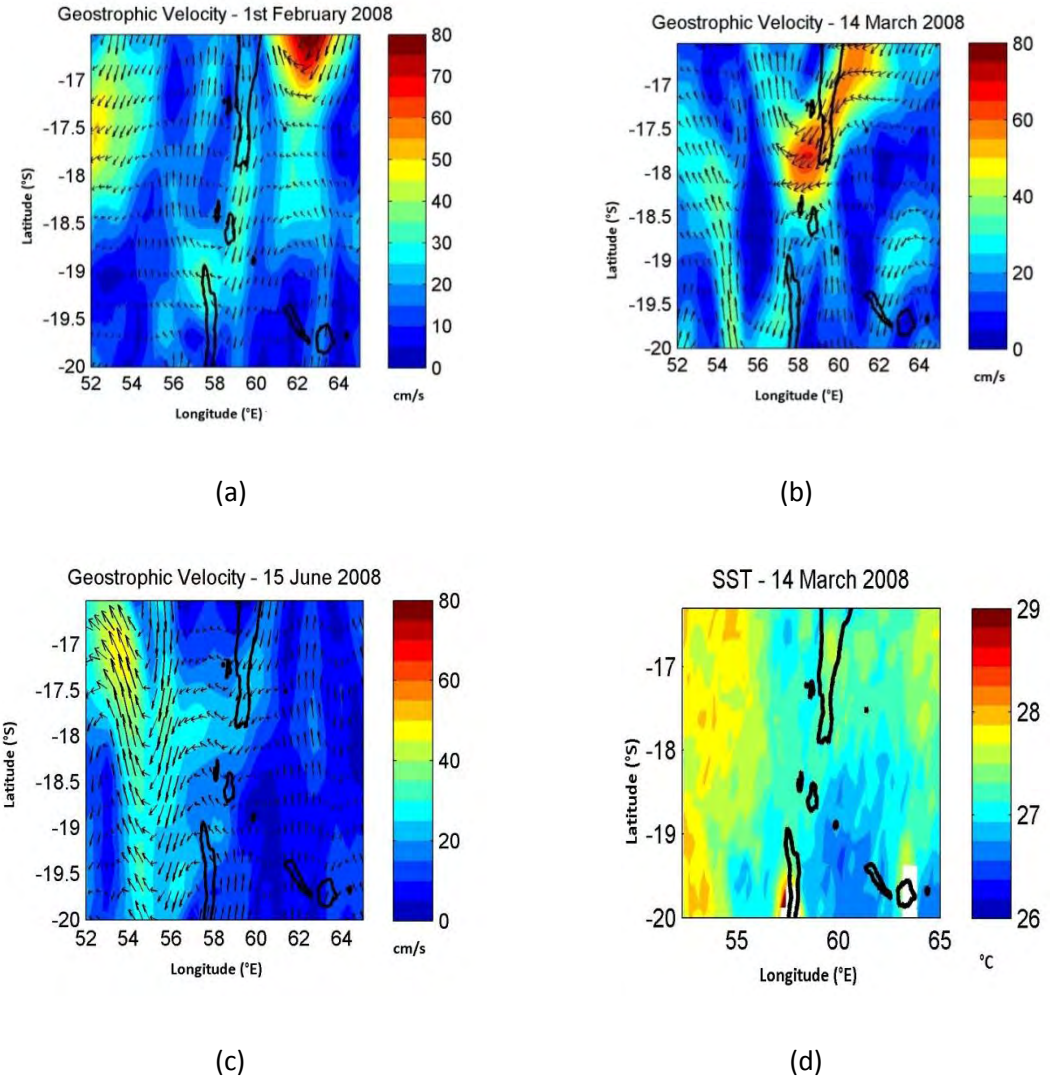

Figure 7. 19: Maps of Geostrophic Velocities (cm/s) and SST (°C) across Cargados-Carajos – Mauritius Gap. 1000m isobath overlaid in black. (a) start (1 February 2008) of the event, (b) maximum geostrophic velocity in the gap (14 March 2008), (c) end of the event (15 June 2008) and (d) temperature variation during the event.

Figure 7.17 shows an event where the geostrophic velocity increases to approximately 33 cm/s (15 cm/s greater than the climatology). (a) Represents the start (1 February 2008) of the event where there is an oscillation in geostrophic velocity (25 cm/s) in gap 3, (b) represents the maximum geostrophic velocity in the gap (14 March 2008) where velocities reach 60 cm/s through the gap whilst (c) represents the end of the event on 15 June 2008 (velocities approximately 20 cm/s) and (d) shows little temperature variation during the event. This event is once again due to an oscillation of the SEC and the oscillation increases the variability of the current in this gap.

The comparison between the 2002 and 2008 average geostrophic velocities through gap 3 indicate 2 periods in the year where the average geostrophic velocities vary drastically. From February – June 2008 there is an increase in geostrophic velocity reaching a peak of approximately 33 cm/s in March. During this same period of the year in 2002 there were no major spikes in the velocity and followed the climatology closely. The reason for the major difference in geostrophic velocity here is due to a major oscillation in the strength of the SEC. The other period in the year where there is a significant difference in geostrophic velocity between 2002 and 2008 is between September – October. During 2002, the average geostrophic velocity dropped to approximately 3 cm/s at the end of September whilst at the end of September during 2008 the velocity reached 16 cm/s. Once again, this is due to no oscillation happening through this gap at this time during 2002.

From the above, key question 5 can be addressed*: What is the nature of the SEC in the region and how do the geostrophic velocities during the 2008 cruise year differ from climatology?*

The South Equatorial Current (SEC) is not a constant current with regards to velocity. The geostrophic velocity through gap 2 and 3 oscillates (2 branches of the SEC). When a re-circulation loop forms in gap 1, it hinders the westward progression of the SEC through the gap as the re-circulation loop contains waters predominantly from the eastward flowing SECC. During 2008 in gap 1 a re-circulation loop developed which increased velocities up to 32 cm/s during September 2008 whereby the climatology during that time was 10 cm/s. Other than during this event, the geostrophic velocities through this gap was similar to the climatology. There was a period of increased geostrophic velocity from mid October 2008 – early February 2009 in gap 2 with a peak in early December 2008 with values of approximately 50 cm/s with climatological values in December of 25 cm/s. This increased velocity was due to an oscillation of geostrophic velocity (nature of the SEC). The geostrophic velocity through this gap was higher than the climatology throughout the year and was of an oscillatory nature. Similarly, due to an oscillation of geostrophic velocity in gap 3 during February – June 2008, velocities reached up to 33 cm/s

during March 2008 where the climatology is approximately 15 cm/s. For the rest of 2008, the geostrophic velocity was lower but there was still an oscillation where the maximum velocity was 18 cm/s during September 2008 (climatology is 12 cm/s). During this event the geostrophic current was lower than the climatology during November 2008 where it was 5 cm/s and the climatology is 10 cm/s.

New information in this section obtained includes:

- Confirmation that a recirculation loop is a regular feature and not an anomaly (observed by New et al, (2007)) through gap 1 and during such an event much of the water which flows westwards through gap 1 recirculates and flows back eastwards via the SECC.
- The SEC is not a constant current with regards to geostrophic velocities. It rather acts as an oscillating current.

7.4 Summary

This chapter made use of satellite estimate to study the seasonal cycle of geostrophic velocities, SST's and eddy kinetic energy. The Mascarene Plateau split the SEC into 3 cores which are subsequently channeled through the 3 main gaps in the Mascarene Plateau. Downstream of the plateau, 2 cores are formed with the strongest core (highest velocity) being the northern core which is composed of the flow between the Saya de Malha and Nazareth Banks and to a lesser degree, the flow between the Seychelles and Saya de Malha Banks. The SST generally decreases from north to south and is of a zonal nature. The SST gradient is the greatest over the Seychelles region probably because this region contains many small islands and shallow water which could increase the SST. The lowest SST gradient in the region is across the Saya de Malha and Nazareth Banks whilst the SST gradient between the Cargados-Carajos Bank and Mauritius is lower than the Seychelles region but higher than the region across the Saya de Malha and Nazareth Banks. Mauritius has the effect of increasing the SST gradient in this region as waters will be warmer closer to the island. Time series of geostrophic velocities during 2008 and maps of geostrophic velocity in the region of the Mascarene Plateau show that there is an increase in velocity through gap 1. This is due to the development of a re-circulation loop where waters from the SECC are drawn south and are channeled through the gap. Similarly, maps of geostrophic velocity and time series during 2008 show that the SEC is not constant in speed in the region as shown by periods of alternating high and low velocities through gap 1. Gap 3 has similar oscillations in velocity. Maps of eddy kinetic energy shows

that areas where EKE is higher than normal are to the east of the Seychelles Bank (downstream of the SECC) and to the west of the 3 major gaps in the Mascarene Plateau (downstream of the SEC). The EKE increases to the west of the Mascarene Plateau due to increased geostrophic velocities caused by the constriction of the gaps

The following chapter investigates the phytoplankton biomass in the region via satellite estimate. The types of water masses and the amount of upwelling (wind stress curl indicates potential upwelling conditions) determines the amount of Chl-a in the region. The climatology and seasonal cycles for phytoplankton biomass will be ascertained over the banks of the Mascarene Plateau and regions offshore of the banks. It will be ascertained whether there are any differences between the seasonal cycles on and off the banks. The variability over the region will also be investigated.

CHAPTER 8: Phytoplankton Biomass in the Mascarene Plateau Region

Chapter 4, 5, 6 and 7 analyzed the physical oceanography of the region. The water masses during the Nansen 2008 cruise were analyzed to determine how much mixing occurred. The westward flowing South Equatorial Current (SEC) contains relatively fresh Indonesian Throughflow Water (ITW) and Tropical Surface Water (TSW). The SEC splits into 3 cores east of the Mascarene Plateau and is channeled through the 3 major gaps of the bathymetric feature. These fresh water masses mix with high salinity Arabian Sea High Salinity Water (ASHSW) over the northern part of the plateau whilst they mix with high salinity Sub Tropical Surface Water (STSW) over the southern part of the plateau. STSW is only found south of gap 2 (the branch of the SEC through gap 2 acts as a barrier to STSW). ASHSW contains nutrient rich waters whilst STSW contains nutrient poor waters. This partly explains the distribution of Chl-a in Fig 8.1. On occasions, a re-circulation loop is formed through gap 1 which increases the amount of nutrient rich ASHSW in the region as most of the water in the loop has its origins in the SECC which contained ASHSW. This chapter will identify the phytoplankton biomass in the region using satellite estimate. Chl-a acts as a proxy for phytoplankton biomass. Along with the type of water mass, the amount of upwelling also determines the nutrient content of waters in the region and wind stress curl estimated from satellite remote sensing is also used below.

Key Question 6. What is the distribution of Chl-a in the region (climatology) and do the banks differ in Chl-a concentration from its surrounding areas?

8.1 Climatology

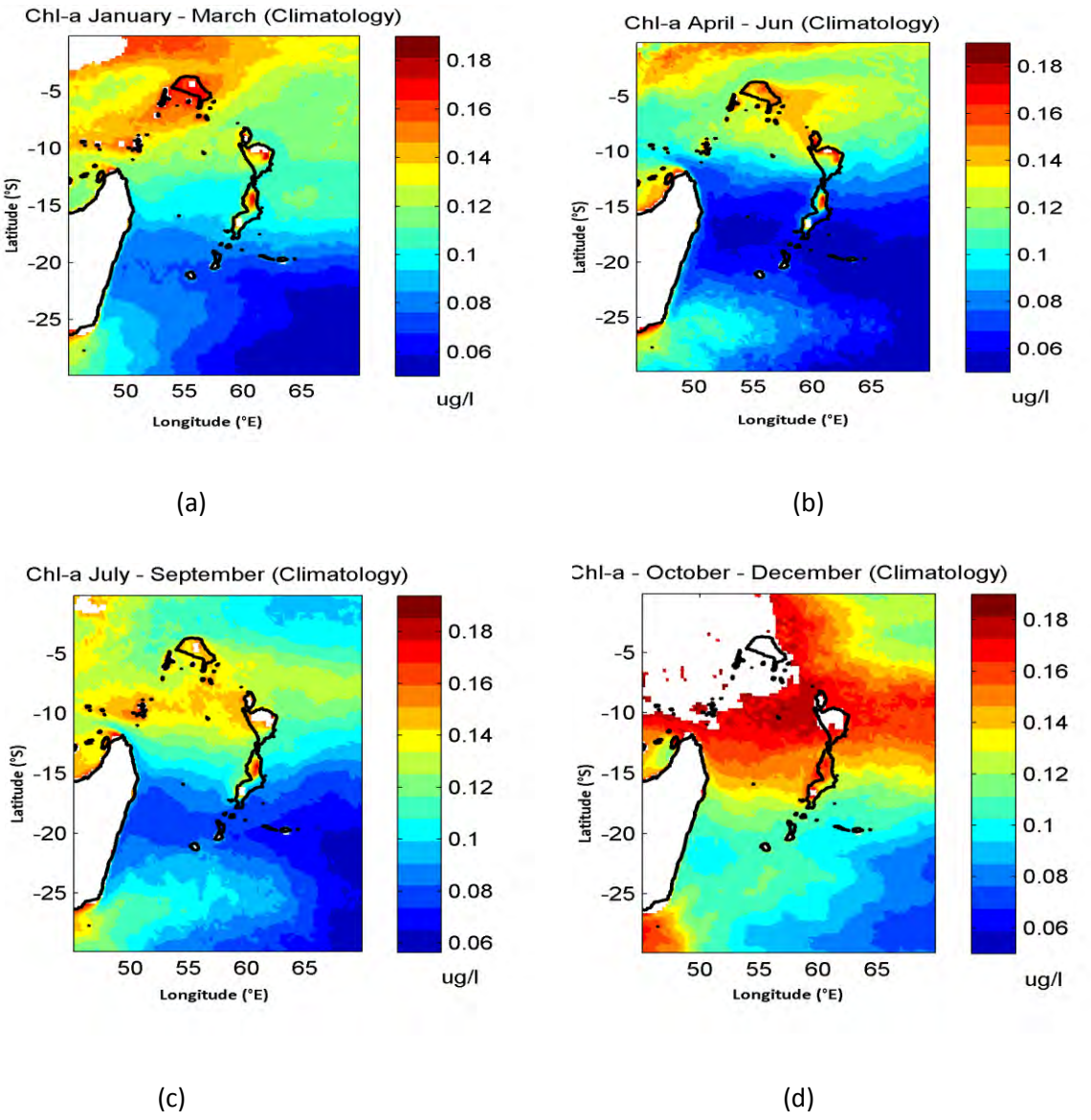

Figure 8. 1: Climatology of Chlorophyll-a (period 1998 – 2010). (a) represents summer, (b) represents autumn, (c) represents winter whilst (d) represents spring. (units: ug/l)

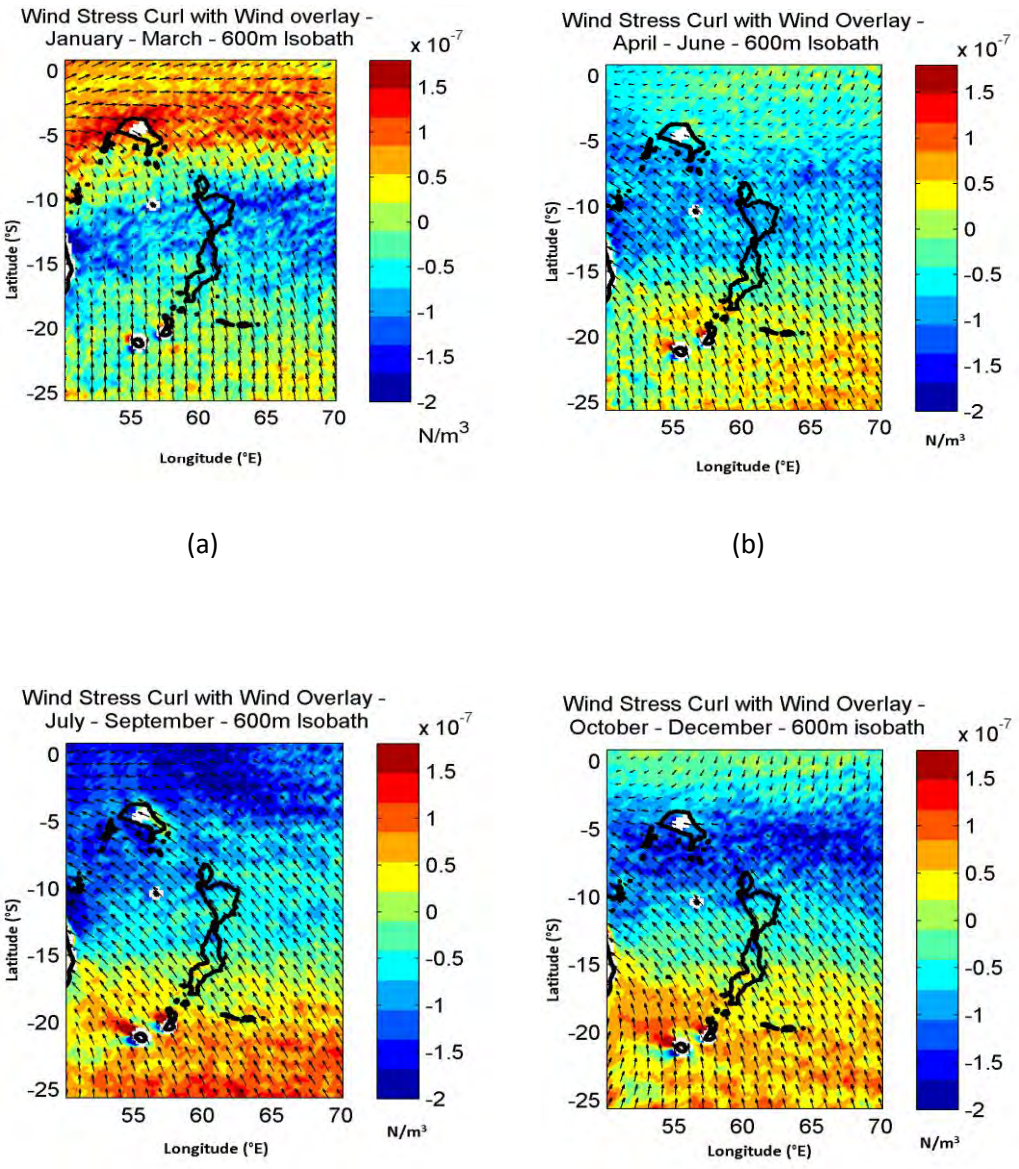

Figure 8. 2: Climatology of Wind Stress Curl (with wind overlay) – period 1998 – 2010. Highest wind stress curl values occur during January – March north of 13° S where values reach 1.5e^{-7} N/m^3. Lowest values occur north of 10° S during July – September where values drop to approximately -1.7e^{-7} N/m^3. (a) Represents summer, (b) represents autumn, (c) represents winter whilst (d) represents spring. 1000m isobath overlaid in black.

Figure 8.1 shows the climatology for Chl-a for January – March (a), April – June (b), July – September (c) and October – December (d) respectively while Figure 8.2 shows the corresponding wind stress curl. During all 4 seasons, the Saya de Malha, Nazareth and Cargados-Carajos Banks retain similar Chl-a values unlike the surrounding regions. During all seasons, Chl-a concentration is higher in the northern region (north of ~ 13° S). Nutrient rich ASHSW is dominant north of approximately 11° S whilst nutrient poor STSW is dominant south of approximately 13° S. Apart from Madagascar (coloured in white), the white patches represent Chl-a values > 2 ug/l. Since Chl-a is an indicator for phytoplankton biomass, ocean colour represents the concentration of phytoplankton biomass in the surface waters.

The period from January – March (Figure 8.1a) had the lowest concentration of Chl-a during the year whilst a strong positive wind stress curl occurred during January – March with values as high as $1.5e^{-7}$ N/m^3 (Figure 8.2a). This positive wind stress curl indicates downwelling and hence a lower Chl-a concentration. However Chl-a values increase northward of approximately 13° S (the latitude between the Saya de Malha Bank and the Nazareth Bank). The other two periods (April – June and July – September) also showed an increase of Chl-a concentration northward of 13° S. October – December showed a dramatic increase in Chl-a values and remain high as far south as the Cargados-Carajos Bank. The concentrations of Chl-a depend not only on upwelling but on the types of water masses in the region. July– September has a negative wind stress curl with values as low as $-1.5e^{-7}$ N/m^3 (Figure 8.2c). This indicates potential upwelling of nutrient rich waters. The northern part of the region (latitudes lower than ~ 13° S) had higher concentrations of Chl-a all year long but no negative value of wind stress curl all year long. This is due to the presence of nutrient rich water masses to the north and nutrient poor water masses to the south.

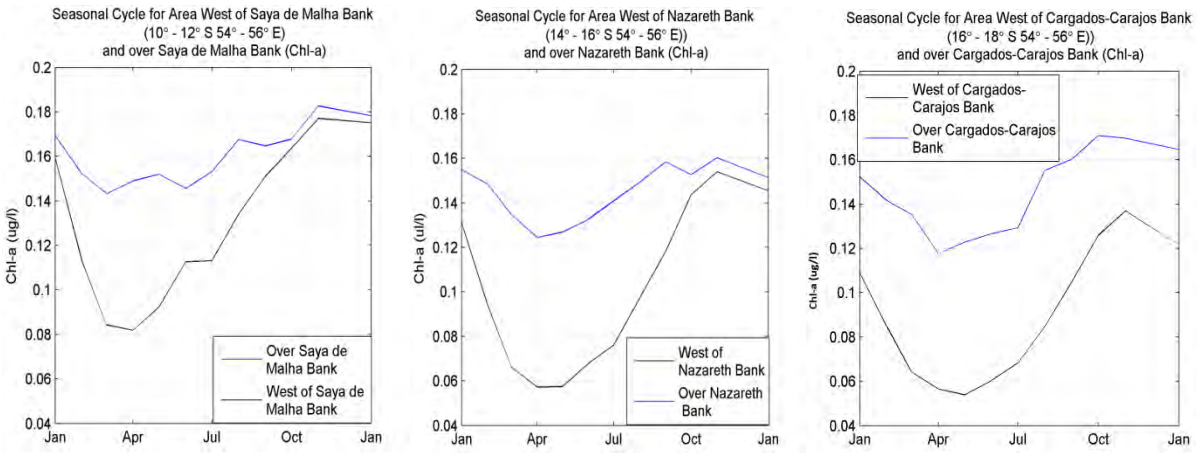

Figure 8. 3: Seasonal cycle of Chl-a over the Saya de Malha Bank, Nazareth Bank, Cargados-Carajos Bank and areas to the west of these banks. The areas to the west have a distinct seasonal cycle whilst over the banks, there is virtually no seasonal cycle.

It appears from Figure 8.3 that the Saya de Malha Bank, Nazareth Bank and Cargados-Carajos Bank retain similar relatively high Chl-a values throughout the year (0.16 ug/l) irrespective of changes in Chl-a adjacent to these banks. The Seychelles Bank had a similar concentration of Chl-a to the surrounding areas throughout the year (varied from approximately 0.13 ug/l to 0.2 ug/l). This indicates that a distinct ecosystem could exist across these banks (excluding the Seychelles Bank) as there were no major currents crossing them and were relatively quiescent (as displayed from shipboard ADCP and maps of satellite geostrophic velocity, the majority of the SEC flowed through the 3 major gaps on the Mascarene Plateau whilst the SECC flows eastward across the Seychelles Bank). The banks also have little seasonality (Figure 8.3) whilst the surrounding areas show marked seasonality (Chl-a values lowest in April and highest in October). The variability across the Saya de Malha, Nazareth and Cargados-Carajos Bank is low compared to the surrounding region (Figure 8.5) where the Standard Deviation is approximately 0.02 ug/l across the banks whilst the surrounding region reaches up to 0.045 ug/l. The Seychelles Bank has the same variability (Standard Deviation) as the surrounding region since the SECC (Standard Deviation ~ 0.035 ug/l) crosses it carrying the nutrient rich water mass (ASHSW). Since these banks may be able to sustain an ecosystem throughout the year there must be a constant supply of nutrients and phytoplankton which could mean that there may be upwelling onto the banks from deeper, nutrient rich waters. New et al, (2013) showed that areas of high chlorophyll concentration on the Saya de Malha Bank is consistent with the breaking of Internal Solitary Waves. Further studies need

to be undertaken to investigate the relationship between chlorophyll concentration and Internal Solitary Waves over the banks of the Mascarene Plateau.

Another factor as to why there are nutrient rich waters to the north of the main branch of the SEC (the branch through gap 2) is due to the uplifting of density surfaces. The upliftment of the density surfaces increases towards the north (Figure 8.4).

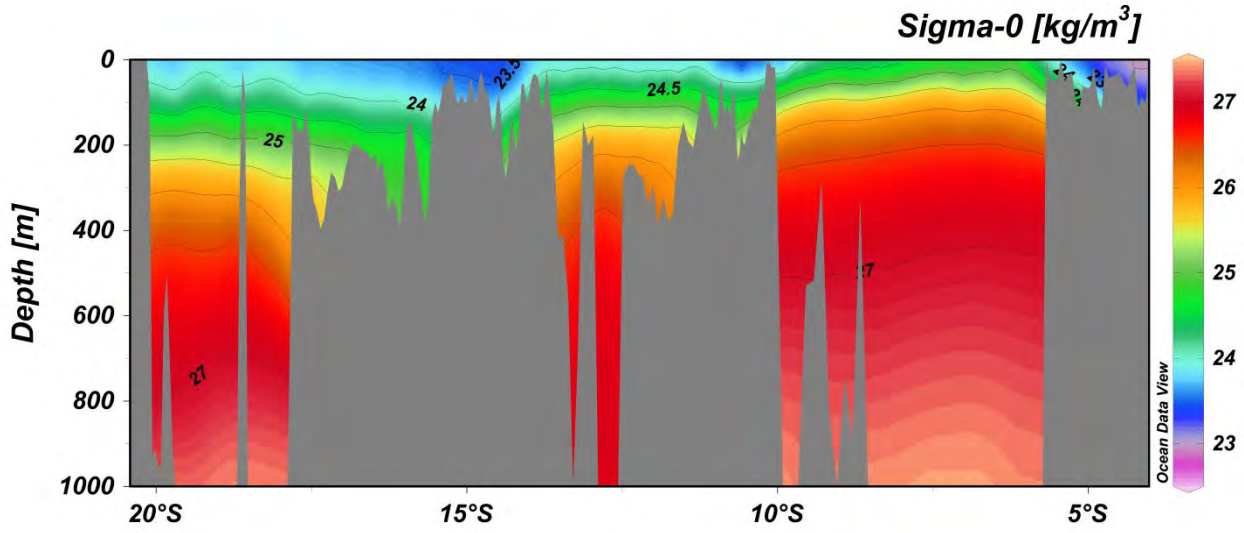

Figure 8.4: Cross section across the Mascarene Plateau of potential density (σ0).

Figure 8.5 shows there is low variability over the Nazareth, Saya de Malha and Cargados Carajos Banks and high variability in the area where nutrient poor waters mix with nutrient rich waters (9° S - 15° S).

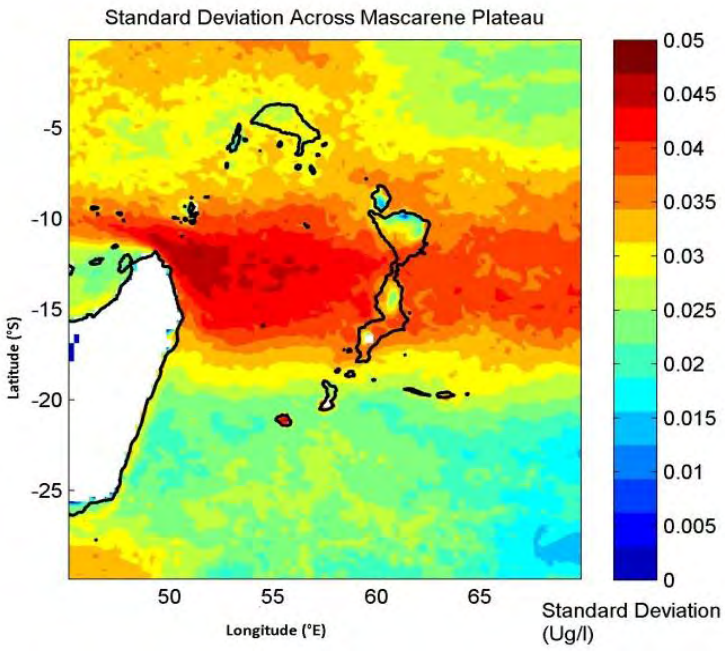

Figure 8. 5: Standard deviation (variability) of Chlorophyll-a. 1000m isobaths overlaid in black.

The highest variability of Chl-a in the region is in the latitude range between 9° S - 15° S (Standard deviation > 0.045 Ug/l) (Figure 8.5). This is the region where nutrient poor water masses to the south mix with nutrient rich water masses to the north and in many areas, the SEC acts as a dividing line between the nutrient rich and nutrient poor water masses. Hence this is a highly variable zone since the SEC is not constantly at the same latitude and Chl-a values shift with the SEC.

The major reasons for the distribution of Chl-a concentration in the region throughout the year is due to the advection of water masses (nutrient rich ASHSW to the north and nutrient poor STSW to the south) and the upliftment of density surfaces (also as determined by New et al, (2007)). Hence, there are very few differences with regards to Chl-a concentration patterns and dynamics between the 2002 and 2008 cruises.

8.2 Conditions during ASCLME Cruise (October/November 2008)

During the ASCLME cruise in October/November 2008, Chl-a values were lower than climatology south of 11° S (latitude across the Saya de Malha Bank). Values were < 0.07 ug/l whilst average climatology values were < 0.1 ug/l (Figure 8.1d). This may be due to excess nutrient poor waters from the south and an above normal positive wind stress curl inducing downwelling. However, north of 11° S and across the Saya de Malha, Nazareth and Cargados-Carajos Banks (distinct ecosystems) Chl-a values were similar to climatology.

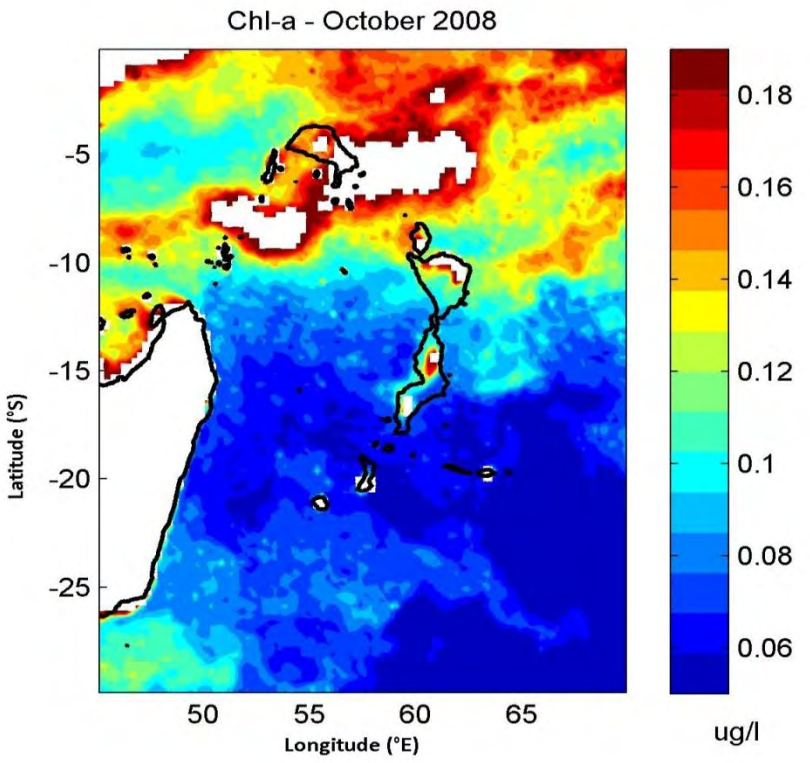

Figure 8. 6: Average October 2008 Chlorophyll-a values (ug/l) estimated from satellite remote sensing during the ASCLME 2008 cruise. 1000m isobath overlaid in black whilst white patches indicate Madagascar or Chl-a values > 2 ug/l.

Figure 8.6 shows nutrient poor waters are found to the south of ~ 13° S and nutrient rich waters are found to the north of ~ 13° S. The Saya de Malha, Nazareth and Cargados-Carajos Banks have nutrient rich waters.

From the above, key question 6 can be addressed: *What is the distribution of Chl-a in the region (climatology) and do the banks differ in Chl-a concentration from its surrounding areas?*

Broadly speaking, the area around the Mascarene Plateau is divided into 2 areas, the northern region (north of approximately 13° S) which is composed primarily of nutrient rich waters (ASHSW – Arabian Sea High Salinity Water) and a southern region which is composed primarily of nutrient poor waters (STSW (Sub Tropical Surface Water). However, climatologically, the period from October – December contains relatively high Chl-a concentrations as far south as the Cargados-Carajos Bank (~ 16° S). The Saya de Malha, Nazareth and Cargados-Carajos Banks retain relatively high Chl-a concentrations (low variability) throughout the year as there are no major currents which flow over them as opposed to its surrounding areas where there is a distinct seasonality and high variability. However, the Seychelles Bank contains similar characteristics to its surrounding region due to the SECC which crosses over it. Hence there is high variability and seasonality over the bank unlike the other banks mentioned. The area with the highest variability is the latitude range between 9° S - 15° S. This is due to nutrient poor water masses mixing with nutrient rich water masses. The SEC acts as a dividing line between the rich and poor water masses and shifts in position throughout the year which increases the variability of Chl-a concentrations in the region. Additionally, the region to the north of the SEC which flows through gap 2 has a higher content of nutrients (higher Chl-a) as there is an upliftment of density surfaces further north.

8.3 Summary

The region around the Mascarene Plateau generally has nutrient poor waters to the south of approximately 13° S and nutrient rich waters to the north. Chl-a concentration depends on both the types of water masses and the amount of upwelling. The major cause for the 2 distinct regions of nutrient rich and poor waters are due to the advection of surface water masses as well as the upliftment of density surfaces north of gap 2. The northern region of the Mascarene Plateau contains nutrient rich ASHSW (Arabian Sea High Salinity Water) whilst the southern sector contains nutrient poor STSW (Sub Tropical Surface Water). The Saya de Malha, Nazareth and Cargados-Carajos Banks retain similar Chl-a values throughout the year (unlike its surrounding areas) with little seasonality and low variability. This indicates that a distinct ecosystem could exist across these banks. The banks retain similar relatively high Chl-a values throughout the year as there are no major currents which flow over them. However,

the Seychelles Bank contains similar characteristics (relatively high Chl-a concentrations, high variability and high seasonality) to its surrounding region as the eastward flowing SECC crosses it. The area with the highest variability in Chl-a concentration is in the latitude range between 9° S - 15° S. This is due to mixing between nutrient poor water masses to the south and nutrient rich water masses to the north. Within this area, a branch of the SEC flows which acts as a division between the water masses. It is not constantly at the same latitude throughout the year which increases the variability of Chl-a as Chl-a concentrations shift with the SEC.

The next chapter investigates the interannual variability around the Mascarene Plateau. In the Indian Ocean, westward travelling Rossby Waves are generated primarily by the positive Indian Ocean Dipole (IOD) and during El Niño via changes in wind. The chapter will investigate whether these propagating Rossby waves are able to cross over sections of the Mascarene Plateau and whether there were any present during the research cruise on board the RRS Charles Darwin during June/July 2002 and the research cruise on board the Dr Fridtjof Nansen during October/November 2008. The effect of these Rossby waves on the general circulation in the region will also be investigated.

CHAPTER 9: Interannual Variability

The Mascarene Plateau may be of important interest with regards to the interannual variability in the Indian Ocean as it lies in the Western Indian Ocean and may have an influence on the westward propagation of Rossby waves. Since the plateau is divided into a series of banks and gaps in a meridional direction, the Rossby waves may be affected differently by the plateau depending on the latitude of the Rossby wave (the speed of Rossby waves differ with latitude) and the topography (depth and width of the banks and gaps in the plateau). The following section will identify whether any Rossby Waves were present over the Mascarene Plateau during the research cruise on board the RRS Charles Darwin during June/July 2002 and the research cruise on board the Dr Fridtjof Nansen during October/November 2008. In addition we will ascertain whether Rossby Waves are able to propagate over certain sections of the Mascarene Plateau. Rossby waves are identifiable on Time-Longitude plots (Hovmöller diagrams of MADT normalized anomalies) by sloping lines increasing with time.

Key Question 7. Were there westward propagating Rossby waves over the Mascarene Plateau during the June/July 2002 cruise on board the RRS Charles Darwin and the October/November 2008 cruise on board the the Dr Fridtjof Nansen? Are these waves capable of crossing every part of the plateau? What effect do these waves have on the general circulation in the region?

9.1 Analysis of Interannual Variability

For clarification, the Mascarene Plateau is divided into 6 different regions where it will be ascertained whether Rossby Waves are able to cross the specified region (Figure 9.1). The 6 regions are the Seychelles Bank (4° - 6° S, 54° – 57° E), Gap 1 (7° – 9° S, 57.5° – 59° E) , the Saya de Malha Bank (10° – 11.5° S, 60° – 62° E), gap 2 (12° – 13.8° S, 60° – 62° E), Nazareth/Cargados-Carajos bank (14° – 16° S, 60° – 61.5° E) and gap 3 (18° - 18.8° S, 58.3° – 60° E). To determine the strength of the Rossby Waves, weekly MADT normalized anomalies from climatology is used (method described in chapter 3).

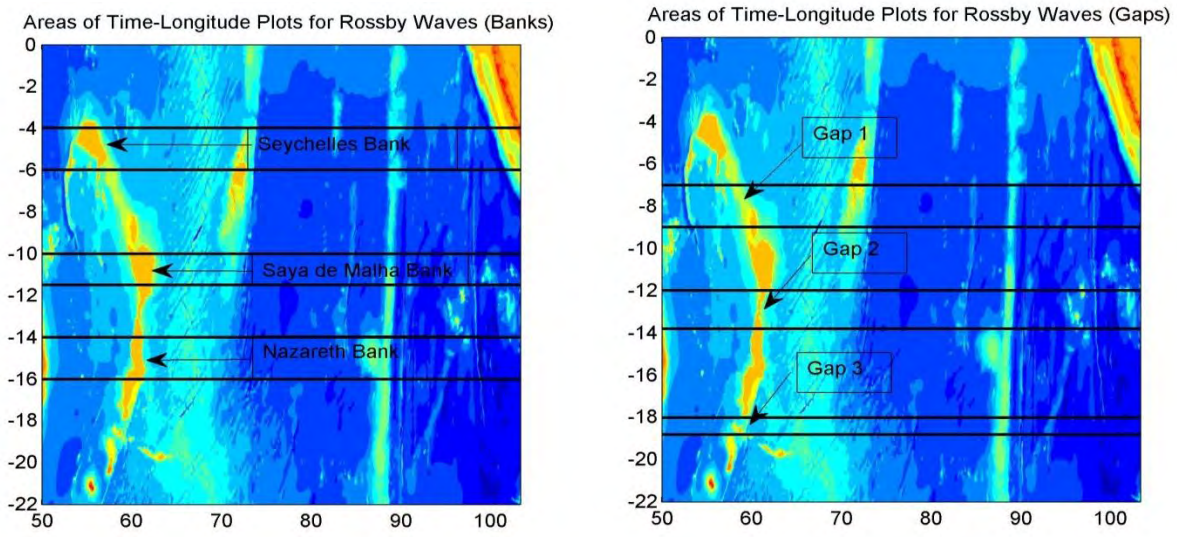

Figure 9. 1: The 6 different regions used in subsequent Hovmöller plots to investigate the effect of Rossby Waves on the Mascarene Plateau. These 6 regions are also chosen to investigate whether Rossby waves were present during the 2 research cruises and whether they are able to cross the specified region.

There were 2 extensive research cruises in the region of the Mascarene Plateau. The first one was conducted on board the RRS Charles Darwin during June/July 2002 whilst the second one was conducted on board the the Dr Fridtjof Nansen during October/November 2008. This section will ascertain whether any Rossby Waves, important regional features, were present in the region of the Mascarene Plateau during the 2 research cruises. Since Rossby Waves affect the thermocline depth, this may have an effect on upwelling and hence there may be less/more nutrient rich waters which enter the mixed layer and result in higher/lower chlorophyll concentrations. With the presence of a Rossby Wave during cruise conditions, an analysis could be undertaken to see differences in upwelling within the 3 major gaps due to differences in the thermocline depth. There could also be an effect on SST.

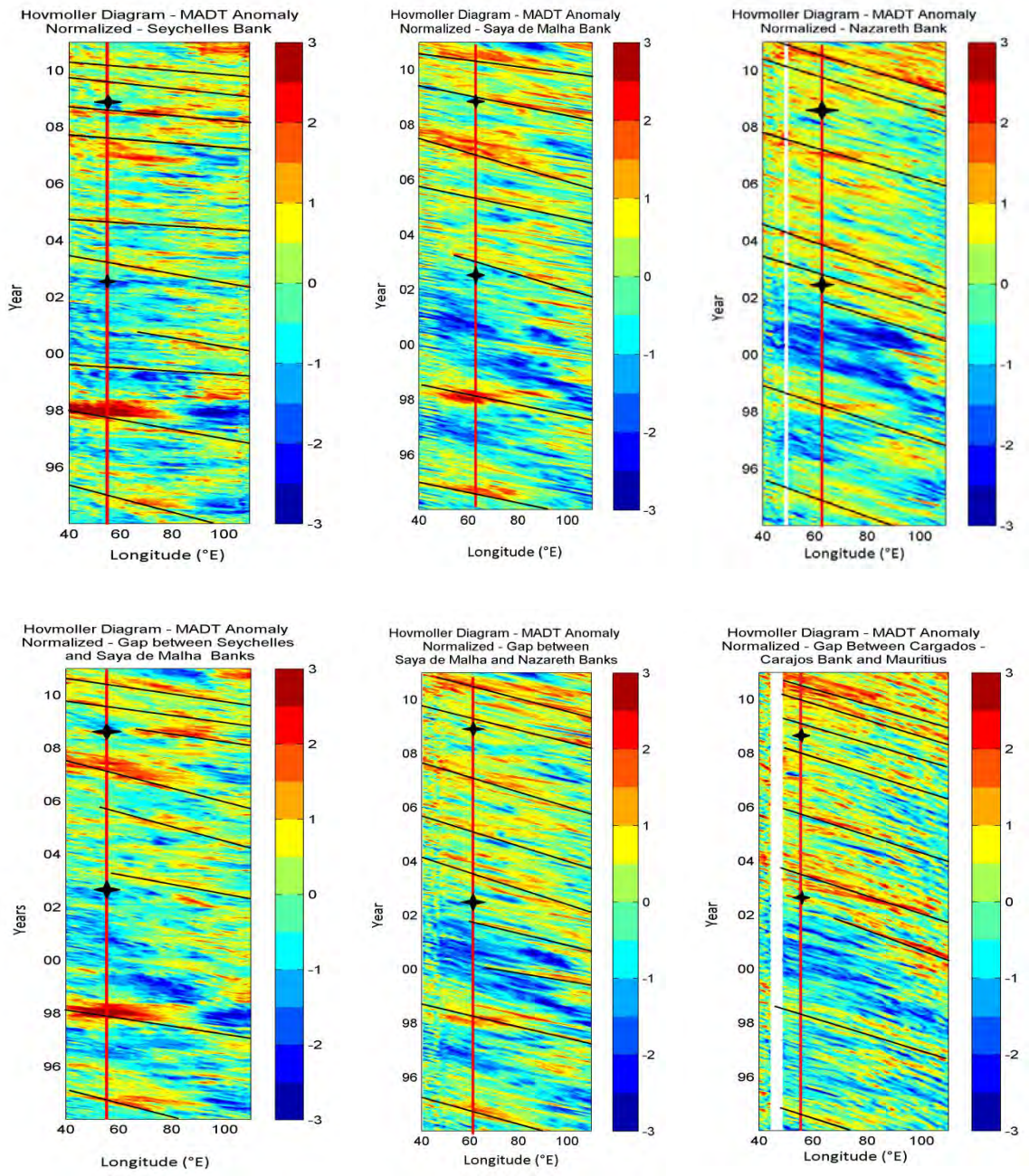

Figure 9. 2: Time – Longitude plots (Hovmöller Diagrams) of MADT Normalized Anomalies depicting propagation of Rossby Waves in the region of the Mascarene Plateau. Sloped lines indicate wave propagation whilst vertical line indicates the particular feature of the plateau (gap/bank). Stars indicate the time of the cruises (June 2002 or October 2008 cruise). Clockwise, figures are labeled a – f.

Figure 9.2 shows the propagation of Rossby waves at various latitudes from 2° – 20° S and over the Mascarene Plateau. Sloped lines indicate wave propagation whilst the vertical red lines indicate the particular feature of the plateau (gap/bank). Stars indicate the time of the cruises (June 2002 or October 2008 cruise). From the Hovmöller plot, there are no major wave propagations (in any of the regions of the Mascarene Plateau) during both of the cruises indicating no major perturbation during the cruises. This indicates that cruise samplings were done during normal conditions with regard to major abnormal events triggered by Rossby wave propagations.

Year	Seychelles Bank	Saya de Malha Bank	Nazareth Bank	Gap 1	Gap 2	Gap 3
2002	-1.3	-0.5	0.5	-1.1	0.1	0.4
2008	-0.3	-0.2	0.6	-1	0.4	0.25

Table 9. 3*: Table of MADT Normalized Anomalies in number of standard deviations over the respective regions of the Mascarene Plateau during the 2 research cruises.*

Table 9.1 indicates the values of MADT normalized anomalies over the particular regions of the Mascarene Plateau. From Table 9.1 there are no MADT normalized anomaly values over 1 standard deviation in any of the regions during both of the cruises. There were no Rossby Waves present during either cruise. This is unfortunate for the scope of the study but it does not prevent the study of Rossby wave propagation in the region since we have several years of altimetry and several clear cases of Rossby wave propagation.

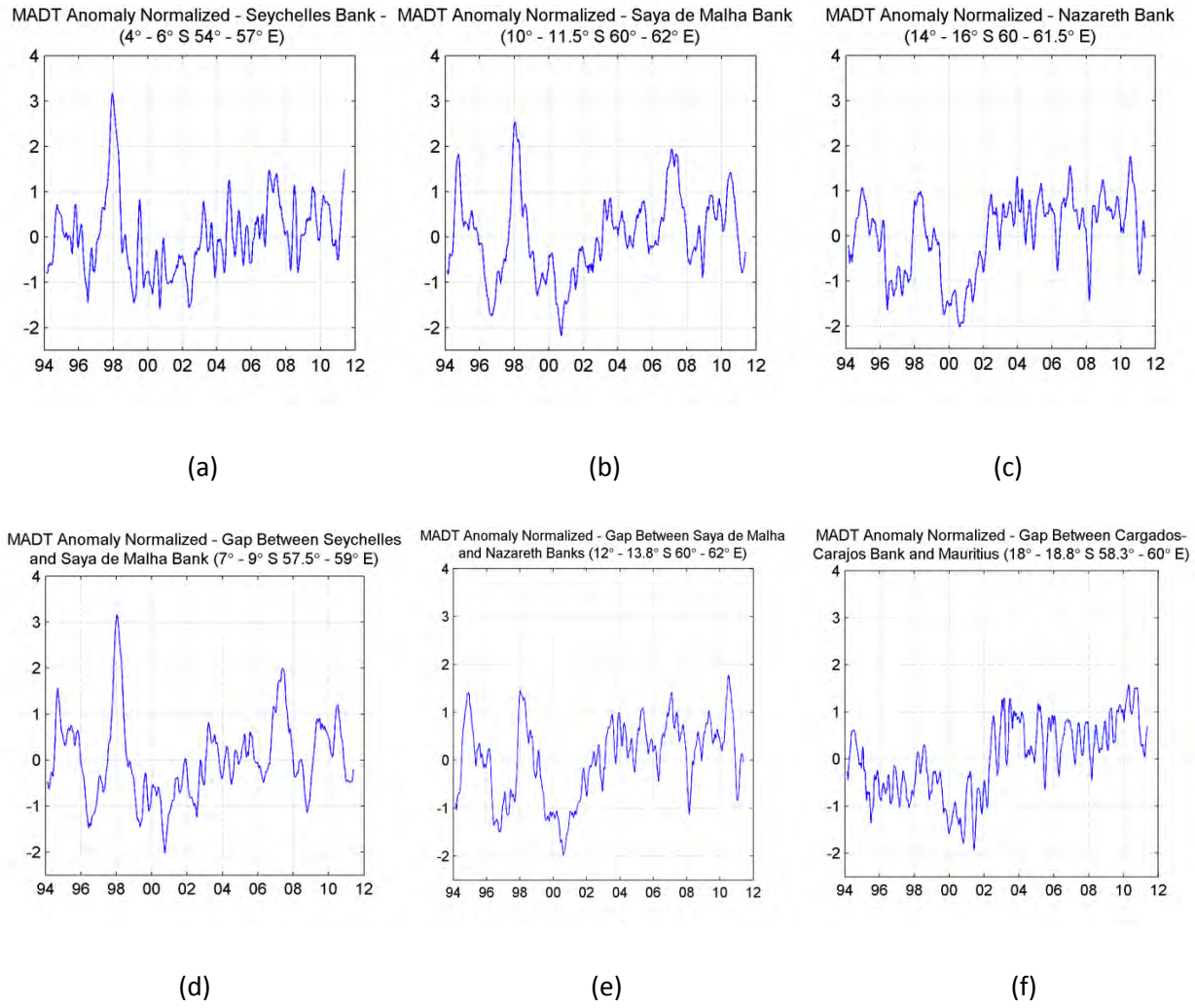

Figure 9. 3: Time series of MADT normalized anomalies (1994 – 2011) for 6 regions of the Mascarene Plateau.

In an attempt to establish the behaviour of Rossby waves when they encounter the Mascarene Plateau, Hovmöller diagrams (Figure 9.2) were analyzed over 6 areas of the Mascarene Plateau. 3 case studies are investigated with regards to the propagation of the waves through the 3 major gaps. The strongest MADT values for each gap over the 17 year period (1994 – 2011) are used for this purpose.

Bank/Gap	MADT Normalized Anomaly	Time (Year and Month)	Corresponding Figure (Hovmöller Diagram)
Seychelles Bank	0.97	Feb 2010	Fig 7.2a
"	1.1	Sep 2009	"
"	1.1	June 2008	"
"	1.4	June 2007	"
"	1.3	July 2004	"
"	1	June 1999	"
"	3.1	Jan 1998	"
"	0.9	Jan 1995	"
Saya de Malha Bank	1.4	May 2010	Fig 7.2b
"	1	Jan 2009	"
"	2	Jan 2007	"
"	0.85	Jun 2005	"
"	0.9	Feb 2003	"
"	2.5	Jan 1998	"
"	1.8	July 1994	"
Nazareth Bank	1.8	Dec 2010	Fig 7.2c
"	0.9	Dec 2009	"
"	1.6	Jan 2007	"
"	1.3	Jan 2004	"
"	0.9	Sep 2002	"
"	1	Jun 1998	"
"	1	Jan 1995	"
Gap 1	1.2	June 2010	Fig 7.2f
"	0.9	June 2009	"
"	2	Mar 2007	"
"	0.7	Dec 2005	"
"	0.9	Feb 2003	"
"	3.1	Jan 1998	"
"	1.5	Jun 1994	"
Gap 2	1.8	Jun 2010	Fig 7.2e
"	1	Jun 2009	"
"	1.5	Mar 2007	"
"	1.1	Jun 2005	"
"	1	July 2003	"
"	1.4	Jan 1998	"
"	1.4	Jan 1995	"
Gap 3	1.5	Jun 2010	Fig 7.2d
"	1	Jan 2010	"
"	1	Jan 2009	"
"	0.9	Jan 2008	"
"	1	Dec 2005	"
"	1.3	Sep 2003	"
"	0.7	July 1994	"

Table 9. 4: Table of MADT Normalized Anomalies over the 6 regions of the Mascarene Plateau with the associated times and corresponding figures representing Rossby wave propagation. Green highlighted rows indicate further investigation with regards to the effect the waves have on the ocean circulation in the region.

For gap 1, the Rossby wave which passed through the gap during January 1998, a well known ENSO/IOD Rossby wave event is investigated. The MADT value of 3.1 standard deviations was reached in January 1998 and the wave propagation is clearly seen in Figure 9.2f across the basin.

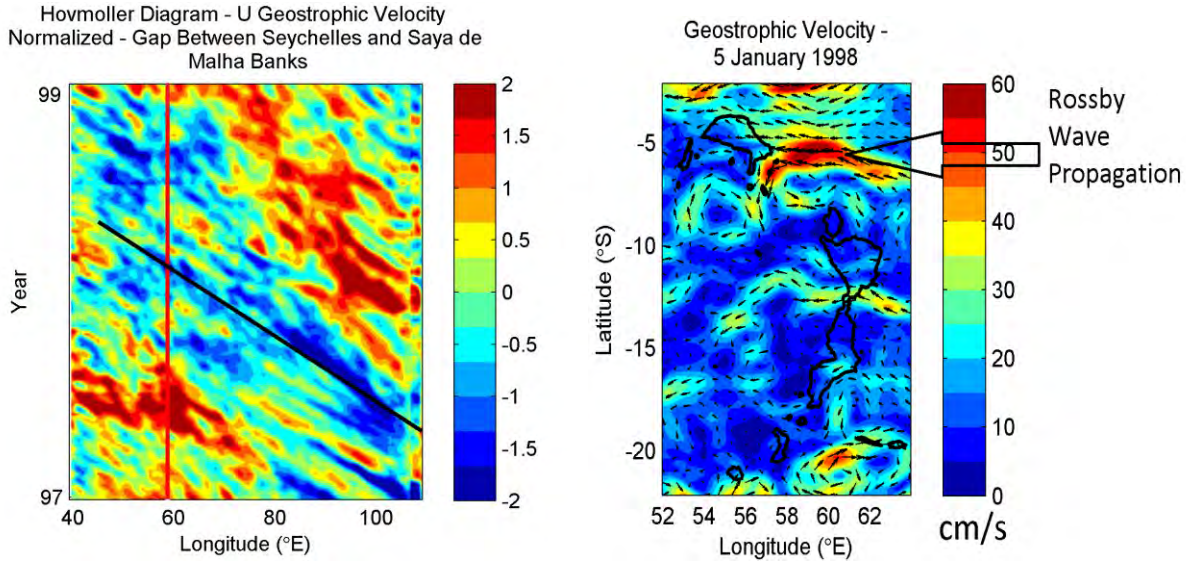

(a) (b)

Figure 9. 4: (a) Hovmöller Diagram of U geostrophic velocity normalized anomaly between 1997 and 1999. Sloped black line indicates Rossby wave propagation whilst vertical red line indicates position of gap 1 and (b) geostrophic velocity in the region of the Mascarene Plateau – 5 January 1998.

During the Rossby wave propagation through gap 1, there is an MADT normalized anomaly of 3.1 standard deviations (Figure 9.2f) and a U normalized geostrophic anomaly of -1 standard deviation (Figure 9.4a). This Rossby wave propagation was associated with the 1997 positive Indian Ocean Dipole (IOD). From Figure 9.4b, it can be seen that velocities reach approximately 55 cm/s through the gap whilst the climatology for January is approximately 19 cm/s (Figure 7.3). It can be ascertained from Figure 9.4a that the higher velocity is due to the propagation of a Rossby wave as the negative anomaly can be traced to 100° E. During the Rossby wave propagation the eastward flowing South Equatorial Counter Current (SECC) shifts northwards and does not cross the Seychelles Bank. There is a westward current across the Seychelles Bank during this time.

For gap 2, the Rossby wave which passed through the gap during June 2010 will be investigated (MADT value of 1.8 during June 2010).

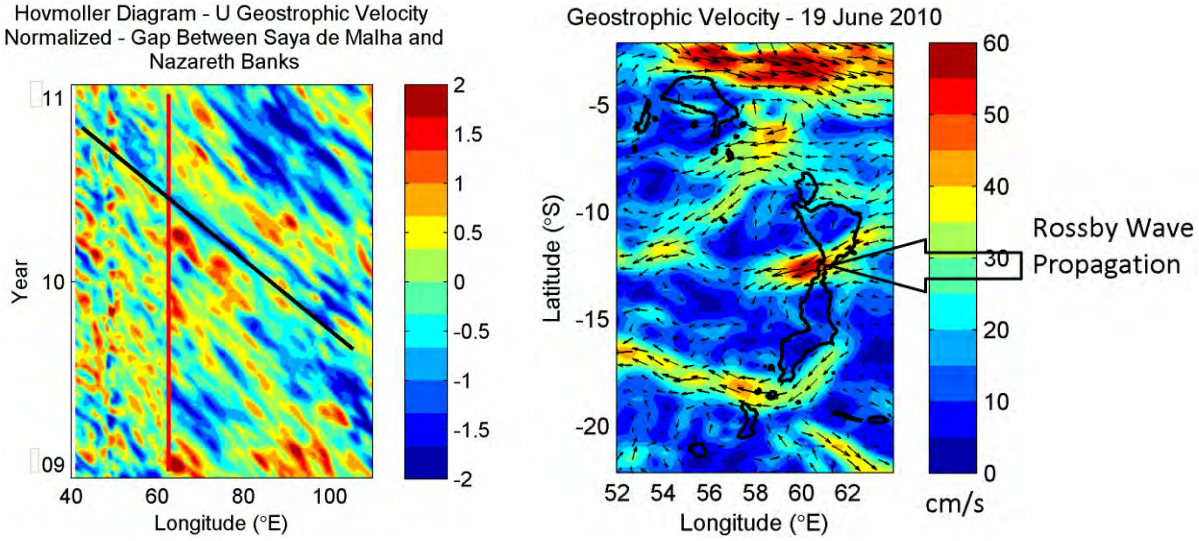

(a) (b)

Figure 9. 5: (a) Hovmöller Diagram of U geostrophic velocity normalized anomaly between 2009 and 2011. Sloped black line indicates Rossby wave propagation whilst vertical red line indicates position of gap 2 and (b) geostrophic velocity in the region of the Mascarene Plateau – 19 June 2010.

During the Rossby wave propagation through gap 2, there is an MADT normalized anomaly of 1.8 standard deviations (Figure 9.2e) and a U normalized geostrophic anomaly of -0.7 standard deviations (Figure 9.5a). The geostrophic velocity through gap 2 is 50 cm/s on 19 June 2010 (Figure 9.5b) whilst the climatology for the same gap in June is 19 cm/s (Figure 7.4). It can be ascertained from Figure 9.5a that the higher velocity is due to the propagation of a Rossby wave as the negative anomaly can be traced to 100° E.

For gap 3, the Rossby wave which passed through the gap during June 2010 will be investigated (MADT value of 1.5 during June 2010).

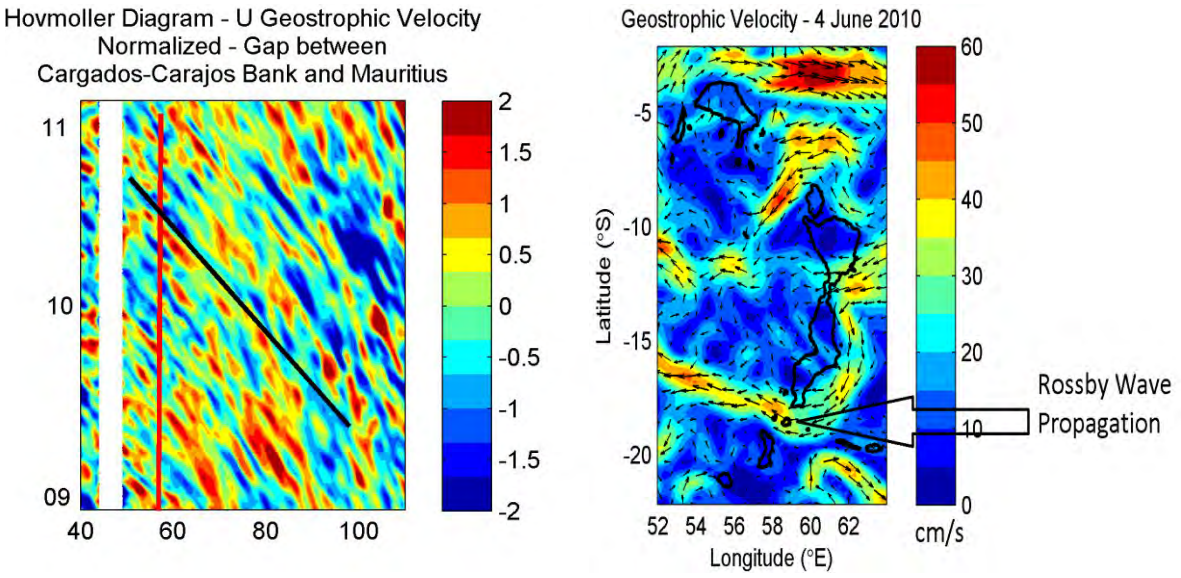

(a) (b)

Figure 9. 6: (a) Hovmöller Diagram of U geostrophic velocity normalized anomaly between 2009 and 2011. Sloped black line indicates Rossby wave propagation whilst vertical red line indicates position of gap 3 and (b) geostrophic velocity in the region of the Mascarene Plateau – 4 June 2010.

During the Rossby wave propagation through gap 3, there is an MADT normalized anomaly of 1.5 standard deviations (Figure 9.2d) and a U normalized geostrophic anomaly of -0.9 standard deviations (Figure 9.6a). It can be ascertained from Figure 9.6a that the higher velocity is due to the propagation of a Rossby wave as the negative anomaly can be traced to 100° E. The geostrophic velocity through gap 3 was 40 cm/s on 5 June 2010 (horizontal geostrophic velocity anomaly of -0.7) whilst the climatology for the same gap in June is 19 cm/s (Figure 7.5).

In analyzing the amount of Rossby waves each section of the Mascarene Plateau encountered during the 17 years of data available (1994 – 2011), time-longitude plots (Hovmöller diagrams) are used (Figure 9.2). The latitude along the Seychelles Bank experienced 10 major Rossby waves whereby 9 propagated across the bank whilst 1 disappeared prior to the bank (Figure 9.2a). The latitude along the Saya de Malha Bank experienced 7 major Rossby Waves during the 17 year period whereby 6 propagated across the bank and 1 faded out as it crossed over (Figure 9.2b). The latitude along the Nazareth Bank experienced 8 major Rossby waves during the period whereby 1 faded out as it encountered the plateau (Figure 9.2c). The latitude along gap 1 experienced 8 major Rossby waves whereby 2 faded out as it

encountered the plateau, 1 faded out before reaching the plateau whilst the rest propagated through the gap (Figure 9.2f). The latitude along gap 2 experienced 9 major Rossby waves whereby 2 faded out whilst encountering the plateau and the rest propagated through the gap (Figure 9.2e). The latitude along gap 3 experienced 9 major Rossby waves whereby 8 propagated through the gap and 1 faded out before reaching the plateau (Figure 9.2d).

From the above, key question 7 can be addressed: *Were there westward propagating Rossby waves over the Mascarene Plateau during the June/July 2002 cruise on board the RRS Charles Darwin and the October/November 2008 cruise on board the the Dr Fridtjof Nansen? Are these waves capable of crossing every part of the plateau? What effect do these waves have on the general circulation in the region?*

There were no Rossby waves which propagated over the Mascarene Plateau during both the cruises. However, there was a propagation towards the end of June 2008 over the Seychelles Bank but it faded out completely by October/November. It has been shown in this study that Rossby waves can propagate over every part of the Mascarene Plateau. Rossby waves can change the circulation patterns in the region. The propagation during 5 January 1998 through gap 1 (associated with the strong 1997 + IOD event) increased the velocity through the gap. The Rossby wave which propagated westward through gap 2 (19 June 2010) and through gap 3 (4 June 2010) had the effect of increasing the geostrophic velocities through the gaps significantly.

9.2 Summary

A major feature of the interannual variability in the region of the Mascarene Plateau is Rossby Waves. During IOD (Indian Ocean Dipole) years or El Niño years, Rossby Waves are generated in the eastern Indian Ocean and propagate westwards. During the westward propagation, a rise in the sea surface of only a few centimeters results in the deepening of the thermocline by tens of metres. This section has shown that there were no Rossby Waves present during the research cruise conducted on board the RRS Charles Darwin during June/July 2002 as well as the cruise conducted on board the Dr Fridtjof Nansen during October/November 2008. Rossby Wave propagation is possible across 6 regions of the Mascarene Plateau. Rossby Waves affect the circulation patterns in the region. These waves which passed through the 3 major gaps in the Mascarene Plateau increased the geostrophic velocity significantly (compared to the climatology). From the maps of MADT normalized anomaly, it has been

shown that most Rossby waves (over the 17 year period 1994 – 2011) propagate across the 6 regions of the Mascarene Plateau described. However, there are instances where the waves fade out in the region. Whether the plateau plays a part in this is unclear.

CHAPTER 10: OGCM (Ocean General Circulation Model)

In this section we will compare observations and satellite estimates obtained around the Mascarene Plateau with OFES model data and ascertain the validity of the model in the region. Modeled SST and Geostrophic Velocity observations will be compared to satellite TRMM SST and satellite derived geostrophic velocities (AVISO data). This is a stringent test for a global model but if validated, it can be used to infer properties not available in space and time which is limited with cruise data and satellite remote sensing as the spatial and temporal resolution is higher in the model than in the satellite data (the model has a spatial and temporal resolution of 1/10° and 3 days respectively whilst satellite data has a spatial and temporal resolution of 1/4° and 7 days respectively (for both SST and altimetry)).

Key Question 8. Is an OGCM (OFES) model viable in the region for further modeling studies?

10.1 Climatological Comparison

Climatological data (2000 – 2009) for surface geostrophic velocity (data obtained via AVISO satellite derived geostrophic velocities) and satellite TRMM SST will be compared to modeled SST and Geostrophic Velocity observations over the Mascarene Plateau. If the comparisons agree reasonably well, this model can be a very useful tool for further studies in the region.

10.1.1 Geostrophic Velocity

Figure 10.1 depicts maps of climatological geostrophic velocity (satellite altimetry and OFES model) for January – March (2000 – 2009). Figure 10.1 shows that velocities through gap 2 are approximately equal (~ 35 cm/s) and both cores of the SEC are evident downstream of the plateau in both the observation and model. The model also manages to capture the geostrophic velocity in gap 3 and hence the 2 cores west of the plateau are present in the model. However, the model does not represent the South Equatorial Countercurrent (SECC) well as velocities in the model are up to 40 cm/s greater. Other than the areas mentioned, the geostrophic velocities are generally greater in the region in the model by approximately 5 cm/s.

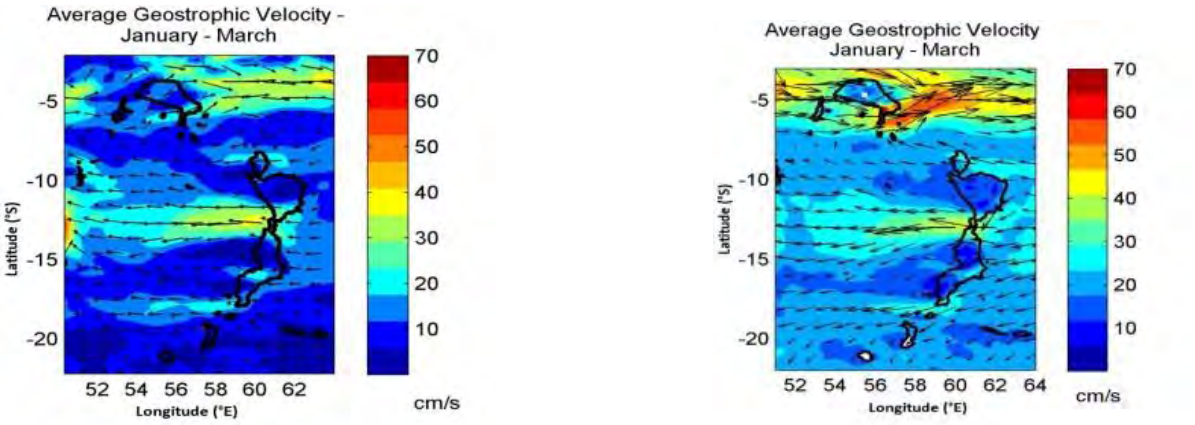

(a) (b)

Figure 10. 2: (a) Climatological Geostrophic Velocity (cm/s) January – March (2000 – 2009) – Satellite Altimetry and (b) Climatological Geostrophic Velocity (cm/s) January - March (2000 – 2009) – OFES Model. 1000m isobath overlaid in black.

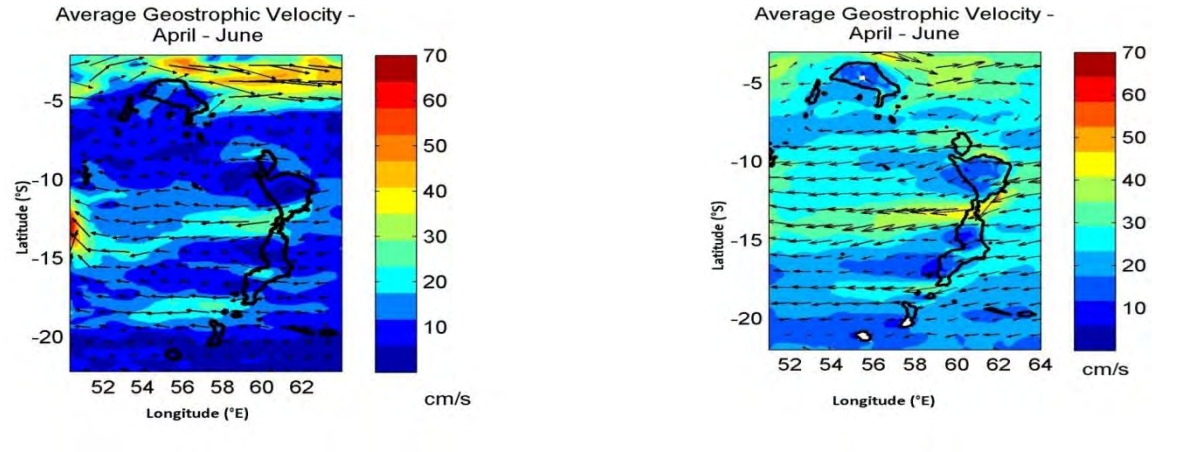

(a) (b)

Figure 10. 3: (a) Climatological Geostrophic Velocity April – June (2000 – 2009) – Satellite Altimetry and (b) Climatological Geostrophic Velocity April - June (2000 – 2009) – OFES Model. 1000m isobath overlaid in black

Figure 10.2 depicts maps of climatological geostrophic velocity (satellite altimetry and OFES model) for April - June (2000 – 2009). Figure 10.2 shows that during the period from April – June, the model manages to capture the 2 cores of the SEC west of the plateau but the model overestimates the geostrophic flow through gap 2. The model captures the SECC but at a lower velocity than the observation by approximately 15 cm/s. Once again, the model generally captures a higher velocity than the observed geostrophic velocity in the rest of the region by approximately 5 cm/s.

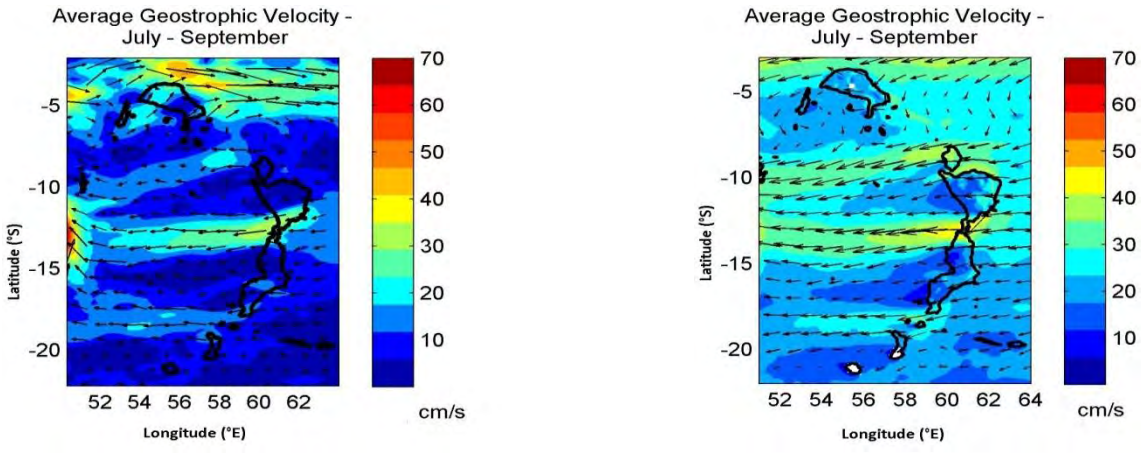

(a) (b)

Figure 10. 4: (a) Climatological Geostrophic Velocity July - September (2000 – 2009) – Satellite Altimetry and (b) Climatological Geostrophic Velocity July - September (2000 – 2009) – OFES Model. 1000m isobath overlaid in black.

Figure 10.3 depicts maps of climatological geostrophic velocity (satellite altimetry and OFES model) for July - September (2000 – 2009). Figure 10.3 shows that during July – September the 2 cores of the SEC west of the Mascarene Plateau are present in the model, however the modeled southern core has greater velocities. The current north of the Saya de Malha Bank is present but stronger in the model. The geostrophic velocity between the Saya de Malha Bank and Nazareth Bank is approximately equal in the satellite estimate and the model. The SECC is not present in the model during this period. Velocities in the area are westward as opposed to the eastward flowing SECC. A possibility for this is that in the model the NEC (North Equatorial Current) shifts south but does not reverse direction (this period is the SW monsoon season where the NEC is supposed to flow eastward).

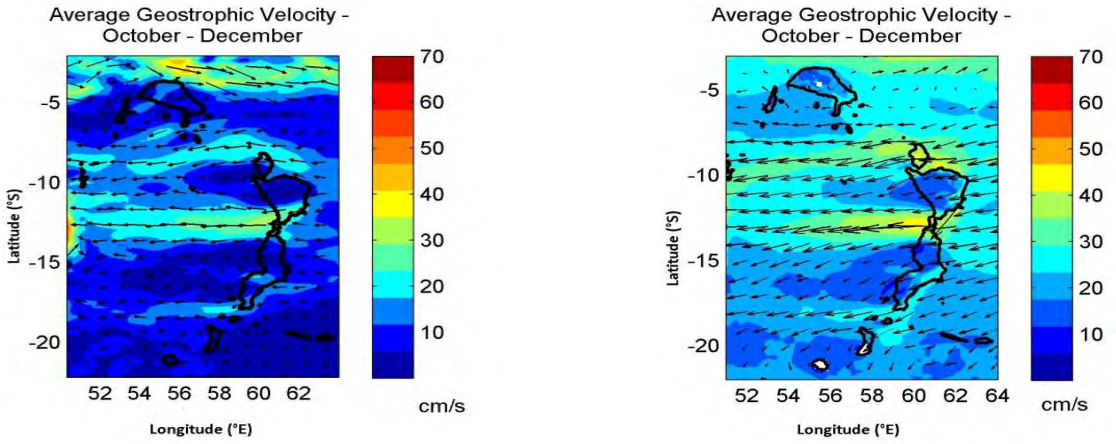

(a) (b)

Figure 10. 5: (a) Climatological Geostrophic Velocity October - December (2000 – 2009) – Satellite Altimetry and (b) Climatological Geostrophic Velocity October - December (2000 – 2009) – OFES Model. 1000m isobath overlaid in black.

Figure 10.4 depicts maps of climatological geostrophic velocity (satellite altimetry and OFES model) for October - December (2000 – 2009). Figure 10.4 shows that during October – December the model captures the SECC however it is weaker than the observed satellite climatology. Velocities are in the order of 5 cm/s lower in the model. Once again, the model captures the northern and southern core of the SEC but the northern core has a higher velocity in the model by approximately 15 cm/s. The remainder of the region has a higher velocity in the model with the exception of the banks where the difference is negligible.

10.1.2 SST

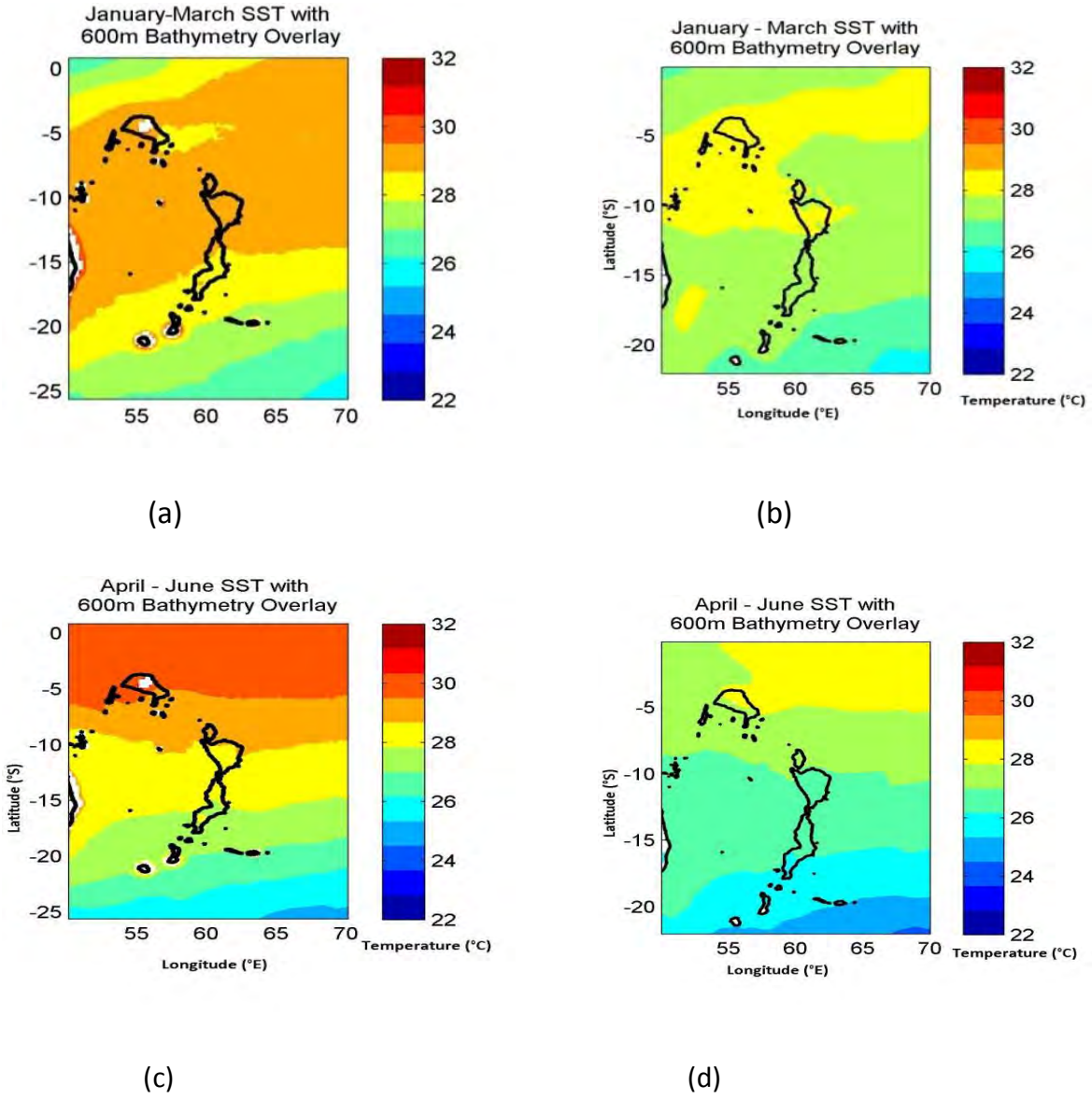

Figure 10. 6: (a) Climatological SST January - March (2000 – 2009) – Satellite Altimetry, (b) Climatological SST January - March (2000 – 2009) – OFES Model, (c) Climatological SST April – June (2000 – 2009) – Satellite Altimetry and (d) Climatological SST April – June (2000 – 2009) – OFES model. 1000m isobath overlaid in black.

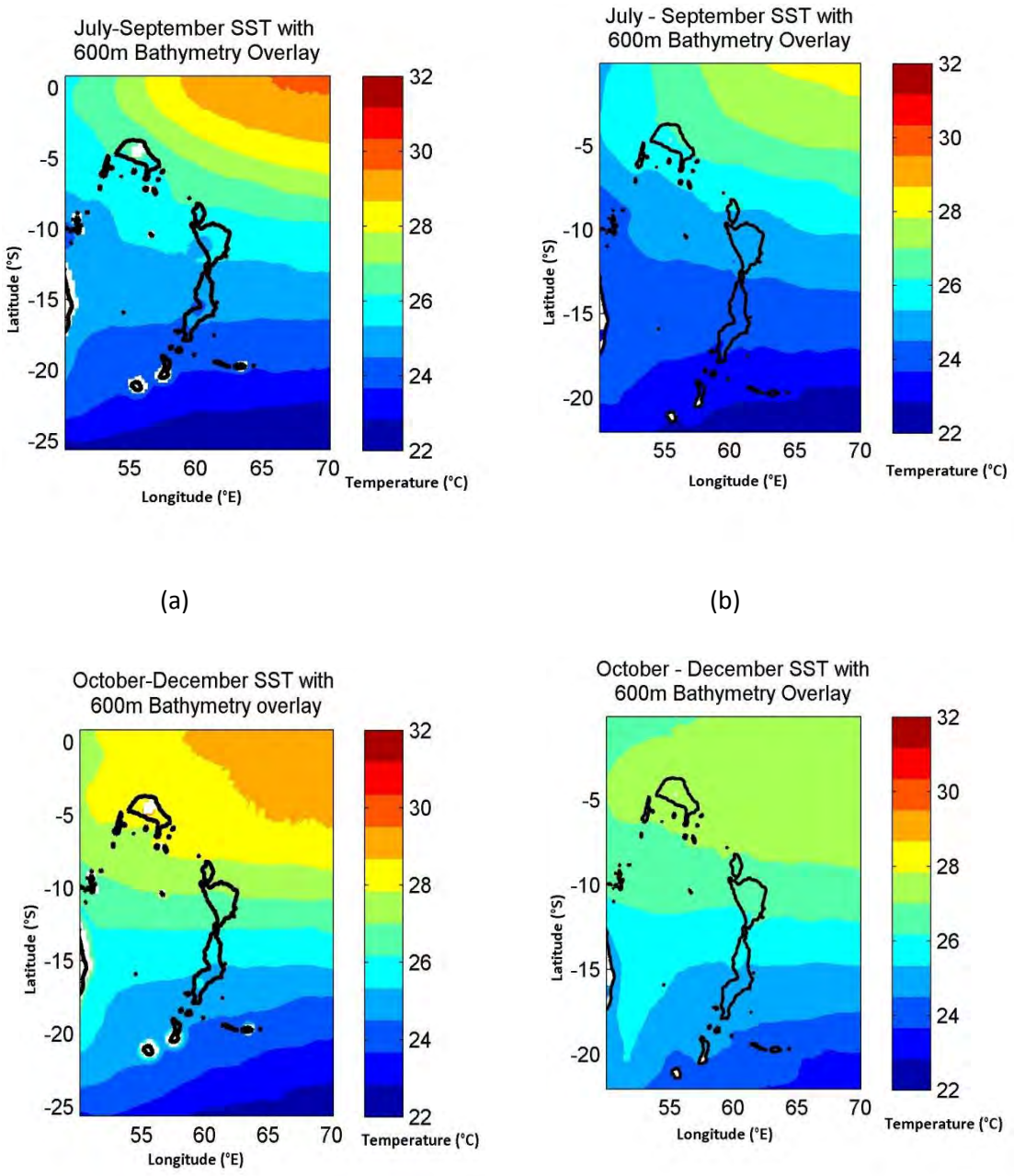

Figure 10. 7: (a) Climatological SST July - September (2000 – 2009) – Satellite Altimetry, (b) Climatological SST July - September (2000 – 2009) – OFES Model, (c) Climatological SST October - December (2000 – 2009) – Satellite Altimetry and (d) Climatological SST October - December (2000 – 2009) – OFES model. 1000m isobath overlaid in black.

Figure 10.5 and Figure 10.6 depicts maps of climatological SST for both satellite altimetry and OFES model (2000 – 2009). From Figure 10.5 and Figure 10.6, it can be seen that south of 15° S the model and observations agree very well with regards to SST whilst north of 15° S the observations are approximately 1° – 2° C warmer than the model (in the region of the Mascarene Plateau). This study highlights a certain degree of confidence when using SST climatology in the OFES model south of 15° S. However, one would need to be cautious when using this model in the region north of 15° S due to the 1° – 2° C disparity.

10.2 Cruise Observations

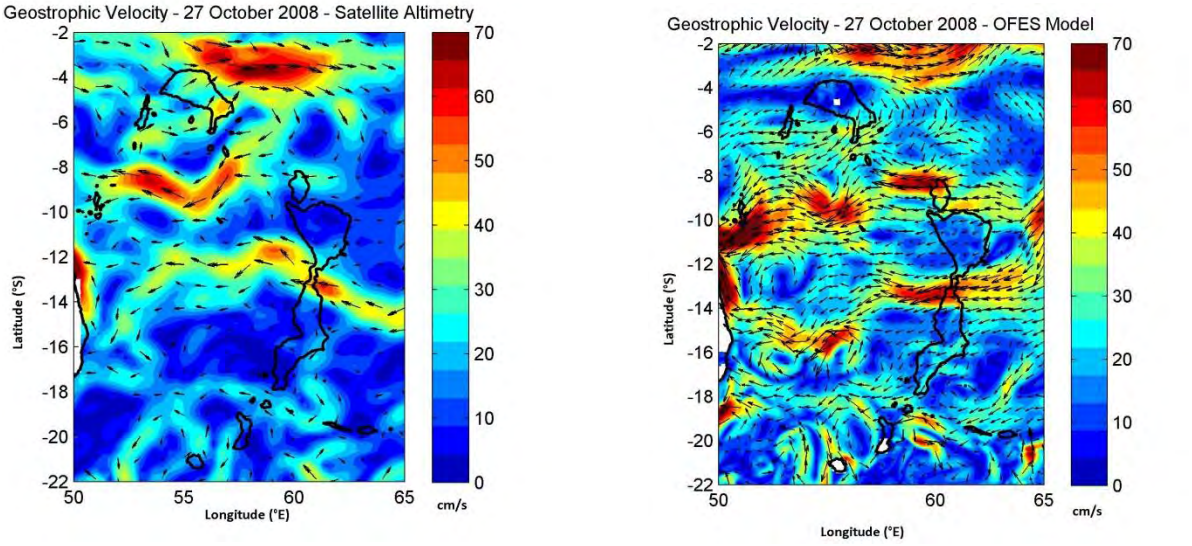

(a) (b)

Figure 10. 8: (a) Geostrophic velocity during the October/November 2008 cruise – satellite altimetry and (b) Geostrophic velocity during the October/November 2008 cruise – OFES model.

During the October/November 2008 cruise there were many similarities between the satellite estimate and the model output. The South Equatorial Current (SEC) was observed through the 3 major gaps in the Mascarene Plateau. Gap 3 had similar velocities which were approximately 25 cm/s. The geostrophic velocities between satellite observations and OFES model output through gap 2 had similar velocities of approximately 45 cm/s whilst the geostrophic velocities through gap 1 were similar but in a different position as depicted in Figure 10.7. The velocities reached up to 50 cm/s through this gap. The

geostrophic velocities to the north-east of the Seychelles Bank (SECC) were similar between the observations and model output where they reached up to 55 cm/s. A major difference was that the Seychelles Bank had velocities of approximately 30 cm/s (SECC) whilst the model output showed that the bank was quiescent with little flow.

10.3 Variability around Mascarene Plateau

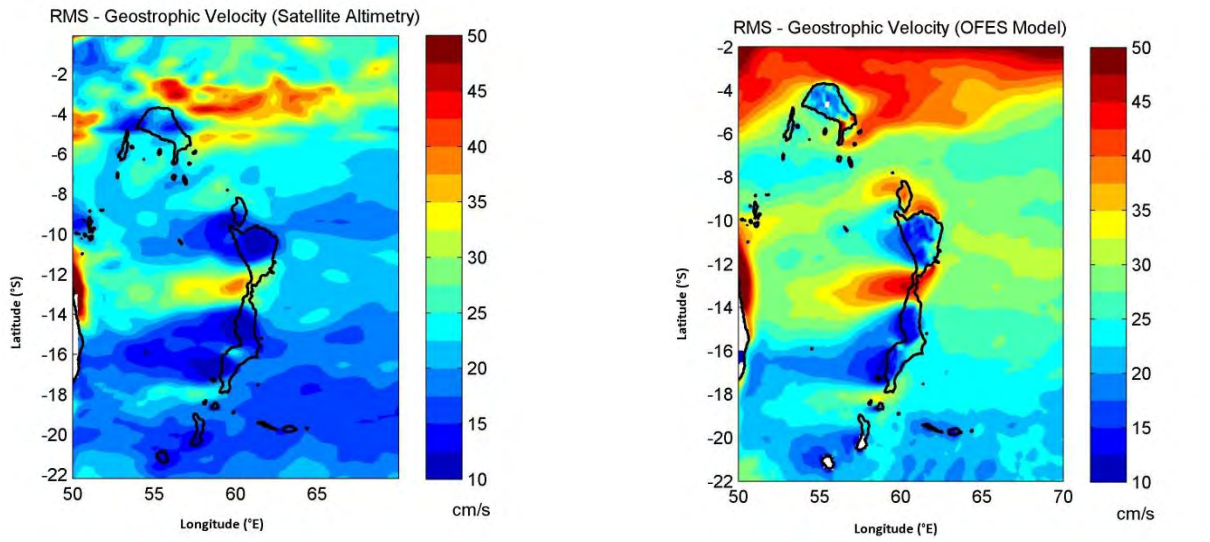

(a) (b)

Figure 10. 9: (a) RMS of Geostrophic Velocity from observations and (b) RMS of Geostrophic Velocity from OFES Model. 1000m isobath overlaid in black.

Figure 10.8a is the root mean square (RMS) of geostrophic velocity, from altimetry from 1 January 2004 to 31 December 2010 whilst figure 10.8b is from OFES, for 7 years climatology of the model run (2004 – 2010). Enhanced levels of RMS geostrophic velocity are representative of mesoscale variability. The model generally shows higher RMS values than satellite altimetry. Both the model and satellite altimetry shows enhanced levels of RMS through the 3 major gaps in the Mascarene Plateau as well as over the northern part of the Seychelles Bank. The RMS values are low and approximately the same (observation and model) on the banks whilst the model shows an RMS value of approximately 32 cm/s in gap 3 and the observation shows an RMS value of 25 cm/s which is an overestimate of 7 cm/s. Gap 2 shows an RMS value of approximately 45 cm/s in the model and 35 cm/s in the observations whilst gap 1 shows

an RMS value of between 32 cm/s and 40 cm/s in the model and values of approximately 22 cm/s in the observation. To the north of the Seychelles Bank, the variability is greatly overestimated in the model by approximately 21 cm/s. This is most likely due to the model overestimating the strength of the South Equatorial Counter Current (SECC).

10.4 Mean Eddy Kinetic Energy

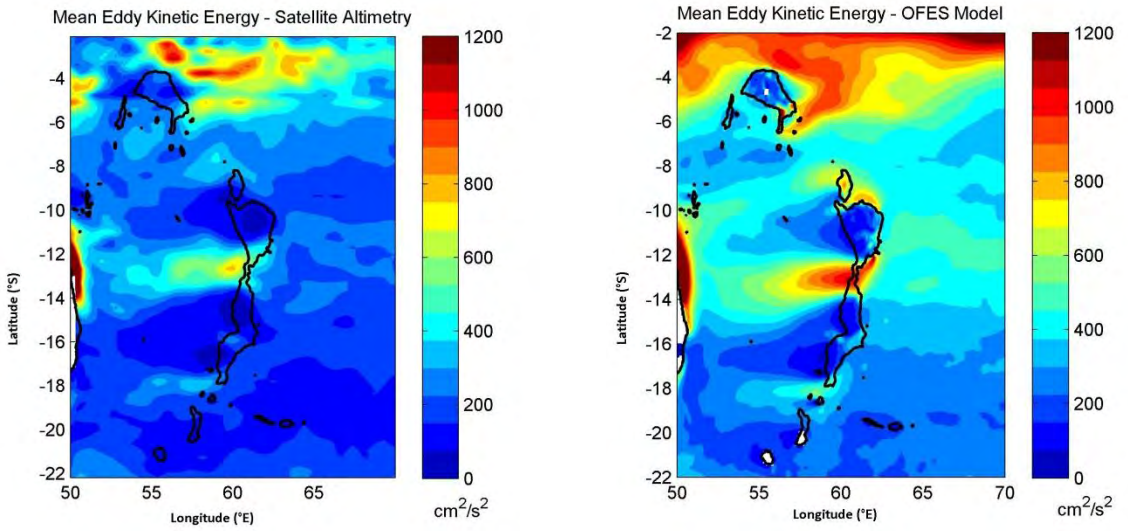

(a) (b)

Figure 10. 10: (a) Mean Eddy Kinetic Energy from observations (climatology 2004 – 2010) and (b) Mean Eddy Kinetic Energy from OFES model (climatology 2004 – 2010). 1000m isobath overlaid in black

Figure 10.8 is consistent with figure 10.9: Strong MEKE results in a strong RMS of geostrophic velocity. The OFES model generally shows higher values of MEKE than through satellite estimates. Similarly to the RMS values, the MEKE values are far greater in the model than in the satellite observations north of the Seychelles Bank. Higher values of MEKE are shown in satellite altimetry north of the Saya de Malha Bank than the surrounding areas (400 cm^2/s^2) whilst in the OFES model values in the same region are greater (700 cm^2/s^2). In gap 2, satellite altimetry shows MEKE values of approximately 750 cm^2/s^2 and the model shows values of approximately 950 cm^2/s^2. The satellite altimetry and OFES model exhibits approximately the same values of MEKE in gap 3 (370 cm^2/s^2). The model shows a stronger production of MEKE than in the satellite altimetry, likely associated with a stronger SEC and SECC in the model.

From the above, key question 8 can be addressed*: Is an OGCM (OFES) model viable in the region for further modeling studies?*

The model managed to pick up the major oceanographic features around the Mascarene Plateau such as the 3 branches of the SEC which were channeled through the 3 major gaps in the plateau, the SECC (except for the climatological period of July – September) and the 2 cores of the SEC downstream of the plateau. South of gap 2, the SST was similar. However there were differences between the model and satellite observations. The SECC was not picked up during July – September. The model either overestimated or underestimated the geostrophic velocities of the 2 major currents in the region (SECC and SEC). The maximum difference in the SECC was 30 cm/s whilst the minimum was 15 cm/s whilst the minimum difference in the SEC was 5 cm/s and the maximum difference was 10 cm/s. As the model does not pick up the SECC during July – September and the RMS and MEKE being overestimated in the region of the SECC (> 25 cm/s and 700 cm^2/s^2 respectively) it would not be advisable to use this model north of the Seychelles. The most likely reason why the model is not as accurate in the northern region as in the southern region is that the OFES global model does not resolve the monsoon seasons and its effects correctly (the different monsoon seasons affect the position and strength of the SECC). This model would be advised to only obtain a rough synoptic view of the region as the geostrophic velocities are either overestimated or underestimated in the model (although in the case of the SEC, only by a maximum of 10 cm/s). The model can be used with most confidence in obtaining the position of the northern and southern core of the SEC downstream of the Mascarene Plateau.

10.5 Summary

There are similarities between the satellite estimates and the OFES model. The OFES model manages to pick up the major oceanographic features around the Mascarene Plateau such as the 3 branches of the SEC which crossed through the major gaps in the plateau, the SECC (with the exception of the climatological period of July – September) and the 2 cores of the SEC downstream of the Mascarene Plateau. The climatological SST was also very similar south of gap 2.

However, there are major differences between the satellite observations and the OFES model. The SECC was not picked up very well in the model. Differences in velocities were great and in the period July – September (climatology), the SECC is not picked up in the model. The model overestimates the observation by 30 cm/s during the period January – March, underestimates the observation by 15 cm/s

during the period April – June whilst the model underestimates the observation by 15 cm/s during the period October – December. The SEC between the Saya de Malha Bank and the Nazareth Bank has velocities greater in the model throughout the year however the maximum difference is 10 cm/s which is small in comparison to the model overestimation of 30 cm/s in the SECC. Similarly, the velocities through gap 3 differ by a maximum of 10 cm/s between the observations and the model. Both the root mean square (RMS) values and the mean eddy kinetic energy (MEKE) values is greater in the model through the 3 main gaps in the Mascarene Plateau but these higher values occur in the same region as in the observations.

Due to the model not picking up the SECC during July – September (Climatology) and the RMS and MEKE being overestimated too much in the region of the SECC (> 25 cm/s and 700 cm^2/s^2 respectively), the model has problems in this region north of the Seychelles. One can use this model satisfactorily for SST south of gap 2. In order to obtain the position of the Northern core and Southern core, the model satisfactorily captures the position, however the strength of the velocity cannot be relied upon. One would have to be cautious to use the model between the 3 major gaps although the difference in climatological velocity is relatively small (~ 10 cm/s).

It would be advisable to use this model only to obtain rough conditions in the Mascarene Plateau region at a certain time of the year such as approximate geostrophic velocities of the SEC, SST's in the region and position of the northern and southern core of the SEC (this can be used with most confidence in the model) as values are either overestimated or underestimated in the model. However, the model captures major oceanographic features of the region such as the SEC splitting into 3 cores which flows through the 3 major gaps, the SECC (apart from July – September), the quiescence in velocity over the banks and the increased RMS and MEKE through the 3 major gaps in the Mascarene Plateau.

CHAPTER 11: Conclusions

11.1 Main Findings

The main objective of this thesis was to analyze cruise data obtained during the October/November 2008 cruise on the Dr Fridtjof Nansen which surveyed the area in the region of the Mascarene Plateau (Water masses and circulation patterns) and to compare SST and ADCP obtained currents on board to satellite data in the hope that the region can be further studied using satellite data. Biologically, Chlorophyll data was used to analyze the region to ascertain where nutrient rich and poor waters occur and whether the banks of the Mascarene Plateau have the ability to sustain separate ecosystems. Additionally, an objective of the thesis was to gain insight into the nature of the South Equatorial Current in the region (a stable, constant velocity current or a current of an oscillatory nature) and how westward propagating Rossby waves impact the geostrophic velocities through the gaps of the Mascarene Plateau. An OGCM (OFES) model was compared to observational data in order to ascertain the viability of the model in the area.

This thesis investigated a relatively understudied feature of the world's ocean, the Mascarene Plateau. It is a submerged volcanic plateau which extends between the Seychelles Bank and Mauritius. The plateau is a complex feature which is oriented in a north-south direction and is shaped similar to a crescent. It is composed of a series of banks (Seychelles, Saya de Malha, Nazareth and Cargados-Carajos Banks) which is separated by 3 deep channels. The primary water mass which was carried by the SEC (South Equatorial Current) was fresh Indonesian Throughflow Water (ITW) where it mixed with high salinity Arabian Sea High Salinity Water (ASHSW) and high salinity Sub-tropical surface water (STSW) through the northernmost gap (gap 1) and southernmost gap (gap 3) channel in the Mascarene Plateau respectively. There are marked differences in water masses between the northern part and the southern part of the Mascarene Plateau. The northern part contained nutrient rich waters (ASHSW) whilst the southern part contained nutrient poor waters (STSW). Intermediate waters consisted of Antarctic Intermediate Water (AAIW) to the south whilst the northern part of the Mascarene Plateau consisted of Red Sea Water (RSW). Towards the centre of the Mascarene Plateau (~ 13° S), mixing occurs between AAIW and RSW. The research cruise conducted during October/November 2008 confirmed that the SEC split into 3 cores to the east of the Mascarene Plateau (similarly to the cruise conducted during June/July 2002). However, the volume transport (via the SEC) differed during the second cruise. During

the cruise conducted during June/July 2002, the volume transport was 50 Sv to the east of the plateau and half of it was channeled through gap 2 whilst equal volumes were channeled through gaps 1 and 3. During the October/November 2008 cruise, the volume transport to the east was 36.53 Sv (lower than the first cruise but most likely an underestimate as there was only an SADCP onboard which reached maximum depths of 450m). The total volume through each gap from north to south was 14.93 Sv (40.87 %), 14.41 Sv (39.4 %) and 6.19 Sv (16.9 %) respectively, whilst there was a small amount of flow (~ 1 Sv) through the minor gap between the Nazareth Bank and the Cargados-Carajos Bank. The difference with the 2002 cruise may be due to the difference in the position of the SEC upstream (different seasons) and/or whether there was a recirculation loop within gap 1. The volume transport across the Saya de Malha, Nazareth and Cargados-Carajos Banks were negligible whilst the Seychelles Bank experienced the eastward flowing SECC (South Equatorial Counter Current). Downstream of the plateau, 2 cores of the SEC formed.

The SST over the Mascarene Plateau generally decreases from north to south and is of a zonal nature. The Seychelles region has the greatest influence on the SST in the region as there are many small islands in the region which increases the SST. The area which has the lowest effect on the SST is the region across the Saya de Malha and Nazareth Banks since this area has on average the deepest waters. An analysis of geostrophic velocities during 2008 reveals an increase in velocity through gap 1 due to the development of a re-circulation loop where waters from the eastward flowing SECC are drawn south and channeled through the gap. The SEC in the region is not constant in speed but is of an oscillatory nature. During 2008, gap 2 and gap 3 experienced oscillations in velocity. Eddy Kinetic Energy (climatology) is higher than normal to the east of the Seychelles Bank and to the west of the 3 major gaps in the Mascarene Plateau. The EKE is generally higher to the west of the plateau due to the increased velocity caused by the constriction of the gaps.

The area around the Mascarene Plateau roughly has 2 regions of nutrient poor waters to the south of 13° S and nutrient rich waters to the north. However, the period from October – December (climatology) contained relatively high concentrations of Chl-a as far south as approximately 16° S as opposed to the rest of the year where the concentration of Chl-a was relatively high north of 13° S. The Saya de Malha, Nazareth and Cargados-Carajos Bank have little seasonality in their concentration of Chl-a where it retains similar values and is generally higher than its surrounding areas. This indicates that a separate ecosystem could exist across these banks. The Chl-a concentrations across these banks have little seasonality as there are no major currents which cross them. However, the Seychelles Bank exhibits

seasonality similar to its surroundings due the SECC which flows across the plateau. The area with the highest variability in Chl-a concentration is in the latitude range between 9° S - 15° S. In this area, nutrient rich and poor water masses mix. The SEC flows and acts as a dividing line between nutrient rich and poor water masses but is not at a constant latitude. This shifting of the position of the SEC during the year increases the variability as Chl-a concentrations shift with the SEC.

A feature of interannual variability in the region of the Mascarene Plateau is westward propagating Rossby waves. During IOD (Indian Ocean Dipole) years, Rossby waves are generated in the eastern Indian Ocean and propagate westwards. This study has shown that there were no Rossby waves present during both the June/July 2002 and October/November 2008 research cruises. Rossby wave propagation is possible over all parts of the Mascarene Plateau. Rossby waves affect circulation patterns in the region. During January 1998, a Rossby wave crossed through gap 1. This increased the geostrophic velocity through the gap and the SECC was located northward of its normal position. The Rossby wave (June 2010) which crossed through gap 2 and gap 3 had the effect of increasing the geostrophic velocities through these gaps significantly.

As there have been few studies around the region of the Mascarene Plateau and in particular only 2 research cruises in the region, modeling studies can prove to be an invaluable mechanism in gaining more knowledge in the region. Here we compared satellite observations to an OFES model to see if this particular model could be used for further studies in the region. The model picked up the major oceanographic features around the Mascarene Plateau such as the 3 branches of the SEC which crossed through the major gaps in the plateau, the SECC (with the exception of the climatological period of July – September) and the 2 cores of the SEC downstream of the plateau. The climatological SST was similar south of gap 2. However there were major differences between the satellite observations and the OFES model. The SECC was not picked up well in the model (either and overestimation of underestimation in the model) whilst the SECC was not picked up at all during the period July – September. The SEC between the Saya de Malha and Nazareth Banks and between the Cargados-Carajos Bank and Mauritius had velocities greater in the model throughout the year. However, the maximum difference was 10 cm/s which were small in comparison to the model overestimation of 30 cm/s in the SECC. Both the root mean square (RMS) values and the mean eddy kinetic energy (MEKE) values were greater in the model through the 3 main gaps in the Mascarene Plateau but these higher values occurred in the same region as in the observations. Due to the model not picking up the SECC during July – September (Climatology), the RMS and MEKE being overestimated too much in the region of the SECC (> 25 cm/s and 700 cm^2/s^2

respectively) it would not be advised to make use of this model in this region north of the Seychelles. One can use this model satisfactorily for SST south of gap 2. In order to obtain the position of the Northern core and Southern core, the model satisfactorily captured the position, however the strength of the velocity cannot be relied upon. One would have to be cautious to use the model for the velocity between the 3 major gaps although the difference in climatological velocity is relatively small (~ 10 cm/s). It would be advisable to use this model only to obtain rough conditions in the Mascarene Plateau region at a certain time such as approximate geostrophic velocities of the SEC, SST's in the region and position of the northern and southern core of the SEC (this can be used with most confidence in the model) as values are either overestimated or underestimated in the model. However, rough conditions can be obtained since the model captures the major oceanographic features of the region such as the SEC splitting into 3 cores which flows through the 3 major gaps, the SECC (apart from July – September), the quiescence in velocity over the banks and the increased RMS and MEKE through the 3 major gaps in the Mascarene Plateau.

This study has proven, via the comparison between cruise data (on board the Dr Fridtjof Nansen), that satellite data (satellite altimetry and TRMM satellite SST) can be used to extend cruise results in both space and time. These findings will prove useful for future studies in the region as there is a lack of in-situ data over the Mascarene Plateau. Various processes such as the nature of ocean circulation patterns in the region, interannual variability (ie. Rossby waves associated with the Indian Ocean Dipole) and phytoplankton biomass can be studied by making use of satellite data in the region. Additionally, an OGCM (OFES) Model was compared to satellite data and proved to capture most of the oceanographic features in the region such as the SST and the position of the 2 branches of the SEC (South Equatorial Current) downstream of the Mascarene Plateau. Although, it is advisable to only use this model for rough estimates of conditions over the plateau, the high resolution of the model (1/10 degree) may be able to capture features such as small eddies which satellite altimetry cannot due to its course resolution. Although this model either captures an underestimate or overestimate of geostrophic velocities in the region (although it captures the velocity of the SEC well as the estimate <10 cm/s), to date this model has proved to be one of the most accurate comparisons to observational data (although other models may be more accurate but has not yet been tested in the region).

The main research questions addressed in this thesis were:

1. *Which water masses are present in the region of the Mascarene Plateau, where are their origins, where do they mix in the region and does the westward flow of the South Equatorial Current (SEC) influence the mixing? (Chapter 4)*
2. *How accurate is satellite data in the region and hence what is its viability for use in the region? (Chapter 5)*
3. *In what way is the flow of the SEC affected by the gaps in the Mascarene Plateau during the 2008 ASCLME cruise and are there differences to the cruise conducted during the June/July 2002 onboard the RRS Charles Darwin? (Chapter 6)*
4. *What seasonal effect does the Mascarene Plateau have on the geostrophic velocities, SST's and eddy kinetic energy in the region? (Chapter 7)*
5. *What is the nature of the SEC in the region and how do the geostrophic velocities during the 2008 cruise year differ from climatology? (Chapter 7)*
6. *What is the distribution of Chl-a in the region (climatology) and do the banks differ in Chl-a concentration from its surrounding areas? (Chapter 8)*
7. *Were there westward propagating Rossby waves over the Mascarene Plateau during the June/July 2002 cruise on board the RRS Charles Darwin and the October/November 2008 cruise on board the the Dr Fridtjof Nansen? Are these waves capable of crossing every part of the plateau? What effect do these waves have on the general circulation in the region? (Chapter 9)*
8. *Is an OGCM (OFES) model viable in the region for further modeling studies? (Chapter 10)*

The questions will be answered one by one in this section:

1. *Which water masses are present in the region of the Mascarene Plateau, where are their origins, where do they mix in the region and does the westward flow of the South Equatorial Current (SEC) influence the mixing?*

North of approximately 8° S, surface waters comprise of mainly ASHSW (Arabian High Salinity Water), intermediate waters comprise of RSW (Red Sea Water) whilst many areas comprise of NIDW (North Indian Deep Water). However, the westward flow of the SEC (South Equatorial Current) which flows through gap 1 influences the surface water composition in the area. The SEC carries fresh TSW (Tropical Surface Water) and fresh ITW (Indonesian Throughflow Water). Areas close to this current undergo mixing. ASHSW mixes with fresher ITW around the SEC. However, ASHSW is still the predominant water mass in the surface waters. The northern branch of the SEC is characterized in the area between 8° S and approximately 13.5° S. RSW mixes with AAIW (Antarctic Intermediate Water) in the intermediate

waters. There is also mixing between STSW and ITW in the surface waters close to the westward transport of the SEC (the northern branch) which contains ITW. The SEC acts as a barrier to STSW as there is no STSW north of it. NIDW exists in this area in areas which are deep enough and SICW is present in the region. The southern branch of the SEC is characterized in the area southward of approximately 13.5° S in the region. The intermediate waters are composed purely of AAIW. Surface waters are composed of STSW and TSW. However, close to the southern branch of the SEC, mixing occurs between STSW and ITW whilst TSW overlies these water masses. SICW and NIDW are present in this region. Hence the westward flow of the SEC influences the mixing since it contains ITW and TSW. The SEC is channeled through the 3 major gaps in the Mascarene Plateau and mixes with water masses in the northern and southern regions of the Mascarene Plateau. In the intermediate waters, RSW has its origins in the north-western region of the Arabian Sea whilst AAIW has its origins south of the Mascarene Plateau. NIDW is a difficult water mass to trace as little is known about its spreading pathways. According to Mantyla and Reid, 1995 it originates from an aged form of NADW which moves southward mixing with a deep saline water mass which underlies RSW. SICW has its origins at approximately 40° – 100° E and spreads along the subtropical gyre. STSW is traced back to the south-eastern quadrant of the Indian Ocean. ITW is traced back to the Indonesian seas as well as TSW whilst ASHSW is traced back to the Arabian Sea.

2. *How accurate is satellite data in the region and hence what is its viability for use in the region?*

The Mascarene Plateau is composed of very small islands and narrow gaps with a complex bathymetry. Satellite data is known to be relatively coarse in resolution and hence there may be significant errors for use in the region. The geostrophic velocity obtained via satellite estimate through the 3 major gaps in the Mascarene Plateau was compared to the ADCP currents obtained on board the October/November 2008 cruise. Average velocities were used through these gaps (as velocities were not constant over the entire length of the gap). The results were encouraging with only a 1.78 cm/s difference through gap 1, 5.48 cm/s through gap 2 and 1.04 cm/s through gap 3. Although the difference was 5.48 cm/s through gap 2, it is acceptable since velocities can easily reach 50 cm/s. The greater difference was due to the narrowness of the gap. These results are very encouraging for the use of satellite altimetry in the region. The greatest difference between SST obtained via cruise data and satellite SST was 1° C which is acceptable since satellite data was available weekly. Since satellite data can be used in the region, cruise data can be extended in space and time.

3. *In what way is the flow of the SEC affected by the gaps in the Mascarene Plateau during the 2008 ASCLME cruise and are there differences to the cruise conducted during the June/July 2002 onboard the RRS Charles Darwin?*

During the cruise in October/November 2008, the SEC transport to the east of the Mascarene Plateau was 36.53 Sv. The volume transport through each of the major gaps in the Mascarene Plateau were 14.93 Sv or 40.87% through gap 1, 14.41 Sv or 39.4% through gap 2 and 6.19 Sv or 16.9% through gap 3. There was approximately an extra 1 Sv or 2.73% which flows through the small gap between the Nazareth and Cargados-Carajos Bank but is not shown on altimetry maps and hence it could be ageostrophic in nature. Downstream of the Mascarene Plateau, 2 cores of the SEC were formed, a northern and southern core. The northern core composed primarily of the flow between the Saya de Malha and Nazareth Banks with a small amount of flow between the Seychelles and Saya de Malha Bank being augmented into it. The southern core comprised of the flow between the Cargados-Carajos Bank and Mauritius with augmented flow from the south. During the June/July 2002 cruise, 50 Sv flowed east of the Mascarene Plateau with half of the flow being channeled through gap 2 with the rest flowing in equal volumes through gap 3 and gap 1. The difference between the 2 cruises may be due to seasonality and a re-circulation loop existed just prior to the October/November 2008 cruise in gap 1 which would increase the geostrophic velocities in the region. The SEC existed in a broad band between 10° – 16° S during June 2002 and between 7° – 12° S in 2008. Hence there was a northward shift during October 2008 which may have contributed to extra (less) flow through the most northerly (southerly) gap in the plateau.

4. *What seasonal effect does the Mascarene Plateau have on the geostrophic velocities, SST's and eddy kinetic energy in the region?*

There are 2 major currents in the region of the Mascarene Plateau, the SEC (South Equatorial Current) and the SECC (South Equatorial Counter Current). The bathymetry of the Mascarene Plateau causes the SEC to split into 3 cores which subsequently flow through the 3 major gaps of the bathymetric feature. Downstream of the Mascarene Plateau, the SEC is composed of a northern and southern core located at approximately 13° S and 18° S respectively. The maximum/minimum geostrophic velocities occur during different times of the year through the 3 major gaps due to the movement of the SEC upstream during the year. A re-circulation loop which forms occasionally through gap 1 also has the effect of increasing the geostrophic velocity through this gap. The SST distribution remains fairly zonal throughout the year (general decrease with increasing latitudes). The gaps experience highest SST's during March with

lowest SST's during August. The Seychelles Bank has the effect of increasing the SST the greatest over the plateau as it is composed of the shallowest bathymetry. Similarly, the region around gap 3 has increased SST's compared to its surroundings mainly due to the gap being narrow and the presence of Mauritius has the effect of increasing the SST (shallow bathymetry). The region around the Saya de Malha Bank and Nazareth Bank has the least effect on the SST over the Mascarene Plateau but SST's are still greater than regions offshore of the Mascarene Plateau. The Mascarene Plateau has the effect of increasing the Eddy Kinetic Energy as the SEC increases its velocity through the Mascarene Plateau and hence the EKE is greater to the west of the plateau. The maximum EKE through gap 1 is approximately 350 cm^2/s^2 during December with the lowest EKE during April with values of approximately 50 cm^2/s^2. The maximum EKE through gap 2 is approximately 360 cm^2/s^2 during January with the lowest EKE during April with values of approximately 160 cm^2/s^2. The maximum EKE through gap 3 is approximately 150 cm^2/s^2 during June with minimum values of approximately 40 cm^2/s^2 during July.

5. *What is the nature of the SEC in the region and how do the geostrophic velocities during the 2008 cruise year differ from climatology?*

The SEC is not a constant current with regards to velocity. The geostrophic velocity through gap 2 and 3 oscillates. When a re-circulation loop forms in gap 1, it hinders the westward progression of the SEC through the gap as the re-circulation loop contains waters predominantly from the eastward flowing SECC. During 2008 in gap 1, a re-circulation loop developed which increased velocities up to 32 cm/s during September 2008 whereby the climatology during that time was 10 cm/s. Other than during this event, the geostrophic velocities through this gap was similar to the climatology. There was a period of increased geostrophic velocity from mid October 2008 – early February 2009 in gap 2 with a peak in early December 2008 with values of approximately 50 cm/s with climatological values in December of 25 cm/s. This increased velocity was due to an oscillation of geostrophic velocity (nature of the SEC). The geostrophic velocity through this gap was higher than the climatology throughout the year and was of an oscillatory nature. Similarly, due to an oscillation of geostrophic velocity in gap 3 during February – June 2008, velocities reached up to 33 cm/s during March 2008 where the climatology is approximately 15 cm/s. For the rest of 2008, the geostrophic velocity was lower but there was still an oscillation where the maximum velocity was 18 cm/s during September 2008 (climatology is 12 cm/s). During this event the geostrophic current was lower than the climatology during November 2008 where it was 5 cm/s and the climatology is 10 cm/s.

6. *What is the distribution of Chl-a in the region (climatology) and do the banks differ in Chl-a concentration from its surrounding areas?*

The area around the Mascarene Plateau is divided into 2 areas, the northern region (north of approximately 13° S) which is composed primarily of nutrient rich waters (ASHSW – Arabian Sea High Salinity Water) and a southern region which is composed primarily of nutrient poor waters (STSW (Sub Tropical Surface Water). The Saya de Malha, Nazareth and Cargados-Carajos Banks retain relatively high Chl-a concentrations throughout the year as opposed to the surrounding areas where there is a distinct seasonality. However, the Seychelles Bank contains similar characteristics to its surrounding region due to the SECC which crosses over it and has distinct seasonality. The area with the highest variability is the latitude range between 9° S - 15° S. This is due to nutrient poor water masses mixing with nutrient rich water masses. The SEC acts as a dividing line between the rich and poor water masses and shifts in position throughout the year which increases the variability of Chl-a concentrations in the region.

7. *Were there westward propagating Rossby waves over the Mascarene Plateau during the June/July 2002 cruise on board the RRS Charles Darwin and the October/November 2008 cruise on board the the Dr Fridtjof Nansen? Are these waves capable of crossing every part of the plateau? What effect do these waves have on the general circulation in the region?*

There were no Rossby waves in the region of the Mascarene Plateau during both cruises. Rossby waves can propagate over all the gaps and banks of the plateau and can change the circulation patterns in the region (geostrophic velocities). However, it has been proven that a few Rossby waves do not cross the Mascarene Plateau and fade away. It was not ascertained in this study as to whether the Mascarene Plateau was the reason for the disappearance of these waves. If they propagate through any of the gaps in the plateau, the geostrophic velocity increases significantly.

8. *Is an OGCM (OFES) model viable in the region for further modeling studies?*

The model managed to pick up the major oceanographic features around the Mascarene Plateau (3 branches of the SEC channeled through the 3 major gaps, the SECC and the 2 cores of the SEC downstream of the plateau). South of gap 2, the SST was similar. However there were differences between the model and satellite observations. The SECC was not picked up during July – September and it either overestimated or underestimated the geostrophic velocities in the region. As the model does not pick up the SECC during July – September and the RMS and MEKE being grossly overestimated in the region of the SECC, it would not be advisable to use this model north of the Seychelles. This model

would be advised to use only to obtain a rough synoptic view of the region as the geostrophic velocities are either overestimated or underestimated in the model. The model can be used with confidence in obtaining the position of the southern and northern cores of the SEC downstream of the plateau.

11.2 Future Work

Although this study has helped gain new knowledge and insight into the oceanic processes occurring over the Mascarene Plateau, there are still many gaps in knowledge. Since there was an absence of Rossby waves during both cruises which have occurred in the region, a cruise would help gain much insight into the knowledge of the region during a Rossby wave propagation (circulation patterns via ADCP, affect the waves have on water masses in the region, nutrient content in the region etc.). The cruise would most likely need to be undertaken during a + IOD year since during these years the plateau has a much greater chance of encountering Rossby waves. More CTD stations would need to be deployed in gap 2 and a LADCP would also need to be deployed since there has only been 1 velocity profile which reached the ocean floor in this region and hence there cannot be a complete understanding of the volume flux through this gap (LADCP deployment during the cruise conducted between June/July 2002). To date there have been very little modeling studies in the region. Since satellite data is relatively course compared to the potential resolution of model data, small features may be able to be detected from model data where satellite data cannot. Although we have learnt that the banks and gaps have a significant role in the evolution of the South Equatorial Current (SEC), one can gain more insight into the affect by removing certain gaps or banks in a model and observing the evolution of the SEC downstream as well as other general oceanographic features such as the position of water masses, the amount and position where water mass mixing occurs. Through this, on a bigger scale we could see the affect the Mascarene Plateau has on the greater region in the South west Indian Ocean such as the circulation in the Mozambique Channel (its eddies) and the greater Agulhas Current system since the waters from the SEC feed into the system. The deployment of moorings in the 3 major gaps in the Mascarene Plateau would assist in understanding the dynamical nature of the volume transport across the Mascarene Plateau. As it was established that there were differences in the volume transport through the 3 gaps during the 2 cruises which occurred during different seasons, through the use of moorings, time series of volume transport can be obtained (as well as velocities) and a better understanding of the change in volume transport due to seasonality can be established.

Bibliography

Ansorge, I. J. and J. R. E. Lutjeharms (2007): *Currents, Continents and Convergences: The Cetacean Environment off Southern Africa. In The Whales and Dolphins of the Southern African Subregion*, P. B. Best and P. A. Folkens, eds. Cambridge University Press. 5 – 13.

Ashok, K.; Z. Guan; and T. Yamagata (2003): A look at the relationship between the ENSO and the Indian Ocean dipole. *Journal of the Meteorological Society of Japan*, 81: 41 – 56.

Aviso. Available:

http://www.aviso.altimetry.fr/en/data/data-access/aviso-cnes-data-center.html.

Backeberg, B. C.; J. A. Johonnessen; L. Bertino and C. Reason (2008): The greater Agulhas Current system: An integrated study of its mesoscale variability. *Journal of Operational Oceanography*, 1: 29 – 44.

Baquero-Bernal, A.; M. Latif; and M. Legutke (2002): On dipole like variability of sea surface temperature in the tropical Indian Ocean. *Journal of Climatology*, 15: 1358 – 1368.

Beal, L. M. and H. L. Bryden (1999): The velocity and vorticity structure of the Agulhas Current at 32° S. *Journal of Geophysical Research*, 104(C3): 5151 – 5176.

Beal, L. M.; A. Field; and A. L. Gordon (2000): Spreading of the Red Sea overflow waters in the Indian Ocean. *Journal of Geophysical Research*, 105: 8549 – 8564.

Behera, S. K.; S. Krishnan and T. Yamagata (1999): Anomalous air-sea coupling in the southern tropical Indian Ocean during the boreal summer of 1994. *Geophysical Research Letters*, 26: 3001 – 3004.

Behera, S. K. and T. Yamagata (2003): Influence of the Indian Ocean dipole on the southern oscillation. *Journal of the Meteorological Society of Japan*, 81: 169 – 177.

Behera, S. K.; A . S. Rao; S. N. Hameed; and T. Yamagata (2003): Comments on "A cautionary note on the interpretation of EOF's". *Journal of Climate*, 16: 1087 – 1093.

Behrenfeld, M; R. O'Malley; D. A. Siegel; C. McClain; J. Sarmiento; G. Feldman; P. Falkowski; E. Boss; and A. Milligan (2006): Climate-driven trends in contemporary ocean productivity. *Nature*, 444: 752 – 755.

Biastoch, A.; C. W. Böning; and J. R. E. Lutjeharms (2008a): Agulhas leakage dynamics affects decadal variability in Atlantic overturning circulation. *Nature*, 456: 489 – 492.

Biastoch, A.; C. W. Boning; F. U. Schwarzkopf; and J. R. E. Lutjeharms (2009): Increase in Agulhas leakage due to poleward shift of Southern Hemisphere westerlies. *Science*, 462: 495 – 499.

Casal, T. G. D.; L. M. Beal; R. Lumpkin; and W. E. Johns (2009): Structure and downstream evolution of the Agulhas Current system during a quasi – synoptic survey in February – March 2003. *Journal of Geophysical Research*, 114(C3): 1978 – 2012.

Chambers, D. P.; B. D. Tapley; and R. H. Stewart (1999): Anomalous warming in the Indian Ocean coincident with El Niño. *Journal of Geophysical Research*, 104: 3035 – 3047.

Chelton, D. B. and M. G. Schlax (1996): Global observations of oceanic Rossby waves. *Science*, 272: 234 – 238.

Chelton, D. B.; M. G. Schlax and R. M. Samelson (2011): Global observations of nonlinear mesoscale eddies. *Progress in Oceanography*, 91: 167 – 216.

Clark, C. O.; P. J. Webster; and J. E. Cole (2003): Interdecadal variability of the relationship between the Indian Ocean Zonal Mode and East African coastal rainfall anomalies. *Journal of Climate*, 16: 548 – 554.

Collins, C (2013): *The dynamics and physical processes of the Comoros Basin.* PhD thesis, University of Cape Town.

Conkright, M. E.; R. A. Locarnini; H. E. Garcia; T. D. O'Brien; T. P. Boyer; C. Stephens; and J. I. Antonov (2002): *World Ocean Atlas 2001: Objective Analysis, Data Statistics, and Figures*. National Oceanographic Data Center, Silver Spring, MD.

Crawford, W. R.; P. J. Brickley; T. D. Peterson and A. C. Thomas (2005): Impact of Haida Eddies on Chlorophyll distribution in the Eastern Gulf of Alaska. *Deep Sea Research Part 2*, 52: 975 – 989.

Demopoulos, A. W. J.; C. R. Smith; and P.A. Tyler (2003): Ecology of the deep Indian Ocean Floor. *Ecosystems of the World,* 28: 219 – 237.

De Ruijter, W. P. M.; A. Biastoch; S. S. Drijfhout; J. R. E. Lutjeharms; R. P. Matano; T. Pichevin; P. J. van Leeuwen; and W. Weijer (1999): Indian-Atlantic inter-ocean exchange: dynamics, estimation and impact. *Journal of Geophysical Research*, 104: 20885 – 20911.

De Ruijter, W. P. M.; H. Ridderinkhof; and M. W. Schouten (2005): Variability of the Southwest Indian Ocean. *Philosophical Transactionsof the Royal Society A*, 363: 63 – 76.

Dierssen, H. M. (2010): Perspectives on empirical approaches for ocean color remote sensing of Chlorophyll in a changing climate. *Proceedings of the National Academy of Sciences*, 107: 17073 – 17078.

Donohue, K. A. and J. M. Toole (2003): A near synoptic survey of the Southwest Indian Ocean. *Deep Sea Research Part 2*, 50: 1893 - 1931.

Emery, W. J. (2001): *Water types and water masses. In Encyclopedia of Ocean Sciences*, J. H. Steele; S. A. Thorpe; and K. K. Turekian, eds. London: Academic Press. 3179 – 3187

Feng, M. and G. Meyers (2003): Interannual variability in the tropical Indian Ocean: a two-year time scale of IOD. *Deep Sea Research Part 2*, 50: 2263 – 2284.

Fine, R. A. (1993): Circulation of Antarctic intermediate water in the South Indian Ocean. *Deep Sea Research Part 1: Oceanographic Research Papers*, 40: 2021 – 2042.

Fischer, A. S.; P. Terray; P. Delecluse; S. Gualdi; and E. Guilyardi (2005): Triggers for tropical Indian Ocean variability and links to ENSO in a constrained coupled climate model. *Journal of Climatology*, 18: 3428 – 3449.

Fu, L.; D. Chelton; P. Le Traon; and R. Morrow (2010): Eddy dynamics from satellite altimetry. *Oceanography*, 23: 14 – 25.

Gadgil, S. (2003): The Indian monsoon and its variability. *Annual Review of Earth and Planetary Sciences*, 31: 429 – 467.

Ganachaud, A.; J. Marotzke; and J. Toole (2000): The meridional overturning and large-scale circulation of the Indian Ocean. *Journal of Geophysical Research*, 105: 26117 – 26134.

Garternicht, U. and F. Schott (1997): Heat fluxes of the Indian Ocean from a global eddy-resolving model. *Journal of Geophysical Research*, 102: 21147 – 21159.

Gnanaseelan, C.; B. H. Vaid; P. S. Polito; and P. S. Salvekar (2005): Interannual variability of Rossby waves in the Indian Ocean and its impact on Indian Ocean Dipole. *Resubmitted to Journal of Geophysical Research (JGR-Oceans)* **.**

GODAE OceanView. Available:

https://www.godae-oceanview.org/science/ocean-forecasting-systems/ocean-models/ [Accessed, 17 August 2015].

Godfrey, J. S. and A. J. Weaver (1991): Is the Leeuwin Current driven by Pacific heating and winds? *Progress in Oceanography*, 27: 225 – 272.

Goes, J. I.; P. G. Thoppil; H. R. Gomes; and J. T. Fasullo (2005): Warming of the Eurasian landmass is making the Arabian Sea more productive. *Science*, 308: 545 – 547.

Gordon, H. R. and A. Y. Morel (1983): *Remote Assessment of Ocean Color for Interpretation of Satellite Visible Imagery: A Review.* Springer-Verlag, New York.

Gordon, A. L. (1986): Interocean exchange of thermocline water. *Journal of Geophysical Research*, 91(C4): 5037 – 5046.

Gordon, A. L.; J. R. E. Lutjeharms; and M. L. Gründlingh (1987): Stratification and circulation at the Agulhas retroflection. *Deep Sea Research*, 34: 565 – 599.

Gordon, A. L. (2005): Oceanography of the Indonesian seas and their throughflow. *Oceanography*, 18: 14 – 27.

Gründlingh, M. L. (1980): On the volume transport of the Agulhas Current. *Deep Sea Research Part A*,27: 557 – 563.

Gründlingh, M. L.; R. A. Carter; and R. C. Stanton (1991): Circulation and water properties of the southwest Indian Ocean, Spring 1987. *Progress in Oceanography*, 28: 305 – 342.

Halpern, D.; M. H. Freilich; and R. A. Weller (1998): Arabian sea surface winds and ocean transports determined from ERS-1 scatterometer. *Journal of Geophysical Research*, 103: 7799 – 7805.

Han, W. and J. P. McCreary (2001): Modelling salinity distributions in the Indian Ocean. *Journal of Geophysical Research*, 106: 859 – 877.

Jensen, T. G. (2003): Cross-equatorial pathways of salt and tracers from the northern Indian Ocean: Modelling results. *Deep Sea Research*, 50: 2111 – 2128.

Jia, F.; L. Wu and B. Qiu (2011): Seasonal Modulation off Eddy Kinetic Energy and its Formation Mechanism in the Southeast Indian Ocean. *Journal of Physical Oceanography*, 41: 657 – 665.

Kalnay, E.; M. Kanamitsu; R. Kistler; W. Collins; D. Deaven; L. Gandin; M. Iredell; S. Saha; G. White; J. Woollen; Y. Zhu; A. Leetmaa; B. Reynolds; M. Chelliah; W. Ebisuzaki; W. Higgins; J. Janowiak; K. Mo; C. Ropelewski; J. Wang; R. Jenne; and D. Joseph (1996): The NCEP/NCAR 40-Year reanalysis project. *Bulletin of the American Meteorological Society*, 77: 437 – 471.

Kawamura, R. (1988): Quasi-biennial oscillation modes appearing in the tropical sea water temperature and 700 mb zonal wind. *Journal of the Meteorological Society of Japan*, 66: 955 – 965.

Kim, E. J.; S. K. Kang; S. T. Jang; J. H. Lee; Y. H. Kim; H. W. Kang; Y. Y. Kwon; and Y. H. Seung (2010): Satellite-Derived SST validation based on In-Situ Data during Summer in the East China Sea and Western North Pacific. *Ocean Science Journal*, 45(3): 159 – 170.

Klein, R. J. T.; R. J. Nicholls; and N. Mimura (1999): Coastal adaptation to climate change: Can the IPCC technical guidelines be applied? *Mitigation and Adaptation Strategies for Global Change*, 4: 239 – 252.

Knox, R. (1976): On a long series of measurements of Indian Ocean equatorial currents near Addu Atoll. *Deep Sea Research*, 23: 211 – 221.

Koch-Larrouy, A.; G. Madec; P. Bouruet-Aubertot; T. Gerkema; L. Bessières; and R. Molcard (2007): On the transformation of Pacific water into Indonesian throughflow water by internal tidal mixing. *Geophysical Research Letters*, 34: L04604.

Kumar, P. S. and T. G. Prasad (1999): Formation and spreading of Arabian Sea High Salinity water mass. *Journal of Geophysical Research*, 104: 1455 – 1464.

Lee, T. and J. Marotzke (1998): Seasonal cycle of meridional overturning and heat transport of the Indian Ocean. *Journal of Physical Oceanography*, 28: 923 – 943.

Levitus, S.; R. Burgett; and T. P. Boyer (1994): *World Ocean Atlas 1994*. U.S. Government Printing Office, Washington DC. 3: 99.

Levy, M. and P. Klein (2004): Does the low frequency variability of mesoscale dynamics explain a part of the phytoplankton and zooplankton spectral variability? *Proceedings of the Royal Society of London*, 460: 1673 – 1683.

Lin, J. L.; G. N. Kiladis; B. E. Mapes; K. M. Weickmann; K. R. Sperber; W. Lin; M. C. Wheeler; S. D. Schubert; A. Del Genio; L. J. Donner; S. Emori; J. F. Gueremy; F. Hourdin; P. J. Rasch; E. Roeckner; and J. F. Scinocca (2006): Tropical intraseasonal variability in 14 IPCC AR4 climate models. Part 1: Convective signals. *Journal of Climate*, 19: 2665 – 2690.

Liu, Z. and M. Alexander (2007): Atmospheric bridge, oceanic tunnel, and global climatic teleconnections. *Reviews of Geophysics*, 45: RG2005.

Longhurst, A.; S. Sathyendranath; T. Platt; and C. Caverhill (1995): An estimate of global primary production in the ocean from satellite radiometer data. *Journal of PlanktonResearch*, 17: 1245 – 1271.

Lumpkin, R. and K. Speer (2007): Global ocean meridional overturning. *Journal of Physical Oceanography*, 37: 2550 – 2562.

Lutjeharms, J. R. E. and H. R. Roberts (1988): The Natal Pulse, an extreme transient on the Agulhas Current. *Journal of Geophysical Research*, 93: 631 – 645.

Lutjeharms, J. R. E. and R. C. van Ballegooyen (1988b): Anomalous upstream retroflection in the Agulhas Current. *Science*, 240: 1770 – 1772.

Lutjeharms, J. R. E. and I. J. Ansorge (2001): The Agulhas return current. *Journal of Marine Systems*, 30: 115 – 138.

Lutjeharms, J. R. E.; O. Boebel; P. C. F. van der Vaart; W. P. M. de Ruijter; T. Rossby; and H. L. Bryden (2001): Evidence that the natal pulse involves the Agulhas Current to its full depth. *Geophysical Research Letters*, 28(18): 3449 – 3452.

Lutjeharms, J. R. E. (2006a): The coastal oceans of south-eastern Africa. *In the Sea*, 14B: 783 – 834.

Lutjeharms, J. R. E. (2006b): The ocean environment off south-eastern Africa: a review. *South African Journal of Science*, 102: 419 – 426.

Madden, R. and P. Julian (1972): Description of global-scale circulation cells in the tropics with a 40 – 50 day period. *Journal of Atmospheric Science*, 29: 1109 – 1123.

Mantyla, A. W. and J. L. Reid (1995): On the origins of deep and bottom waters of the Indian Ocean. *Journal of Geophysical Research*, 100: 2417 – 2439.

Masumoto, Y.; H. Sasaki; T. Kagimoto; N. Komori; A. Ishida; Y. Sasai; T. Miyama; T. Motoi; H. Mitsudera; K. Takahashi; H. Sakuma; and T. Yamagata (2004): A fifty-year eddy – resolving simulation of the world ocean: Preliminary outcomes of OFES (OGCM for the Earth simulator). *Journal of the Earth Simulator*, 1: 35 – 56.

McCartney, M. S. (1982): The subtropical circulation of mode waters. *Journal of Marine Research*, 40: 427 – 464.

McCreary, J. P.; R. Furue; T. Jensen; H. W. Kang; B. Bang; and T. Qu (2007): Interactions between the Indonesian Throughflow and circulations in the Indian and Pacific Oceans. *Progress in Oceanography*, 75: 70 – 114.

McWilliams, J. C. (2013): The nature and Consequences of Oceanic Eddies. In *Ocean Modeling in an Eddying Regime*. M. W. Hecht and H. Hasumi, Eds. Washington, D.C.: American Geophysical Union: 5-15.

Morrow, R.; F. Birol; D. Griffin and J. Sudre (2004): Divergent pathways of cyclonic and anti-cyclonic ocean eddies. *Geophysical Research Letters*, 31(L24311).

Murtugudde, R.; J. P. McCreary; and A. J. Busalacchi Jr (2000): Oceanic processes associated with anomalous events in the Indian Ocean with relevance to 1997 – 1998. *Journal of Geophysical Research*, 105: 3295 – 3306.

Nagura, M. and M. Konda (2007): The seasonal development of an SST anomaly in the Indian Ocean and its relationship to ENSO. *Journal of Climatology*, 20: 38 – 52.

New, A. L.; K. L. Stansfield; D. Smythe-Wright; D. A. Smeed; A. J. Evans; and S. G. Alderson (2005): Physical and biochemical aspects of the flow across the Mascarene Plateau in the Indian Ocean. *Philosophical Transactions of the Royal Society*, A363: 151 – 168.

New, A. L.; S. G. Alderson; D. A. Smeed; and K. L. Stansfield (2007): On the circulation of water masses across the Mascarene Plateau in the South Indian Ocean. *Deep Sea Research Part 1: Oceanographic Research Papers*, 54(1): 42 – 74.

New, A. L.; J.M. Magalhaes; and J. C. B. da Silva (2013): Internal Solitary Waves on the Saya de Malha Bank of the Mascarene Plateau: SAR observations and interpretation. *Deep Sea Research Part 1: Oceanographic Research Papers*, 79: 50 – 61.

Nigam, S. and H. S. Shen (1993): Structure of oceanic and atmospheric low-frequency variability over the tropical Pacific and Indian Oceans. Part 1: COADS observations. *Journal of Climate*, 6: 657 – 676.

Pacanowski, R.C. and S. M. Griffies (1999): *The MOM3 Manual, NOAA/Geophysical Fluid Dynamics Laboratory*. Princeton, USA.

Palastanga, V.; P. van Leeuwen; and W. de Ruijter (2006): A link between low-frequency mesoscale eddy variability around Madagascar and the large-scale Indian Ocean variability. *Journal of Geophysical Research*, 111: C09029.

Payet, R. (2005): Research, assessment and management on the Mascarene Plateau: a large marine ecosystem perspective. *Philosophical Transactionsof the Royal Society A*, 363: 295 – 307.

Pickard, G. L. and W. J. Emery (1990): *Descriptive Physical Oceanography.* Pergamon Press, Oxford.

Piola, A. R. and A. L. Gordon (1989): Intermediate waters in the Southwest South Atlantic. *Deep Sea Research Part A*, 36: 1 – 16.

Rao, S. A.; S. K. Behera; Y. Masumoto; and T. Yamagata (2002): Interannual variability in the subsurface tropical Indian Ocean with a special emphasis on the Indian Ocean dipole. *Deep Sea Research part 2*, 49: 1549 – 1572.

Rao, L. V. G. and P. Shree Ram (2005): *Upper Ocean Physical Processes in the Tropical Indian Ocean*. National Institute of Oceanography, Goa, India.

Rasmusson, E. M. and T. H. Carpenter (1982): Variations in tropical sea surface temperature and surface wind fields associated with the Southern Oscillation / *El Niño. Monthly Weather Review, 110: 354 – 384.*

Read, J. F. and R. T. Pollard (1993): Structure and transport of the Antarctic circumpolar current and Agulhas return current at 40° E. *Journal of Geophysical Research*, 98: 12281 – 12295.

Reason, C. J. C.; R. J. Allan; J. A. Lindesay; and T.J. Ansell (2000): ENSO and climatic signals across the Indian Ocean basin in the global context: Part 1, Interannual composite patterns. *International Journal of Climatology*, 20: 1285 – 1327.

Reason, C. J. C.; D. Jagadheesha; and M. Tadross (2003): A model investigation of interannual winter rainfall variability over southwestern South Africa and associated ocean-atmosphere interaction. *South African Journal of Science*, 99: 75 – 80.

Richardson, P. L. (2007): Agulhas leakage into the Atlantic estimated with subsurface floats and surface drifters. *Deep Sea Research Part 1: Oceanographic Research Papers,* 54(8): 1361 – 1389.

Ridderinkhof, H.; P. M. van der Werf; J. E. Ullgren; H. M. van Aken; P. J. van Leeuwen and W. P. M. de Ruijter (2010): Seasonal and interannual variability in the Mozambique Channel from moored current observations. *Journal of Geophysical Research – Oceans*, 115(C06010).

Roman, R. E. and J. R. E. Lutjeharms (2009): Red Sea intermediate water in the source regions of the Agulhas Current. *Deep Sea Research Part 1*, 56: 939 – 962.

Royal Geographical Society. n.d. Shoals of Capricorn 1998 – 2001. Available: http://www.rgs.org/OurWork/Fieldwork+and+Expeditions/Resources/Past+Field+Programmes/Indian+Ocean/Shoals+of+Capricorn+1998-2001.htm. [Accessed, 12 September 2014]

Saji, N. H.; B. N. Goswami; P. N. Vinayachandran; and T. Yamagata (1999): A dipole mode in the tropical Indian Ocean. *Nature*, 401: 360 – 363.

Saji, N. H. and T. Yamagata (2003): Structure of SST and surface wind variability during Indian Ocean Dipole Mode years: COADS observations. *Journal of Climatology*, 16: 2735 – 2751.

Salby, M. L. and H. H. Hendon (1994): Intraseasonal behavior of clouds, winds, and temperature in the tropics. *Journal of Atmospheric Science*, 51: 2344 – 2367.

Sasaki, Y. N.; S. Minobe; N. Schneider; T. Kagimoto; M. Nonaka; and H. Sasaki (2008): Decadal sea level variability in the South Pacific in a global eddy-resolving ocean model hindcast. *Journal of Physical Oceanography*, 38: 1731 – 1747.

Schott, F. A. and J. P. McCreary (2001): The monsoon circulation of the Indian Ocean. *Progress in Oceanography,* 51(1): 1 – 123.

Schott, F. A.; S. P. Xie; and J. P. McCreary Jr (2009): Indian Ocean circulation and climate variability. *Reviews of Geophysics*, 47(1): 1 – 46.

Schouten, M. W.; W. P. M. de Ruijter; P. J. van Leeuwen; and J. R. E. Lutjeharms (2000): Translation, decay and splitting of Agulhas rings in the south-east Atlantic Ocean. *Journal of Geophysical Research*, 105: 21913 – 21925.

Siedler, G.; M. Rouault; and J. R. E. Lutjeharms (2006): Structure and origin of the subtropical South Indian Ocean countercurrent. *Geophysical Research Letters*, 33: L24609.

Slingo, J. M.; K. R. Sperber; J. S. Boyle; J. P. Ceron; M. Dix; B. Dugas; W. Ebisuzaki; J. Fyfe; D. Gregory; J. F. Gueremy; J. Hack; A. Harzallah; P. Inness; A. Kitoh; W. K. M. Lau; B. McAvaney; R. Madden; A. Matthews; T. N. Palmer; C. K. Park; D. Randall; and N. Renno (1996): Intraseasonal oscillations in 15 atmospheric general circulation models: Results from an AMIP diagonostic subproject. *Climate Dynamics*, 12: 325 – 357.

Smith, W. H. F. and D. T. Sandwell (1997): Global seafloor topography from satellite altimetry and ship depth soundings. *Science*, 277: 1956 – 1962.

Song, Q.; A. L. Gordon; and M. Visbeck (2004): Spreading of the Indonesian throughflow in the Indian Ocean. *Journal of Physical Oceanography*, 34: 772 – 792.

Stramma, L. and J. R. E. Lutjeharms (1997): The flow field of the subtropical gyre in the South Indian Ocean into the Southeast Atlantic Ocean: A case study. *Journal of Geophysical Research*, 99: 14053 – 14070.

Talley, L. D. and J. Sprintall (2005): Deep expression of the Indonesian throughflow: Indonesian intermediate water in the South Equatorial Current. *Journal of Geophysical Research*, 110: C10009.

Thompson, R. O. R. Y. (1984): Observations of the Leeuwin Current off Western Australia. *Journal of Physical Oceanography*, 14: 623 – 628.

Tokinaga, H. and Y. Tanimoto (2004): Seasonal transition of SST anomalies in the tropical Indian Ocean during El Niño and Indian Ocean dipole years. *Journal of the Meteorological Society of Japan*, 82: 1007 – 1018.

Tomczak, M. and J. S. Godfrey (2003): *Regional Oceanography: an Introduction.* Daya Publishing House, Delhi.

Toole, J. M. and B. A. Warren (1993): A hydrographic section across the subtropical South Indian Ocean. *Deep Sea Research Part 1: Oceanographic Research Papers*, 40: 1973 – 2019.

Tourre, Y. M. and W. B. White (1995): ENSO signals in global upper-ocean temperature. *Journal of Physical Oceanography*, 25: 1317 – 1332.

Tourre, Y. M. and W. B. White (1997): Evolution of the ENSO Signal over the Indo-Pacific Domain. *Journal of Physical Oceanography*, 27: 683 – 696.

Vaid, B. H.; C. Gnanaseelan; P. S. Polito; and P. S. Salvekar (2006): Influence of El Nino on the Biennial and Annual Rossby waves propagation in the Indian Ocean with special emphasis on Indian Ocean Dipole. *IITM Research Report*, RR-109.

Valentine, H. R.; J. R. E. Lutjeharms; and G. B. Brundrit (1993): The water masses and volumetry of the southern Agulhas current region. *Deep Sea Research*, 40: 1285 – 1305.

Van Ballegooyen, R. C.; M. L. Gründlingh; and J. R. E. Lutjeharms (1994): Eddy fluxes of heat and salt from the Southwest Indian Ocean into the Southeast Atlantic Ocean: A case study. *Journal of Geophysical Research*, 99: 14053 – 14070.

Van Leeuwen, P. J.; W. P. M. De Ruijter; and J. R. E. Lutjeharms (2000): Natal Pulses and the formation of Agulhas Rings. *Journal of Geophysical Research*, 105: 6425 – 6436.

Van Sebille, E; P. Spence; M. R. Mazloff; M. H. England; S. R. Rintoul; and O. A. Saenko (2013): Abyssal connections of Antarctic bottom water in a Southern Ocean State Estimate. *Geophysical Research Letters*, 40: 2177 – 2182.

Voldsund, A. (2011): *The dynamics of the East Madagascar current system and its influence on the biological production associated to the shelf – an observational study*. Masters thesis, University of Bergen.

Volkov, D. L.; T. Lee and L. L. Fu (2008): Eddy-induced meridional heat transport in the ocean. *Geophysical Research Letters*, 35(20).

Warren, B. A. (1981): *Deep circulation of the World Ocean. In Evolution of Physical Oceanography*, B. A. Warren and C. Wunsch, Eds. Cambridge, Massachusetts: MIT Press. 6 – 41.

Weijer, W. (2008): Normal modes of the Mascarene Basin. *Deep Sea Research Part 1*, 55: 128 – 136.

Woodberry, K.; M. Luther; and J. J. O'Brien (1989): The wind-driven seasonal circulation in the southern tropical Indian Ocean. *Journal of Geophysical Research*, 94: 17985 – 18002.

Wyrtki, K. (1971): Oceanographic Atlas of the International Indian Ocean Expedition. *National Science Foundation Publication*: 531.

Wyrtki, K. (1973): An equatorial jet in the Indian Ocean. *Science*, 181: 262 – 264.

Xie, S. P.; H. Annamalai; F. A. Schott; and J. P. McCreary (2002): Structure and mechanisms of south Indian Ocean climate variability. *Journal of Climatology*, 15: 864 – 878.

Yamagata, T.; S. K. Behera; S. A. Rao; Z. Guan; K. Ashok; and H. N. Saji (2002): The Indian Ocean dipole: A physical entity. *CLIVAR Exchanges*, 7: 15 – 22.

Yamagata, T.; S. K. Behera; S. A. Rao; Z. Guan; K. Ashok; and H. N. Saji (2003): Comments on "Dipoles, Temperature Gradient, and Tropical Climate Anomalies". *Bulletin of the American Meteorological Society*, 84: 1418 – 1422.

Yamagata, T.; J. J. Luo; S. Masson; M. Jury; and S. A. Rao (2004): *Coupled ocean-atmosphere variability in the tropical Indian Ocean. In Earth Climate: The Ocean – Atmosphere Interaction,* C. Wang; S. P. Xie; and J. A. Carton, Eds. Washington, DC: Geophysical Monograph Series. 189 – 212.

Yoo, S. H.; J. Fasullo; S. Yang; and C. H. Ho (2010): On the relationship between Indian Ocean sea surface temperature and the transition from El Niño to La Nina. *Journal of Geophysical Research*, 115: D15114.

Yu, J. Y. and K. M. Lau (2004): Contrasting Indian Ocean SST variability with and without ENSO influence: A coupled atmosphere – ocean GCM study. *Meteorology and Atmospheric Physics*, 90: 179 – 191.

Zaneveld, J. R. V. (1973): Variation of optical sea parameters with depth. *In Optics of the Sea* (Interface and In Water Transmission and Imagery) (AGARD – NATO lecture series 61).

Zhang, Z. G.; W. Wang and B. Qiu (2014): Oceanic mass transport by mesoscale eddies. *Science*, 345: 322 – 324.